International Journal of Vehicular Technology

Vehicular Ad Hoc Networks

Guest Editors: Syed R. Rizvi, Stephan Olariu, Cristina M. Pinotti, Shaharuddin Salleh, Mona E. Rizvi, and Zainab Zaidi

Vehicular Ad Hoc Networks

International Journal of Vehicular Technology

Vehicular Ad Hoc Networks

Guest Editors: Syed R. Rizvi, Stephan Olariu,
Cristina M. Pinotti, Shaharuddin Salleh, Mona E. Rizvi,
and Zainab Zaidi

Editorial Board

Contents

Hindawi Publishing Corporation
International Journal of Vehicular Technology
Volume 2011, Article ID 256542, 2 pages
doi:10.1155/2011/256542

Editorial
Vehicular Ad Hoc Networks

Syed R. Rizvi,[1] Stephan Olariu,[1] Cristina M. Pinotti,[2] Shaharuddin Salleh,[3] Mona E. Rizvi,[4] and Zainab Zaidi[5]

[1] *Old Dominion University, Norfolk, VA 23529, USA*
[2] *Department of Computer Science, University of Perugia, 06123 Perugia, Italy*
[3] *University of Technology, 81310 Johor, Malaysia*
[4] *Norfolk State University, Norfolk, VA 23504, USA*
[5] *NICTA, Australia*

Correspondence should be addressed to Syed R. Rizvi, srizvi@cs.odu.edu

Received 24 March 2011; Accepted 24 March 2011

Vehicular ad hoc networks (VANETs) have recently been proposed as one of the promising ad hoc networking techniques that can provide both drivers and passengers with a safe and enjoyable driving experience. VANETs can be used for many applications with vehicle-to-vehicle (V2V) and vehicle-to-infrastructure (V2I) communications. In the United States, motor vehicle traffic crashes are the leading cause of death for all motorists between two and thirty-four years of age. In 2009, the National Highway Traffic Safety Administration (NHTSA) reported that 33,808 people were killed in motor vehicle traffic crashes. The US Department of Transportation (US-DOT) estimates that over half of all congestion events are caused by highway incidents rather than by rush-hour traffic in big cities. The US-DOT also notes that in a single year, congested highways due to traffic incidents cost over $75 billion in lost worker productivity and over 8.4 billion gallons of fuel. Some of the significant applications of VANETs are road safety applications including collision and other safety warning systems, driver convenience and information systems, and, in the future, intelligent traffic management systems.

This special issue on VANETs presents current groundbreaking research, projects, and standardization efforts that have been done in the area of vehicular communications. In both the review process, and the production process we have aimed for the highest possible quality and speed. Papers in this special issue have been rigorously peer-reviewed. With an internationally acclaimed Editorial Board, we have selected some high-quality research work in the field of VANETs. Critical reviews were received from S. Olariu, G. Yan, S. El-Tawab (Old Dominion University, USA), C. M. Pinotti (University of Perugia, Italy), S. Salleh (University of Technology, Malaysia), M. E. Rizvi and S. Zehra (Norfolk State University, USA), Z. Zaidi (NICTA, Australia), and X. Chen (University of Oklahoma, USA).

In "*Spectrum sensing for cognitive vehicular networks over composite fading*," the authors consider shared utilization of the radio spectrum via cognitive radio systems to increase spectrum efficiency and quality of vehicular services. A cognitive radio system is a mechanism which allows unlicensed cognitive users (CUs) to utilize idle unused bands. Spectrum sensing is the first step that should be carried out before permitting cognitive clients to approach an authorized channel. A viable choice for spectrum sensing due to its simplicity, low computational cost, and ability to be applied on any kind of deterministic signal is energy detection (ED). However, hidden terminal and low SNR problems due to shadow-fading put fundamental limits to the sensing performance and practical entailments in designing of cognitive vehicular networks. Extensive modeling efforts are then being carried out to cope with varying channel characteristics, particularly multipath fading and shadowing. In this paper, the authors examine the performance of spectrum sensing using ED over Gamma-shadowed Nakagamim composite fading channel to cater both small and large-scale fading. The results highlight the notable impact of shadowing spread and fading severity on detection performance.

In "*Disseminating large amount of data to vehicular network in an urban area*," the problem of distributing large amount of data from multiple sources in an urban area is

investigated. The authors have shed light on an opportunistic approach for information collection in which a vehicle obtains information about resources from encountered vehicles. Due to the highly dynamic nature of the underlying vehicular network topology, reliable dissemination is introduced from multiple sources when each node in the network shares a limited amount of its resources for cooperating with others. By using rateless coding at the road side unit (RSU) and using vehicles as data carriers, an efficient way to achieve reliable dissemination to all nodes is described.

Recently, the *IntelliDriveSM* initiative has been proposed by the US Department of Transportation (USDOT) to enhance on-road safety and efficiency. In "*The effect of intellidrive on the efficiency of highway transportation systems*," a mathematical framework which predicts the effect of *IntelliDrive* on the efficiency of multilane highway systems prior to their real-life deployment is covered. The authors have shown that intervehicular communications improves the flow of vehicles by reducing the perception-reaction (P-R) times of drivers and, in some cases, allowing for more efficient lane-changing operations.

The paper "*Heterogeneous wireless sensor network for transportation system applications*," outlines the author's experience in the Embedded Middleware in Mobility Applications (EMMA) project and provides an illustration of the important role that wireless sensor technology can play in future transport system. The paper presents the employment of heterogeneous sensors to develop transportation system applications and focuses on how cooperation between vehicle and infrastructure can be addressed. It also presents encouraging results obtained from the experiments in investigating the feasibility of utilizing wireless sensor in vehicle and vehicle-to-infrastructure communication in real transportation applications.

In "*Evaluation of selective broadcast algorithms for safety applications in vehicular ad hoc networks*," evaluation focusing on the performance with respect to safety, rather than to classical network aspects like throughput, loss, and delay is presented. In this research, four new performance criteria are defined to address the effectiveness, efficiency, timeliness, and overhead of the candidate broadcast algorithms in terms of safety warning delivery. Four different selective broadcast algorithms used for information dissemination in VANETs are simulated. The results obtained help the readers to understand better the design requirements of a high-performance selective broadcast algorithm.

In "*Time in privacy preserving LBSs: an overlooked dimension*," privacy issues in location-based services (LBSs), that is, traffic monitoring, congestion-based, and "pay-as-you-go" road pricing, are considered. The main privacy threat in such services is the possibility to identify the user that requests a given service and his/her location at the time of the request. To specify a level of anonymity, a feeling-based model has been recently introduced which allows a user to define his/her desired level of anonymity simply by specifying a given area (e.g., a shopping mall). The entropy of the selected area is used to describe the area's popularity. In turn, the popularity is expressed in terms of footprints of the visitors—these being a representation of the amount of time a user spends in a given area—in the selected area. While this privacy model is claimed to be independent from the specific knowledge of the adversary about users' footprints, in this paper, the authors argue that an adversary that has a more structured knowledge over time can pose a threat to the privacy guarantees of the model. The claim is supported with both analysis and a concrete example on the mobility traces of cabs of San Francisco.

Acknowledgment

We are very pleased and thankful to receive the brilliant contributions and supports from many distinguished authors and organizations all over the world. I give my sincerest appreciation to Ghada Ali, Hindawi Publishing Corporation, for her timely support, excellent advice, and kind words of encouragement. Without her support, this special issue certainly would not have been possible. I thank the authors, all members of the Editorial Board, and members of publishing team in Hindawi Publishing Corporation for their efforts in providing significant supports and suggestions and organizing this special issue from ground zero.

Syed R. Rizvi
Stephan Olariu
Cristina M. Pinotti
Shaharuddin Salleh
Mona E. Rizvi
Zainab Zaidi

Hindawi Publishing Corporation
International Journal of Vehicular Technology
Volume 2011, Article ID 630467, 9 pages
doi:10.1155/2011/630467

Research Article

Spectrum Sensing for Cognitive Vehicular Networks over Composite Fading

Haroon Rasheed[1] and Nandana Rajatheva[1,2]

[1] *Telecommunications, Pathumthani 12120, SET, Asian Institute of Technology, Thailand*
[2] *Center for Wireless Communications, University of Oulu, 90570 Oulu, Finland*

Correspondence should be addressed to Haroon Rasheed, st105893@ait.ac.th

Received 16 August 2010; Revised 29 December 2010; Accepted 8 January 2011

Academic Editor: Cristina Pinotti

Recent advancement in vehicular wireless applications is also a major contributing factor in spectrum scarcity. Cognitive radio system is a mechanism which allows unlicensed cognitive users (CUs) to utilize idle unused bands. Fast and reliable detection of primary legacy user is the key component of cognitive radio networks. However, hidden terminal and low SNR problems due to shadow fading put fundamental limit to the sensing performance and practical entailments in design of the cognitive vehicular networks. Extensive modeling is being carried out to specify varying channel characteristics, particularly multipath fading and shadowing. Energy detection-(ED-) based spectrum sensing is a viable choice for many vehicle-to-vehicle (V2V) and vehicle to-road-side infrastructure (V2I) communications. This paper examines the performance of spectrum sensing using ED over Gamma-shadowed Nakagami-m composite fading channel to cater for both small-and-large scale fading. The results highlight the notable impact of shadowing spread and fading severity on detection performance. The relevant simulation results are presented to support our analytical results for average detection probability. Furthermore, these results are investigated and compared to other compound and classical channels.

1. Introduction

Radio spectrum is a limited resource, and almost all frequency bands are allocated to licensed users. The underutilization of spectrum bands extends to the definition of term *spectrum hole* as shown in Figure 1. It is actually an allotted band of frequencies, but at a specific time and geographic perspective, the band is not being employed by that user [1]. Cognitive radio is a compelling and innovative need for future wireless demands. There is a tremendous possibility to improve spectrum efficiency and quality of services through shared utilization. This system has also attracted a lot of interest in intelligent transportation networks (ITS). Cognitive radio-based vehicular transportation system in V2I and V2V communications and even interactions among on board devices within vehicles will help improve radio resource, energy efficiency, traffic network management, vehicular diagnostics and reduce accidents by road traffic awareness and route planning [2].

Spectrum sensing is the first step, as it should be carried out before permitting a cognitive client to approach an authorized channel. Fast and reliable detection of licensed user is the key component of cognitive radio networks. Thus, CUs need to have such cognitive abilities along with monitoring of substitute spectral route for possible band evacuation and minimum interference aggregation to other CUs [1].

In wireless communication, fading effect degrades signal propagation. This also places a primary constraint on sensing performance. Many propagation campaigns have been performed to investigate the statistics of shadow-fading in radio environments. Vehicle-to-roadside communications such as an automatic toll collection system has to grapple several channel variations particularly shadowing and multipath fading. Although the vehicle-mounted antenna ensures line-of-sight (LOS) connection to the beacon antenna, the shadow-fading due to reflections and scattering from the vehicle's own motor-hood or from other nearby large vehicles is a common problem as presented in Figure 2.

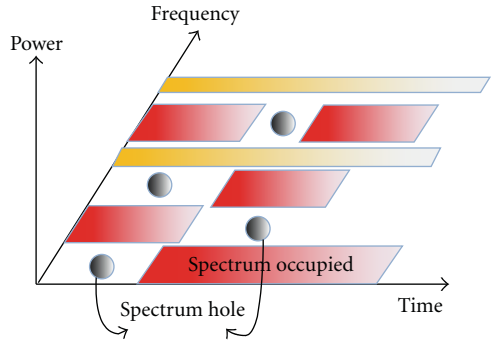

Figure 1: Spectrum holes concept.

Composite fading models like Suzuki, Loo, Rice-lognormal and Nakagami-lognormal, and so forth, are used to represent combine multipath and shadowing effects in wireless communications [3, pages 72–74]. They all rely on conventional lognormal distribution to model shadowing. However, capacity measurement and performance of spectrum sensing and access under multipath and shadowing using lognormal fading channel are somehow complex and do not lead to closed-form solutions. Alternatively, Gamma distribution is proposed to model the variations of average power which interprets shadow fading as close as lognormal distribution [4].

Energy detection [5] is proposed for spectrum sensing in cognitive radios due to its simplicity, low computational cost and ability to be applied on any kind of deterministic signal. In cognitive vehicular ad hoc network (VANET), ED can be applied to increase bandwidth efficiency. Licensed TV bands holders are primary users whereas vehicles and roadside infrastructure on highways and suburban cities will act as secondary users. As most of TV bands are blank, CUs in vehicular communication will perform ED-based sensing to find many unused spectrum bands. This assumption provides opportunistic spectrum access for wireless V2V and V2I communications. These ED-based cognitive vehicular systems lead to increased safety and information agility for vehicles on the road affected by multipath fading and shadowing. Moreover, the primary user transmission is modeled as a signal with known power, and hence energy detector is optimal [6, page 141]. In addition to cognitive radio, ED has found many applications in ultra wide-band technologies. Thus, performance analysis of energy detector in vehicular wireless networks with a variety of integrated techniques, is of particular interest.

The vehicular environment vision requires reliable, low latency wireless communication methods. One core issue is to detect and understand the nature of the wireless channel encountered by vehicular radios. The fading channels considered for are classical lognormal and Rayleigh fading channels. Previous research has primarily focused and examined ED, without (explicitly) taking into account fading channels that consist of composite distributions. The investigation over Gamma-shadowed Nakagami-m channel in [7, 8] consisted mainly on error performance, whereas spectrum sensing or estimation of detection probability is still an unexplored region.

This paper specifically focuses the performance analysis of energy detector in vehicular networks under Gamma-shadowed Nakagami-m fading channel model. The organization of the paper is as follows. In Section 2, detailed model of ED for spectrum sensing is discussed with its significance in vehicular networks. Section 3 defines the statistics of composite fading model with Gamma PDF as an alternative replacement for lognormal distribution. Composite fading channel statistics and signal-to-noise ratio (SNR) analysis for ED with respect to shadow-fading parameters are characterized in Section 4. The approximated expression for average detection probability over composite fading is obtained in Section 5 using series representation of Marcum-Q function. Further, Section 6 contains numerical and simulation results which also verify our theoretical formulations, and discussion about sensing and receiver performance in terms of fading parameters. Finally, Section 7 contains some concluding remarks.

2. Energy Detection in Vehicular Technologies

Energy detection is an efficient and fast noncoherent technique that essentially computes a running average of the signal power over a window of prespecified spectrum length. This is the simplest sensing method that requires no a priori knowledge about the transmitted signals. In addition to vehicular communications, the significance of energy detector finds many applications in wide-band technologies [9]. Performance analysis of ED over a variety of fading channels in vehicular network is considerably important and requires detailed investigation.

ED has already been recognized as an efficient sensing method for cognitive radio. In vehicular networks cognitive radio is a new paradigm to alleviate the bandwidth scarcity problem which will be an issue in near future. Similar to many cognitive radio systems, cognitive VANET faces the challenge of spectrum sensing, that is, the vehicles need to detect the presence or absence of licensed primary users with high reliability [9].

The block diagram of the energy detector is shown in Figure 3. The signal $x(t)$ is received and filtered with a bandpass filter (BPF) in order to limit the noise and to select the bandwidth of interest. The noise in the output of the filter has a band-limited, flat spectral density. Next, the energy detector consists a squaring device and a finite time integrator. The output signal Y from the integrator as given in [5]

$$Y = \frac{1}{T}\int_{t-T}^{t} |x(\tau)|^2 d\tau. \tag{1}$$

Finally, this output signal Y is compared to the threshold λ, in order to decide whether a signal is present or not. The threshold is set according to the statistical properties of the output Y when only noise is present. Thus, spectrum sensing is equivalent to detect the presence of an unknown

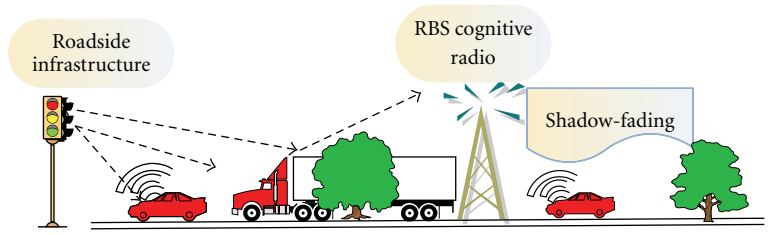

Figure 2: Shadowing in spatial environment.

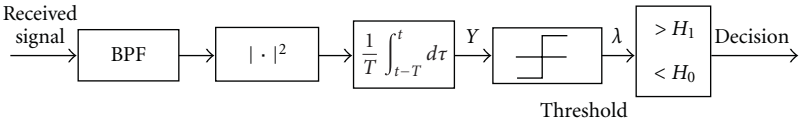

Figure 3: Block diagram of energy detector.

deterministic signal in the radio spectrum band which generally defines a binary hypothesis-testing problem as

$$y(t) = \begin{cases} n(t) & H_0 : \text{signal is absent}, \\ hx(t) + n(t) & H_1 : \text{signal is present}, \end{cases} \quad (2)$$

where h is the channel response and $n(t)$ is the Gaussian random variable with zero mean and $N_{01}W$ variance; $n \sim N(0, N_{01}W)$ where N_{01} is the single sided noise spectral density and W is the bandwidth. A sample function of time period T of a process which is band limited to W can be approximately described by a set of $2u$ number of sample values, that is, $u = TW$, where T and W are selected to limit u to an integer value [5]. Using this fact, the statistics of the detector decision variable Y of the primary signal is a sum of $2u$ zero and non zero mean Gaussian random variables under H_0 and H_1 respectively. The approximated noise energy over a time period $(0, T)$ for detector Y is formulated as [10]

$$Y = \frac{2}{N_{01}} \int_0^T n^2(t)dt = \sum_{i=1}^{2u} \left(\frac{n_i}{\sqrt{N_{01}W}} \right)^2 : H_0. \quad (3)$$

Similarly, Y under H_1 is constructed as

$$Y = \frac{2}{N_{01}} \int_0^T y^2(t)dt = \sum_{i=1}^{2u} \left(\frac{h_i x_i + n_i}{\sqrt{N_{01}W}} \right)^2 : H_1. \quad (4)$$

Here, we assume that the h is constant over the $2u$ samples.

Thus, the probability density function (PDF) of Y is a central chi-square variable χ^2_{2u} with $2u$ degrees of freedom for H_0 and noncentral chi-square variable $\chi^2_{2u}(2\gamma)$ with $2u$ degrees of freedom and a noncentrality parameter 2γ under H_1 respectively, which can be written as

$$f_Y(y) = \begin{cases} \frac{1}{2^u \Gamma(u)} y^{u-1} e^{-y/2} : H_0, \\ \frac{1}{2} \left(\frac{y}{2\gamma} \right)^{(u-1)/2} e^{-(2\gamma+y)/2} I_{u-1}(\sqrt{2\gamma y}) : H_1, \end{cases} \quad (5)$$

where γ is the SNR, that is, $\gamma = h^2 E_s / N_{01}$ and E_s is defined as observed signal energy, $\Gamma(\cdot)$ is gamma function and $I_n(\cdot)$ is nth order modified Bessel function of the first kind. The exact closed-form equations for probabilities of detection P_d, false alarm P_f, and missed detection P_m over additive white Gaussian noise (AWGN) channel are given by [10]

$$P_d = P_r\{Y > \lambda \mid H_1\} = Q_u\left(\sqrt{2\gamma}, \sqrt{\lambda}\right), \quad (6)$$

where λ is the threshold for signal sample and $Q_M(\cdot, \cdot)$ is generalized Mth order Marcum-Q function defined as [11, Equation (2.1-122), page 44]

$$Q_M(\alpha, \beta) = \int_\beta^\infty \frac{t^M}{\alpha^{M-1}} e^{-(t^2+\alpha^2)/2} I_{M-1}(\alpha t)dt, \quad (7)$$

where $I_{M-1}(\cdot)$ is the modified Bessel function of $(M-1)$th order. The probability of false alarm is expressed as

$$P_f = P_r\{Y > \lambda \mid H_0\} = \frac{\Gamma(u, \lambda/2)}{\Gamma(u)}, \quad (8)$$

where $\Gamma(\cdot, \cdot)$ is an upper incomplete gamma function which is defined as $\Gamma(m, n) = \int_n^\infty t^{m-1} e^{-t} dt$ [12, Equation (8.350-2), page 899]. Since γ does not appear in (8), average false alarm probability over any fading channel will be similar (8).

Threshold λ for ED is calculated for a specified P_f using (8), whereas conventional optimality principle, Neyman-Pearson criterion maximizes P_d for a given P_f and equivalent to the likelihood ratio test (LRT) of Y indicated as $\mathrm{LR}(Y)$. In general, there is no LOS path present between the secondary user and the primary transmitter. Hence, the received primary signal is a superposition of many non LOS signals and is well approximated to Gaussian random variables according to central limit theorem [13]. In our consideration, when both the primary signal and noise are treated as Gaussian processes, energy detector can meet any desired P_d and P_f simultaneously, hence the threshold λ is optimal [14]. Finally, the probability of missed detection can be evaluated as

$$P_m = 1 - P_r\{Y > \lambda \mid H_1\} = 1 - Q_u\left(\sqrt{2\gamma}, \sqrt{\lambda}\right). \quad (9)$$

Since P_f is independent of SNR due to the concept of no signal transmission, P_d in (6) is dealt only for nonfading environment, where channel h is deterministic. While a varying h due to shadowing and multipath fading gives probability of detection on the instantaneous SNR γ [15]. In this case, the average probability of detection P_d is assessed by averaging (6) over fading statistics.

The IEEE 802.22 draft standard addresses fixed-access devices and targets rural area applications. Energy detector has been tested for spectrum sensing in cognitive radio. Also ED is a non coherent reception technique which is implementable either using analog or digital design. The experimental test bed description and algorithms of ED in cognitive radio are given in [16, 17]. The SNR limitation is dealt with the help of collaboration of users [18] and continuous research work is ongoing to overcome ED limitations.

3. Composite Channel Model for Shadow Fading

In vehicular communication, a signal is assumed to pass through a large number of attenuating materials before reaching to the destination. Owing to the short range of typical V2V and V2I links, a more precise description of the fluctuations is often given by small-scale fading models. These fluctuations are caused by constructive and destructive interference between multipath components. Nakagami distribution can model fading conditions like Rayleigh or Rician statistics, depending on whether or not there is a LOS. The fading statistics for V2V propagation channel under realistic suburban driving conditions is modeled and analyzed by Nakagami distribution [19].

The PDF $f_X(x)$ of the envelope X, under Nakagami fading conditions describes the magnitude of the received envelope by the distributions given as

$$f_X(x) = \frac{2m^m x^{2m-1} e^{-(m/p)x^2}}{\Gamma(m) p^m}, \quad x \geq 0.5, \tag{10}$$

where $\Gamma(\cdot)$ is the gamma function and m is the Nakagami fading parameter. $p = E[x^2]$ is the average power of the received signal, $E[\cdot]$ represents statistical average operator.

The average power p is deterministic in the absence of shadowing. However, V2I and V2V channel variations due to obstructions and large size vehicles, and so forth, exhibit shadowing effect. Thus, mean power of the signal becomes random and (10) can be written by conditioning the envelope as [20]

$$f_{X|P}(x \mid p) = \frac{2m^m x^{2m-1} e^{-(m/p)x^2}}{\Gamma(m) p^m}, \quad x, p > 0. \tag{11}$$

The composite PDF with fading and shadowing is therefore written as

$$f_X(x) = \int_0^\infty f_{X|P}(x \mid p) f_P(p) dp, \tag{12}$$

where $f_P(p)$ is the PDF of average power due to shadowing. If $f_P(p)$ is lognormally distributed and $m \neq 1$, $f_X(x)$ will be Nakagami-lognormal composite distribution. Nevertheless, due to the inherent analytical complication of handling correlated lognormal random variables, it is often inconvenient for further performance measurements and will not lead to a closed-form solution [15, 20].

3.1. Gamma Distribution: Alternative to Lognormal Distribution. Lognormal distribution is generally used to model average power variations. Empirical studies have shown that p has a lognormal PDF [21, Equation (1.5), page 21], that is,

$$f_P(p) = \frac{1}{p\sqrt{2\pi\sigma^2}} \exp\left(-\frac{(20\log p - \mu_{\text{dBm}})^2}{2\sigma^2}\right), \quad p > 0, \tag{13}$$

where σ is the standard deviation for shadowing, whereas $\sigma \to 0$ corresponds to no shadowing. The local mean power p fluctuates about a constant area mean power μ_{dBm}, that is, $\mu_{\text{dBm}} = 30 + 10E[\text{Log}_{10}p]$ [21, Equation (2.202), page 98]. Composite fading channel with Nakagami PDF and lognormally distributed power has involved complicated integral form, also from above discussion even fitting this PDF to real data in vehicular communications is a difficult task. Hence, a closed-form expression for various system computations is a challenging problem. Based on theoretical results and measured data, an alternative substitute is the two-parameter Gamma distribution, which approximates several PDFs and justifies the lognormal distribution [4, 22].

Lognormal and Gamma PDFs are interchangeable in simulating real data when σ_{dB} is not large, that is, ≤ 6 [23]. For this, we compared the average detection probability variations over Gamma and lognormal fading channels in Figure 4 for Gamma shadowing parameter m_0 with respective lognormal σ_{dB} spreads. It is evident from simulation results that for $\sigma_{\text{dB}} < 6$, Gamma PDF is a good fit for lognormal distribution. Furthermore, when signal amplitude follows Nakagami-m distribution, the PDF of SNR γ, which is the sum of n independent and identically distributed (i.i.d) exponential random variables is Gamma distributed.

Considering $P = X^2$, the obtained result will be the PDF of P can be expressed as [11, Equation (2.1-105), page 41]

$$f_P(p) = \frac{1}{\sqrt{2\pi\sigma^2 p}} \exp\left(-\frac{p}{2\sigma^2}\right), \quad p \geq 0 \tag{14}$$

if P is defined as $P = \sum_{i=1}^{n} X_i^2$, where $i = 1, 2, \ldots, n$ are statistically i.i.d Gaussian random variables with zero mean and variance σ^2. The characteristics function of P is represented as [11, Equation (2.1-107), page 41]

$$\phi_P(jv) = \frac{1}{(1 - j2v\sigma^2)^{n/2}}. \tag{15}$$

The inverse transform of this characteristic function leads to central chi-square distribution with n degree of freedom, that is,

$$f_P(p) = \frac{p^{(n/2)-1}}{\sigma^n 2^{n/2} \Gamma(n/2)} \exp\left(-\frac{p}{2\sigma^2}\right), \quad p \geq 0, \tag{16}$$

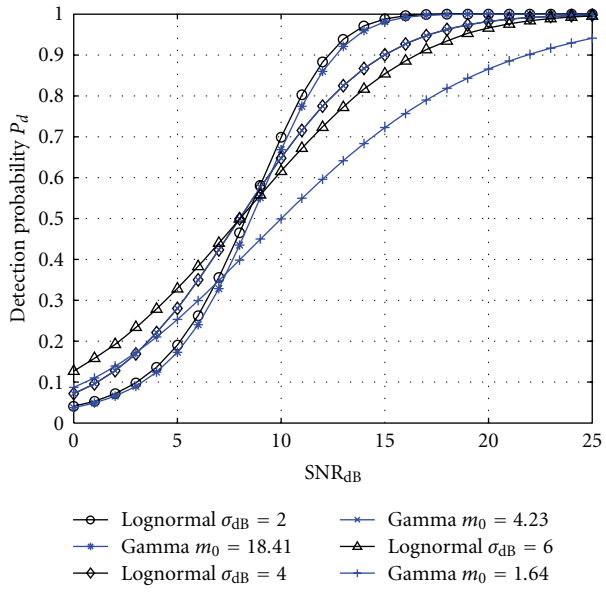

Figure 4: A comparison of average detection probability (P_d) variations between lognormal σ_{dB} spread and Gamma distributions shadowing parameter m_0 values, keeping time bandwidth product $u = 5$ and false alarm probability $P_f = 0.01$.

Table 1: Gamma m_0 and lognormal σ_{dB} values relationships.

σ_{dB}	2	4	6
m_0	18.41	4.23	1.64

substituting $p_0 = 2\sigma^2$ and $m_0 = n/2$ is simplified to Gamma PDF as

$$f_P(p) = \frac{p^{m_0-1}}{\Gamma(m_0)p_0^{m_0}} \exp\left(-\frac{p}{p_0}\right), \tag{17}$$

where p_0 is the measure of average power and m_0 is the order of Gamma PDF that inversely reflects shadowing severity. By changing m_0, several distributions like lognormal, Gaussian, and so forth, can be obtained [8, 20]. The parameters m_0 and p_0 of Gamma distribution are related with their respective lognormal mean and the variance as $m_0 = 1/(e^{\sigma^2} - 1)$ and $p_0 = \mu\sqrt{(m_0+1)/m_0}$, where $\sigma = \sigma_{dB}/8.686$ and μ are defined as the standard deviation and average power related to lognormal PDF respectively. The equivalent values of σ_{dB} and m_0 are found accordingly and indicated in Table 1.

3.2. Gamma-Shadowed Nakagami-m Fading Distribution for Multipath and Shadowing. In radio propagation, shadowing and multipath fading appear simultaneously. Conversely, the channel model most frequently employed in vehicular communication do not distinguish the two effects. The Gamma-shadowed Nakagami-m (composite) distribution provides analytical restraint in terms of simplicity with which parameters can be computed. By substituting (17) and (11)

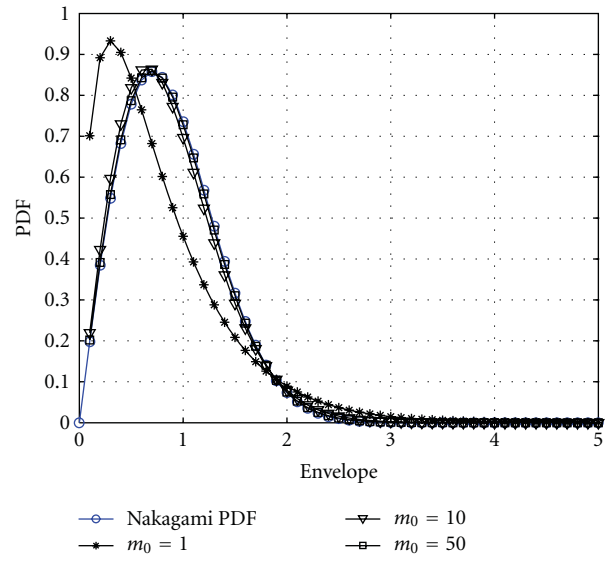

Figure 5: The composite PDF over various shadowing parameter m_0 values with corresponding Nakagami-m keeping $m = 0.8$.

in (12), the compound envelope of X consists of both multipath and shadowing is obtained in (18) as [20]

$$\begin{aligned} f_X(x) &= \int_0^\infty f_{X|P}(x \mid p)\, f_P(p)\, dp \\ &= \frac{2c}{\Gamma(m_0)\Gamma(m)} \left(\frac{cx}{2}\right)^{m_0+m-1} K_{m_0-m}(cx), \quad x > 0, \end{aligned} \tag{18}$$

where $c = 2\sqrt{m/p_0}$ and $K_{m_0-m}()$ is the modified Bessel function of order $(m_0 - m)$.

The numerically evaluated PDFs of composite and Nakagami fading are plotted in Figure 5. It is found that when the effect of shadowing is decreased at large value of $m_0 = 50$, the composite PDF exactly overlaps the Nakagami PDF and represents both multipath and shadowing effects.

4. Composite Fading Channel Statistics

The moments of the compound envelope PDF are expressed as [20]

$$E_c[X^t] = \frac{\Gamma(m_0 + t/2)\Gamma(m + t/2)}{\Gamma(m_0)\Gamma(m)} \left(\frac{2}{c}\right)^t. \tag{19}$$

From above formula, amount of fading (AF) defined as A_f can be obtained as [20]

$$\begin{aligned} A_f &= \frac{\text{variance}[X^2]}{E[X^2]^2} \\ &= \frac{mm_0 + m^2 m_0 + mm_0^2}{m^2 m_0^2} > 0. \end{aligned} \tag{20}$$

The value of A_f ranges from zero to infinity, corresponding to no fading to severe multipath fading and shadowing. By

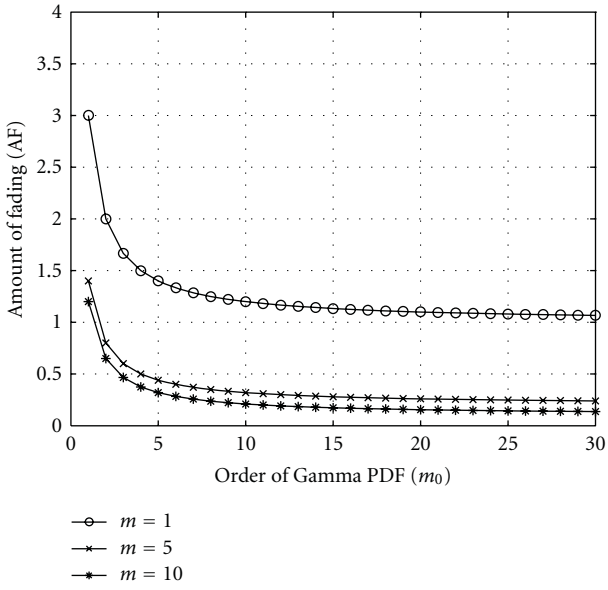

Figure 6: Amount of fading with respect to shadowing parameter m_0 taking different values of fading severity parameter m.

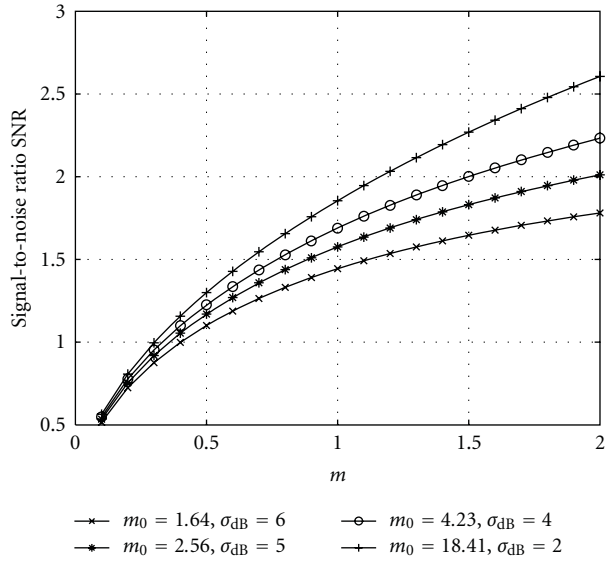

Figure 7: Composite fading channel signal-to-noise ratio (SNR) as a function of shadowing parameter m_0 over different values of fading severity parameter m.

using (20) AF curves are simulated over a range of m_0 for various m values as depicted in Figure 6. It is found that AF is related inversely with fading severity, and become independent for shadowing parameter $m_0 > 5$ corresponds to $3.71\sigma_{dB}$ spread.

For a given noise uncertainty, there exist a SNR wall, below which the ED cannot notice the existence of unknown deterministic signal [14]. Due to shadowing and fading effects, it is possible that user experiences very low SNR conditions and hence, its performance diminishes. For detection improvement in such situations, channel SNR values associated with the shadow-fading condition must be monitored carefully. The SNR of composite envelope is obtained from (19) as given by [20]:

$$\text{SNR} = \frac{1}{\sqrt{m_0 m[\Gamma(m_0)\Gamma(m)/\Gamma(m_0+0.5)\Gamma(m+0.5)]^2 - 1}}. \tag{21}$$

By using (21), we plotted SNR variations as a function of fading severity index m depicted in Figure 7. It is observed that larger values of m_0 correspond to high SNR values. However, for $m > 0.5$ change in SNR gradually decreases. When the user is in shadow fading environment with low SNR, the detection threshold λ of ED should be adjusted adaptively.

5. Average Detection Probability over Composite Fading Channel

The average probability of detection $\overline{P}_d$ over fading statistics is determined as [10]:

$$\overline{P}_d = \int_0^\infty Q_u\left(\sqrt{2\gamma}, \sqrt{\lambda}\right) f_\gamma(\gamma)\, d\gamma, \tag{22}$$

where $f_\gamma(\gamma)$ is the PDF of SNR under shadow fading.

When envelope of received signal due to shadow-fading is modeled as Nakagami distribution the SNR PDF can be modeled as Gamma distribution [20]

$$f_{\gamma|\overline{\gamma}}(\gamma) = \frac{m^m \gamma^{m-1}}{\Gamma(m)\overline{\gamma}^m} \exp\left(-\frac{m\gamma}{\overline{\gamma}}\right), \quad \gamma \geq 0,\ m \geq 0.5, \tag{23}$$

where $\Gamma(\cdot)$ is the gamma function and m is the Nakagami fading parameter. $\overline{\gamma} = E[h^2 E_b/N_{01}]$ is the average SNR or average power of the received signal being random, hence reflects the existence of shadowing. The two-parameter Gamma distribution which has shown a good justification of lognormal PDF is defined as

$$f_{\overline{\gamma}_0}(\gamma) = \frac{m_0^{m_0} \gamma^{m_0-1}}{\Gamma(m_0)\overline{\gamma}_0^{m_0}} \exp\left(-\frac{\gamma}{\overline{\gamma}_0}\right), \tag{24}$$

where $\overline{\gamma}_0$ is the measure of average power and is related to the average SNR $\overline{\gamma}$, m_0 is order of Gamma PDF and a measure of channel shadowing. The PDF of received SNR in combined shadow fading situation is given as [20]

$$f_\gamma(\gamma) = \int_0^\infty f(\gamma \mid \overline{\gamma}) f_P(p). \tag{25}$$

Substituting (23) and the two-parameter Gamma PDF from (24) in (25), and by changing variables $f_\gamma(\gamma)$, the PDF of received SNR in combined shadow fading environment can be obtained as [8]

$$f_\gamma(\gamma) = \frac{2}{\Gamma(m)\Gamma(m_0)}\left(\frac{c_0}{2}\right)^{m_0+m} \times \gamma^{((m_0+m)/2)-1} K_{m_0-m}\left(c_0\sqrt{\gamma}\right), \quad \gamma > 0, \tag{26}$$

where $c_0 = 2\sqrt{mm_0/\overline{\gamma}_0}$ is scaling parameter related to $\overline{\gamma}$ and $K_{m_0-m}(\cdot)$ is the modified Bessel function of order $(m_0 - m)$.

The probability of detection over fading environment is evaluated using complicated integral forms involving Marcum-Q function. Further, these integrals cannot be solved in closed-forms in general with the available integral results [24]. In order to avoid such mathematical difficulties and to evaluate integrals involving Marcum-Q function with exponentials and Bessel functions having complicated arguments, alternative series representation of Marcum-Q function is used.

The generalized Marcum-Q function $Q_u(a,b)$ in its alternative series representation for $\sqrt{2\gamma} > \sqrt{\lambda} \geq 0$, as given in [24]

$$Q_u\left(\sqrt{2\gamma},\sqrt{\lambda}\right) = 1 - e^{(-(2\gamma+\lambda)/2)} \sum_{n=u}^{\infty} \left(\frac{\lambda}{2\gamma}\right)^{n/2} I_n\left(\sqrt{2\lambda\gamma}\right), \tag{27}$$

where $I_n(\cdot)$ is the nth order modified Bessel function of the first kind. By substituting (27) and (26) in (22), the average detection probability over compound fading channel P_d can be written as

$$\overline{P}_d = \int_0^{\infty} \left(1 - e^{(-(2\gamma+\lambda)/2)} \sum_{n=u}^{\infty} \left(\frac{\lambda}{2\gamma}\right)^{n/2} I_n\left(\sqrt{2\lambda\gamma}\right)\right) \times \frac{2}{\Gamma(m)\Gamma(m_0)} \left(\frac{c_0}{2}\right)^{m_0+m} \gamma^{((m_0+m)/2)-1} K_{m_0-m}\left(c_0\sqrt{\gamma}\right) d\gamma. \tag{28}$$

By using the fact $\int_0^{\infty} f_\gamma(\gamma)d\gamma = 1$, (28) will be simplified as,

$$\overline{P}_d = 1 - \frac{2e^{-\lambda/2}}{\Gamma(m)\Gamma(m_0)} \left(\frac{c_0}{2}\right)^{m_0+m} \sum_{n=u}^{\infty} \left(\frac{\lambda}{2}\right)^{n/2} \times \int_0^{\infty} e^{-\gamma} \gamma^{(-n+m_0+m)/2-1} I_n\left(\sqrt{2\lambda\gamma}\right) K_{m_0-m}\left(c_0\sqrt{\gamma}\right) d\gamma. \tag{29}$$

However, integral of the Bessel functions product $I_n(\cdot)$ and $K_{m_0-m}(\cdot)$ with exponentials and powers does not lead to a closed-form, therefore we evaluated (29) numerically and compared it with our simulation results.

6. Numerical and Simulation Results

The performance of energy detector over composite fading channel for vehicular communications is presented in terms of average detection probability $\overline{P}_d$ and complementary receiver operating characteristic (ROC) curves, that is, P_m versus P_f. By varying the average SNR $\overline{\gamma}_0$, while keeping all the other parameters such as threshold λ, time bandwidth product u, fading metric m and shadowing parameter m_0 constant, the behavior of $\overline{P}_d$ is shown. In the second scenario, detector performance is evaluated by means of complementary ROC curves similar to [10], that is, $\overline{P}_m$ versus P_f where $\overline{P}_m = 1 - \overline{P}_d$.

Detector behavior characterization over various parameters is important in order to adjust numerous vehicular environments. The detector threshold λ is calculated for

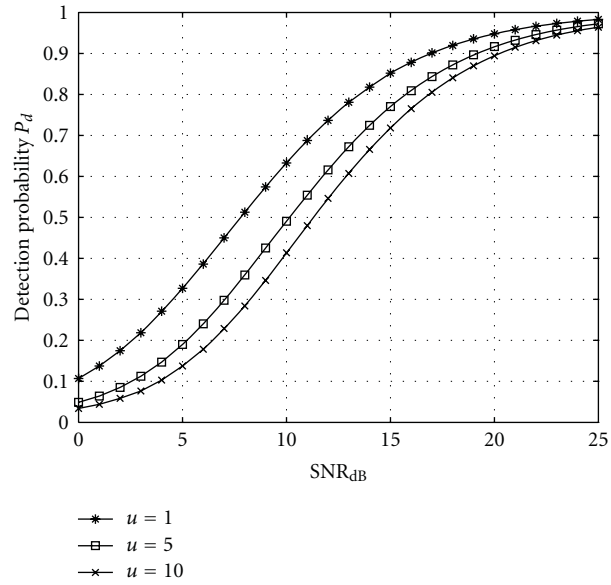

Figure 8: Average detection probability ($\overline{P}_d$) variations over various time bandwidth product (u) values in compound fading channel while taking false alarm probability $P_f = 0.01$.

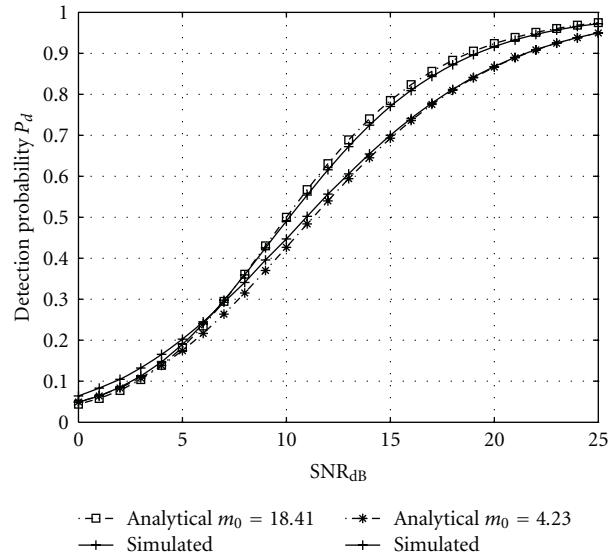

Figure 9: Average detection probability ($\overline{P}_d$) both analytical and simulation for composite fading taking $m = 1$, $u = 5$, and $P_f = 0.01$.

$P_f = 0.01$ from (8) taking $u = 1, 5, 10$ as shown in Figure 8. It can be observed that the detector performance with smaller number of samples (lower u) for energy E_s is better if compared with that obtained from greater number of samples. The detector threshold λ is found at specified P_f. An increase in the threshold value of the detector, that is, larger u leads to reduction in both the false alarm and detection probabilities.

By using (29) average $\overline{P}_d$ over varying $\overline{\gamma}_0$ is computed with the help of MATHEMATICA 7. Figure 9 illustrates

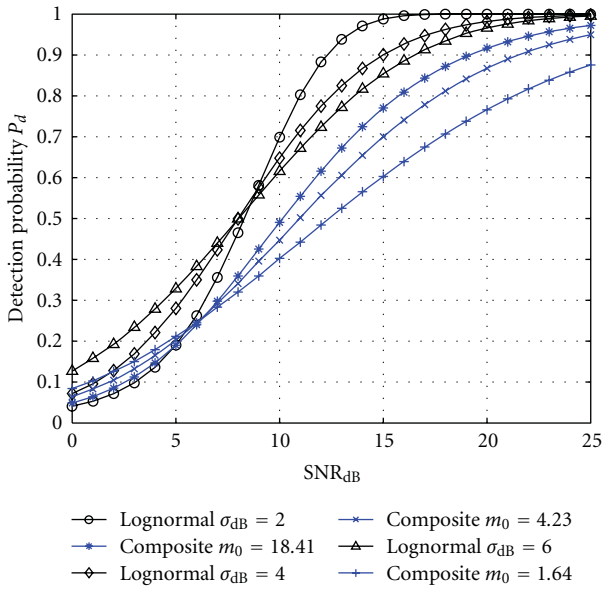

FIGURE 10: A comparison of average detection probability ($\overline{P}_d$) variations between lognormal and composite fading channel keeping fading severity parameter $m = 1$, time bandwidth product $u = 5$ and false alarm probability $P_f = 0.01$.

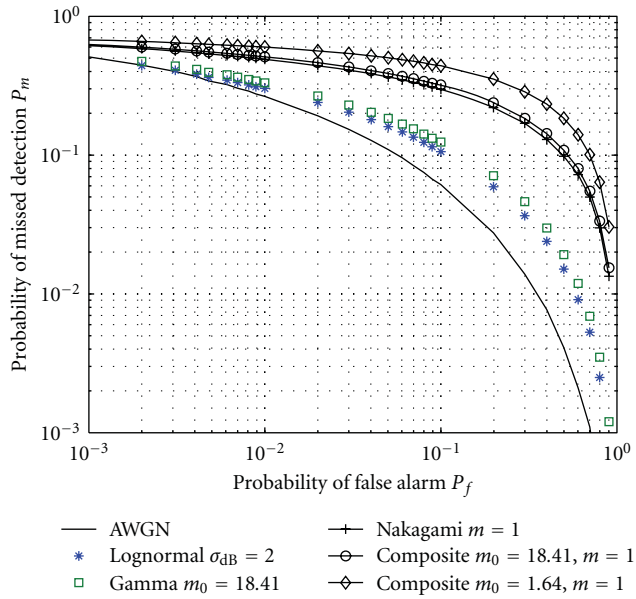

FIGURE 11: Complementary ROC (P_m versus P_f) of composite fading channel over different shadowing parameter m_0 values in comparison with Nakagami-m fading channel. AWGN curve is provided for reference.

the average P_d variations over composite fading channel at $m_0 = 18.41$ and 4.23 corresponding to $\sigma_{dB} = 2$ and 6 respectively. Both analytical and simulated results interpret sufficient detector performance over high average SNR, that is, SNR > 10 dB, also higher values of m_0 reflects better detection over specified SNR$_{dB}$. However, for low SNR region the deteriorating performance can be improved using spatial diversity and appropriate combining techniques.

The detection performance of composite fading channel rendering both multipath and shadowing effects at different range of m_0 is evaluated in Figure 10. The better detection is illustrated as the effect of shadowing diminishes at higher values of m_0, keeping fading characteristics $m = 1$ unchanged. The similar phenomenon is obtained at smaller values of lognormal shadowing statistics $\sigma_{dB} \leq 2$ referring to light to moderate shadowed scenario. Whereas for heavier shadowed region, that is, $\sigma_{dB} > 6$ to achieve a good fit is not possible. However, fading severity index $m > 1$ keeps composite channel to overcome the shadowing and LOS communication can be considered which is common in vehicular networks.

Complementary ROC plot (P_m versus P_f) for composite channel is plotted in contrast to Gamma, lognormal and Nakagami channels as shown in Figure 11. Both the Gamma and lognormal are offering similar detection characteristics for the selected parameters.It is evident that composite fading channel exhibits the combine fading properties of Gamma and Nakagami-m fading channel.

In Figure 12 the ROC curve of Gamma-shadowed Nakagami-m composite fading clearly indicates a substantial detection performance improvement in contrast to Loo and

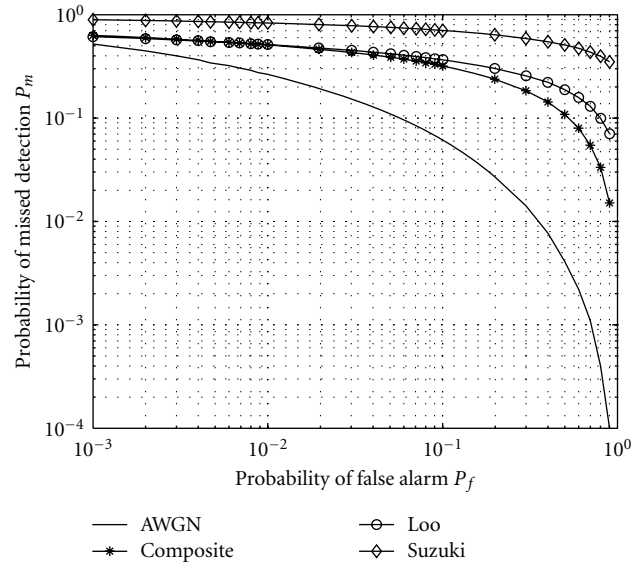

FIGURE 12: Complementary ROC (P_m versus P_f) of different mixed distribution fading channel over shadowing factor $\sigma_{dB} = 2$ and fading severity parameter $k = m = 1$. AWGN curve is provided for reference.

Suzuki mixed distribution channels where k represents carrier to multipath ratio in Loo distribution. Another prominent feature of the versatile Gamma-shadowed Nakagami-m composite channel is having minimum set of parameters as summarized in Table 2 from which diverse shadow fading environments can be approximated.

Table 2: Input parameters of different shadow fading distributions.

Channel/parameter	m	m_0	σ_{dB}	k	μ_{dB}
Composite	1	18.41	—	—	—
Loo	—	—	2	5	−6
Suzuki	—	—	2	—	−6

7. Conclusion

In the standardization process of vehicular networks, channel models are required to evaluate and select the proposed physical layer modulation and coding schemes. We have presented spectrum sensing using energy detection over Gamma-shadowed Nakagami-m composite fading model. The scheme can be effectively deployed in vehicular networks and help to combat against spectrum scarcity. To avoid computational complexities of the integrals involving Marcum-Q function, we apply PDF-based approximation and alternative series representation of generalized Marcum-Q function. Employing these approaches the average detection probability is evaluated. Analytical and simulation results are provided to support the theoretical formulations and derivations. The presented results show that spectrum sensing and access in vehicular communication can be improved by modeling the wireless environment precisely. Gamma-Shadowed Nakagami-m fading channel based energy detection provides fast and reliable sensing in cognitive vehicular networks. The numerical and simulation results provide insight and can serve as a quick way of assessing performance. From the presented results it is clear that a channel model composed of mixed distributions is useful for designing vehicular wireless systems and networks.

References

[1] S. Haykin, "Cognitive radio: brain-empowered wireless communications," *IEEE Journal on Selected Areas in Communications*, vol. 23, no. 2, pp. 201–220, 2005.

[2] H. Hannes and P. L. Kenneth, Eds., *VANET: Vehicular Applications and Inter-Networking Technologies*, John Wiley & Sons, New York, NY, USA, 2010.

[3] E. G. Corazza, *Digital Satellite Communications*, Springer, New York, NY, USA, 2007.

[4] A. Abdi and M. Kaveh, "On the utility of gamma PDF in modeling shadow fading (slow fading)," in *Proceedings of the 49th IEEE Vehicular Technology Conference*, vol. 3, pp. 2308–2312, May 1999.

[5] H. Urkowitz, "Energy detection of unknown deterministic signals," *Proceedings of the IEEE*, vol. 55, pp. 523–531, 1967.

[6] S. Kay, *Fundamentals of Statistical Signal Processing: Detection Theory*, Prentice-Hall, Englehood Cliffs, NJ, USA, 1998.

[7] P. M. Shankar, "Error rates in generalized shadowed fading channels," *Wireless Personal Communications*, vol. 28, no. 3, pp. 233–238, 2004.

[8] I. M. Kostic, "Analytical approach to performance analysis for channel subject to shadowing and fading," *IEE Proceedings on Communications*, vol. 152, no. 6, pp. 821–827, 2005.

[9] L. Catalin, K. V. Rama, A. Onur, B. Dusan, and S. Ivan, "Evaluation of energy-based spectrum sensing algorithm for vehicular networks," in *Proceedings of the Software Defined Radio and Dynamic Spectrum Access Technical Conference*, Washington, DC, USA, December 2009.

[10] F. F. Digham, M. S. Alouini, and M. K. Simon, "On the energy detection of unknown signals over fading channels," *IEEE Transactions on Communications*, vol. 55, no. 1, pp. 21–24, 2007.

[11] J. G. Proakis and M. Salehi, *Digital Communications*, McGraw Hill, New York, NY, USA, 5th edition, 2008.

[12] S. I. Gradshteyn and M. I. Ryzhik, *Table of Integrals, Series, and Products*, Academic Press, 7th edition, 2007.

[13] J. Ma, G. Zhao, and Y. Li, "Soft combination and detection for cooperative spectrum sensing in cognitive radio networks," *IEEE Transactions on Wireless Communications*, vol. 7, no. 11, pp. 4502–4507, 2008.

[14] A. Sahai, N. Hoven, and R. Tandra, "Some fundamental limits on cognitive radio," in *Proceedings of the 42nd Allerton Conference on Communication, Control, and Computing*, 2004.

[15] A. Ghasemi and E. S. Sousa, "Collaborative spectrum sensing for opportunistic access in fading environments," in *Proceedings of the 1st IEEE International Symposium on New Frontiers in Dynamic Spectrum Access Networks (DySPAN '05)*, pp. 131–136, November 2005.

[16] D. Cabric, A. Tkachenko, and R. Brodersen, "Experimental study of spectrum sensing based on energy detection and network cooperation," in *Proceedings of the 1st ACM International Workshop on Technology and Policy for Accessing Spectrum (TAPAS '06)*, 2006.

[17] T. Ohno, H. Murata, K. Yamamoto, and S. Yoshida, "Field trial of cooperative sensing technique with energy detection," in *Proceedings of the 20th IEEE International Symposium on Personal, Indoor and Mobile Radio Communications*, pp. 2926–2929, 2009.

[18] J. Wu, T. Luo, J. Li, and G. Yue, "A cooperative double-threshold energy detection algorithm in cognitive radio systems," in *Proceedings of the 5th International Conference on Wireless Communications, Networking and Mobile Computing (WiCOM '09)*, pp. 1–4, September 2009.

[19] L. Cheng, B. Henty, D. Stancil, F. Bai, and P. Mudalige, "Mobile vehicle-to-vehicle narrow-band channel measurement and characterization of the 5.9 GHz dedicated short range communication (DSRC) frequency band," *IEEE Journal on Selected Areas in Communications*, vol. 25, pp. 1501–1516, 2007.

[20] P. M. Shankar, "A compound scattering pdf for the ultrasonic echo envelope and its relationship to K and Nakagami distributions," *IEEE Transactions on Ultrasonics, Ferroelectrics, and Frequency Control*, vol. 50, no. 3, pp. 339–343, 2003.

[21] L. G. Stuber, *Principles of Mobile Communication*, Kluwer Academic Publishers, Boston, Mass, USA, 2001.

[22] J. D. Lewinskey, "Non stationary probabilistic target and cluttering scattering models," *IEEE Transactions on Aerospace and Electronic Systems*, vol. 31, pp. 490–498, 1983.

[23] H. Rasheed, N. Rajatheva, and F. Haroon, "Spectrum sensing with energy detection under shadow-fading condition," in *Proceedings of the 5th IEEE International Symposium on Wireless Pervasive Computing (ISWPC '10)*, pp. 104–109, May 2010.

[24] S. P. Herath and N. Rajatheva, "Analysis of equal gain combining in energy detection for cognitive radio over Nakagami channels," in *Proceedings of the IEEE Global Telecommunications Conference (GLOBECOM '08)*, pp. 1–5, November 2008.

Hindawi Publishing Corporation
International Journal of Vehicular Technology
Volume 2011, Article ID 627968, 8 pages
doi:10.1155/2011/627968

Research Article

Disseminating a Large Amount of Data to Vehicular Network in an Urban Area

Mina Taheri and Faramarz Hendesi

Department of Electrical and Computer Engineering, Isfahan University of Technology, Esfahan 84156-83111, Iran

Correspondence should be addressed to Mina Taheri, mina.taheri.h@gmail.com

Received 13 August 2010; Accepted 31 December 2010

Academic Editor: Shaharuddin Salleh

The problem of distributing a large amount of data from multiple sources in an urban area is investigated. We explore an opportunistic approach for information collection, in which a vehicle obtains information about resources from encountered vehicles. This protocol could be applied in both dense and sparse vehicular networks. Due to the highly dynamic nature of the underlying vehicular network topology, we depart from architectures requiring centralized coordination, reliable MAC scheduling, or global network state knowledge, and instead adopt a distributed paradigm with simple protocols. In other words, a reliable dissemination is introduced from multiple sources when each node in the network shares a limited amount of its resources for cooperating with others. By using rateless coding at the Road Side Unit (RSU) and using vehicles as data carriers, an efficient way to achieve reliable dissemination to all nodes (even disconnected clusters in the network) is described.

1. Introduction

Recently, many researches have been done to use vehicular ad hoc networks (VANET) for safety and commercial purposes [1–3].

The integration of communication technology in state-of-the-art vehicles has begun years ago: car phones and internet access based on cellular technologies as well as Bluetooth adapters for the integration of mobile devices are popular examples. However, the direct communication between vehicles using an ad hoc network, referred to as intervehicle communication (IVC) or vehicle ad hoc networks (VANETs), is a relatively new approach. Compared to a cellular system, IVC has three key advantages: lower latency due to direct communication, broader coverage, and having no service fee.

Recently, the promises of wireless communications to support vehicular safety applications have led to several research projects around world: the Vehicle Safety Communications Consortium, developing the DSRC Technology (USA), the Internet ITS Consortium (Japan), the PREVENT project (Europe), and the "Network on Wheels" project (Germany) are some samples.

To cater to the emerging wireless communication needs with regard to vehicles, in July 2003, ASTM and IEEE adopted the Dedicated Short Range Communication (DSRC) standard (ASTM E 2213-03) [4]. The aim of this standard is to provide wireless communications capabilities for transportation applications within a 1000 m range at typical highway speeds. It provides seven 10 MHz channels at the 5.9 GHz licensed band for ITS applications, with different channels designated for different applications, including one specifically reserved for vehicle-to-vehicle communications. The specific properties of VANETs allow the development of attractive new services.

Vehicular communications have many different facets. Applications range from safety support [5] (e.g., collision warnings, slow-down warnings), to entertainment for passengers, to local news delivery and advertisement [6] (e.g., electronic toll collection, map download, video download, Internet transactions, Parking Space availability). The key parameter for providing these applications is message dissemination. According to above classification, the messages which are exchanged between vehicles can be categorized into three classes.

(1) Event driven safety messages: which are the results of the detection of an unsafe situation, (e.g., a car crash, the proximity of vehicles at high speed, etc.).

(2) Periodic safety messages: also called beacon messages, are needed to make vehicles aware of their environment and also commercial purposes. Thus, they will be able to avoid emergency or unsafe situations even before they appear. Therefore, beacon messages essentially contain the state of the sending vehicle, that is, position, direction, speed, and so forth, and also aggregated data regarding the state of their neighbors.

(3) Comfort messages: all other types of data packets are included in comfort messages (e.g., data packets include internet access, video conferencing, etc.).

In this paper, a protocol which is able to disseminate a large amount of commercial data to urban areas from roadside units is proposed. This protocol can be used for both dense and sparse networks. Moreover, In previous works, neighbors are assumed to be recognized by beacons which are periodically sent by carriers. In this approach, there is no need to send these beacons.

The protocol should answer to these questions: when and how the act of forwarding should happen; in other words, how does the carrier decide to forward the message? Does it need to keep a copy message for itself?

The remainder of this paper is organized as follows. In Section 2, a brief review of previous works about distributing data in vehicular networks is propounded. In Section 3, we introduce the application of commercial advertisements in VANET. In Section 4, characteristics of vehicular ad hoc networks will be expressed. Section 5 reviews the DMRC method investigated in [7]. Our proposed scheme and simulation tools are described in Section 6. Finally, the paper is concluded in Section 7.

2. Related Work

Advertisements are one of the most important sources of revenue for companies. The advertisement application is a type of data dissemination from an information source to a large number of clients. In this work, we will take some steps to answer questions concerning data dissemination in the context of disseminating information packets from a large array of Road Side Units (RSU) to a bidirectional linear highway vehicular network. Vehicular ad hoc networks (VANETs) can be considered as a category of partitioned ad hoc networks [8]. Since density of vehicles is highly variable with space and time, the network changes from a sparsely disconnected to a densely connected in a short period of time. As a result of these topology variations, traditional routing and forwarding methods do not have a reasonable performance in VANET scenarios. In order to have message dissemination in partitioned ad hoc networks, the idea of Store-Carry-Forward (SCF) was proposed [1]. In SCF, a node carries information while there is not any other node in its vicinity. As soon as another node is detected, the forwarding phase starts. In recent years, several works have been done in using SCF which are more compatible with VANET environment. The most important of these works are SODAD [2], VADD [3], and MDDV [9]. A weak point in SCF is that sometimes the message transfer speed is limited by nodes' velocities. This increases end-to-end delay from a source to a destination. Fortunately, comfort applications of VANET are Delay Tolerant and applying SCF cannot be a major problem. Although SCF seems to be the proper answer for sparse scenarios, designing a routing protocol that can seamlessly handle the two extreme cases: well-connected networks and disconnected networks is still a challenge. In our proposed mechanism, an opportunistic approach of SCF is used. In opportunistic forwarding [10], message dissemination happens when a forwarding opportunity is detected. After forwarding a packet, a copy may be kept in the original node for further forwarding, if needed. For VANETs, opportunity can be defined as a situation where two vehicles meet each other. In [7], disseminating a large amount of data in highways is investigated. The characteristic of highways is that vehicles have approximately constant speed during their moving across the highways.

3. Commercial Advertisement in Vanet

Consider a downtown area with many stores and entertainment centers. Each store has different products and services. Some of products are on sale, some of the entertainment seats are available, and some foods are close to expiration date. Now consider many vehicles which carry many passengers in the downtown area. If store owners advertise their sale or activity information in nearby area, they have the opportunity to find some customers out of these passengers. With this motivation, any store is willing to use a special device to become a Roadside Advertising Unit (RSAU). In a conventional VANET, four primary data transfers can be assumed: (1) vehicle-to-vehicle (v2v) data transfer, (2) vehicle-to-roadside data transfer (v2r), (3) roadside-to-vehicle date transfer (r2v), and (4) roadside-to-roadside date transfer (r2r).

In this work, we continued the DMRC [7] approach for urban area. Therefore, at first the DMRC scheme will be introduced and we develop it for the roads containing vehicles with various speeds and different traffic loads. In our approach, the typical traffic is advertisement data generated by roadside advertising units (RSAU). Each RSAU is equipped with a short range wireless broadcast point which broadcasts the advertisements to the vehicles (r2v). Vehicles are collecting these data when they are moving toward the RSAU and distributing the data when they are moving in opposite direction. In this paper, a new approach that merges the *vehicle-to-vehicle* and *roadside-to-vehicle* communication typologies in order to support reliable data dissemination in an urban area without the need of complex routing protocols is presented. Also our focus in this paper is on sparse networks. In the following, we first reminisce the characteristics of disconnected ad hoc networks.

4. Characteristics of Disconnected Vehicular Ad Hoc Networks

Realizing that a Vehicular Ad hoc Network is prone to network fragmentation, it becomes essential to capture VANET's traffic characteristics for a better understanding of this phenomenon. Based on investigations in [11], it is observed that vehicles tend to move in clusters where two consecutive clusters of vehicles are normally separated by a relatively large distance. Also, it is observed that the probability distribution of the spacing between equipped vehicles in a network with can be approximated as an exponential distribution with parameter λ_s, given by

$$f_s(s) = \lambda_s e^{-\lambda_s s}. \tag{1}$$

4.1. Average Intracluster Spacing ($E[S_{\text{intra}}]$). In this subsection, we are particularly interested in characterizing the intracluster spacing between adjacent vehicles i and $i+1$ which travel in the same cluster. Since the two vehicles belong to the same cluster, the distance between them should be less than the transmission range R. Given that the intervehicle spacing S has an exponential distribution, it follows that the Probability Distribution Function (PDF) of S_{intra} can be expressed as

$$f_{S_{\text{intra}}}(S_{\text{intra}}) = P_r[S \mid S \le R] = \frac{\lambda_s e^{-\lambda_s S_{\text{intra}}}}{1 - e^{-\lambda_s R}}. \tag{2}$$

4.2. Average Inter-Cluster Spacing ($E[S_{\text{inter}}]$). Obviously, in line with the concept of clusters, the distance between the last vehicle of the leading cluster and the first vehicle of the following cluster should be larger than transmission range R. Given that the interarrival spacing S follows an exponential distribution, PDF of S_{intra} can be expressed as

$$f_{S_{\text{inter}}}(S_{\text{inter}}) = P_r[S \mid S > R] = \lambda_s e^{-\lambda_s (S_{\text{inter}} - R)}. \tag{3}$$

Based on expressed lemmas in [12], the intervehicle spacing is exponentially distributed with the parameter λ_s, then the expected inter-cluster spacing is given by

$$E[S_{\text{inter}}] = \frac{1}{\lambda_s} + R. \tag{4}$$

Also, if the intervehicle spacing is exponentially distributed with parameter λ_s, the expected number of vehicles in a cluster is

$$E[C_N] = e^{\lambda_s R}. \tag{5}$$

4.3. Average Cluster Length ($E[C_L]$). The size of a cluster can also be described by its length between the first vehicle and the last vehicle in a cluster.

If the intervehicle spacing is exponentially distributed with parameter λ_s, then the average cluster length is given as

$$E[C_L] = \left(\frac{1}{P_d} - 1\right)\left(\frac{1}{\lambda_s} - \frac{R e^{-\lambda_s R}}{1 - e^{-\lambda_s R}}\right). \tag{6}$$

The proof of (1), (2), (3), and (6) is amplified in [11].

Let V_0 be the average speed of every vehicle on the road and $M_n(L)$ denote the number of clusters a collector vehicle meets during a travel along a road of length L (note that collector and carrier vehicles move in opposite directions, with respect to an RSU). Further, let M_t denote the time duration that a collector vehicle spends in contact with a cluster of carrier vehicles. Given that the intervehicle spacing follows an exponential distribution, $M_n(L)$ and M_t could be achieved by

$$E[M_n(L)] \approx \frac{2L}{(e^{\lambda_s R} - 1)((1/\lambda_s) - (R e^{-\lambda_s R}/(1 - e^{-\lambda_s R}))) + R + (1/\lambda_s)}, \tag{7}$$

$$E[M_t] = \frac{\left(e^{\lambda_s R} - 1\right)\left((1/\lambda_s) - \left(R e^{-\lambda_s R}/\left(1 - e^{-\lambda_s R}\right)\right)\right) + 2R}{2v_0}. \tag{8}$$

The proof of (7) and (8) is mentioned in [16] in detail.

5. Overview of DMRC

DMRC suggests the application of a new class of packet-level coding schemes referred as rateless codes for the reliable and efficient data dissemination in VANETs [14, 15]. Several aspects of rateless codes make them suitable for such applications.

In this strategy, each RSU packetizes its message into smaller data packets of the same size. These packets are then encoded into a set of slightly bigger size using rateless coding. Then the RSU broadcasts the set of encoded packets. Vehicles divided in two groups: collectors and carriers. Collector vehicles are approaching to the specific RSU and try to collect its packets. After receiving the required number of packets, they could decode these packets in order to obtain the message of the RSU. By crossing over each RSU, collector vehicles apply rateless coding on the received message. From this point, they act as Carriers and keep packets in their buffer and broadcast them periodically. In order to the better understanding, Figure 1 shows the difference between collectors and carriers.

In this scheme, each carrier node can potentially carry packets from several RSUs simultaneously. Thus, it can act as a carrier and collector for different RSUs at the same time. Every time a collector node listens to a carrier node it receives packets which are innovative (by the rateless encoding property). The number of sufficient packet by which a collector could perform the rateless decoding is limited to $\mathcal{l}$. By this strategy, it is showed that because of the limited buffer in vehicles, they could not carry out infinite packets.

The parameter DD (*Decoding Distance*) is the basic performance metric we consider which can provide insight to the throughput. By collecting sufficient packet, each collector could decode the message of each RSU before entering its communication range (at decoding point). The distance

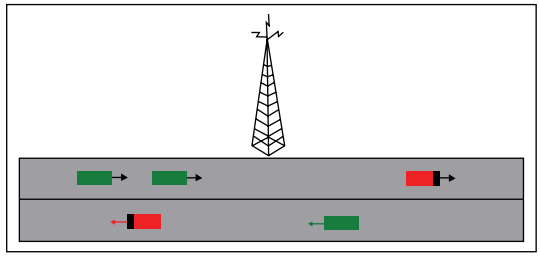

Figure 1: Collector and carrier vehicles.

between each RSU and related decoding point is considered as DD.

To describe DMRC scheme, the basic network model is considered. RSUs are placed uniformly in the road with distance d from each other. The space between two consecutive sources is named as segment. ϕ_i is representing the ith source in the road. If a vehicle is located in jth segment from source ϕ_i, it is in segment ϕ_{ij}.

It can be shown that for any source ϕ_i, DD is directly proportional to the number of packets from the corresponding source ($m_{i,j}$), that carriers posses per each segment ϕ_{ij}. In order to maximize DD, we need to find a solution for $m_{i,j}$'s subject to the buffer limit constraint. Since sources are all the same, we can omit the first index in $m_{i,j}$ and find a generic solution m_j for all sources. We assume that the number of packets carrier posses from ϕ_i cannot be increased. Also, buffer updating for a carrier node occurs when it crosses a new source and enters a new segment (e.g., from ϕ_{ij} to ϕ_{ij+1}). Just after crossing ϕ_i the carrier node has m_0 encoded packets from the source and reduces them gradually as $\cdots \le m_2 \le m_1 \le m_0$ and $m_j = 0$ for $j \ge \Delta$. By considering N_j as the total number of collected packets in segment j, DD can be formally stated as

$$\begin{aligned} \text{DD} &= \min_{m_j} d, \\ \text{S.t.} \quad & \sum_{i=0}^{d} E[N_{\Delta-i}] \ge \mathbb{1}. \end{aligned} \tag{9}$$

Since [7] suggests that only the tail behavior of the distribution of m_j's is important and because m_j is nonincreasing with j, one can see that the maximum value of DD is achieved when m_Δ (and hence all the previous segments) has its maximum value [16]. Further, the buffer limit constraint implies that $\sum_{i=0}^{\Delta} m_i \le B$. Therefore, a solution can be formulated as

$$m_0 = m_1 = m_2 = \cdots = m_\Delta = \frac{B}{\Delta + 1}. \tag{10}$$

This solution is only applied for a single road with a fixed velocity. To find the maximum distribution for m_j's in an urban area, we set the desired value for DD (DD*) and calculate the value of m_0 for all sources.

6. Proposed Approach for Data Dissemination

6.1. Proposed Scheme. As mentioned previously, we are interested in solving the problem of distributing large amount of data from multiple sources in an urban area. A network in which roads are separated by junctions is considered. Each road has its own characters. Characters of each road are defined as the average speed of vehicles and the rate of vehicle entering in the road. These two parameters determine the traffic load in each road. RSUs in such a network are uniformly distributed along the roads. Upon crossing an RSU, every node that has been successful in decoding the RSU's message acts as a carrier for that source. Then, every carrier node generates some encoded packets from the RSU's information packets and stores them. The number of stored packets is determined for maximum performance, given that the storage buffer is limited to B.

Upon crossing the ith source, every carrier node generates some encoded packets and puts $m_{i,j}$ packets in their buffer in jth segment from source ϕ_i. In the basic model, segments have the same length of d. The number of stored packets is determined for maximum performance, given that the storage buffer is limited to B. Each collector could gather packets from the vehicle clusters. Consider a collector vehicle meets a cluster of vehicles in ϕ_{ij}. The number of broadcast packets during the meet time M_t follows the Poisson distribution with the mean ρ, because carriers send encoded packets randomly and without coordination. Thus, based on [13], the maximum throughput occurs when ρ is equal to 1/2 of packet transfer time and is equal to $1/2e$. By using (6) and (7) and considering that a received packet is of collector's interest (i.e., the packet is from ϕ_i) with the probability of $m_{i,j}/B$, the maximum expected number of collected packets from a cluster (N_j^C) and total number of collected packets N_j^T, that could be obtained from the segment ϕ_{ij}, are given by ψ

$$\begin{aligned} E\left[N_j^c\right] &= \rho_{\max} \times E[M_t] \times \frac{m_{ij}}{B}, \\ E\left[N_j^T\right] &= E\left[N_j^c\right] \times M_n(d). \end{aligned} \tag{11}$$

To find the maximum distribution for m_j's in an urban area, the desired value for DD (DD*) is set and the value of m_0 for all sources would be calculated.

A network in which the velocity of vehicles is V_1 is considered. We are interested in achieving the message of RSUs at DD* from each source. The goal is to find the value of m_{i0} for the ith source. N is considered as the number of RSUs that a carrier node keeps their packets in its buffer. Based on DMRC scheme, $N = B/m_{i0}$. The value of m_{i0} for all sources could be obtained as follows:

$$\rho_{\max} \times E[M_t] \times \frac{m_{i0}}{B} \times M_n(N \times d - d^*) = \mathbb{1}. \tag{12}$$

Using (7) and (8) in (12), the value of m_{i0} for each source would be calculated. Now, in order to find a suitable distribution for an urban area, a large road consisting of segments with different traffic loads is considered. In each segment, the average speed of vehicles and the rate of vehicle

entering the segment are different. By considering the specific value for DD* and based on vehicle velocity and intervehicle spacing in each segment of the road, we can calculate the required number of stored packets in the collector buffer corresponding to each RSU. The value of DD* determines the segment (or segments) in which collector could collect the required number of packets. We assume that the nature of information is commercial advertisement and it is only useful in a nearby geographical area. By this assumption, we could consider the end for our simulated road. Based on the parameters of jth segment, $E[N_j^c]$ would be determined. The assumption is that messages from sources located in the last segment are collected by the collectors in that segment. Therefore, the value of m_{i0} for these sources will be calculated using (12). For these sources, $m_{0i} = \Delta$ is assumed.

Using the value of m_{i0} for sources located in the last segment (Δ), the value of m_{i0} corresponding to the other sources should be calculated one by one. Therefore, the value of m_0 for the last source in the last segment but one (m_{0j}) is calculated. The number of sources located in the range of DD* from the above source is defined as k. As a result, $((B - m_{0j} - K\Delta)/\Delta) \times d$ determines the distance in which the collector collects packets for the jth source. Consequently, the value of m_{0j} is calculated using the following equation:

$$\rho_{\max} \times E[M_t] \times \frac{m_{0j}}{B} \times M_n\left(\frac{\left(B - m_{0j} - K\Delta\right)}{\Delta} \times d\right) = \mathbb{1}. \tag{13}$$

It should be notified that the value of $E[M_t]$ is varied for each segment. In (13), $E[M_t]$ is calculated based on the parameters of the last segment. Based on the above algorithm, the value of m_0 for other sources could be calculated, too. The point is that, for each source, the parameters of segments in which the collector collects packets should be determined. Regarding these values, (13) would be altered for each source. For example, for some sources, the last segment may not be included in the distance in which the packets are collected. Accordingly, instead of using Δ and k for calculating their m_0, the m_0 and k values should be determined corresponding to the source of the other segments.

Based on these extracted values for all sources, the trend of dropping packets from the buffer of carriers could not follow the expressed algorithm in DMRC scheme.

The algorithm of the proposed scheme for urban area changes as follows: upon crossing new source in the road i, the value of m_{0i} packets from corresponding source would be stored in the buffer. In order to fix the number of B (buffer size) packets in the buffer, by reaching a new source, collector vehicle should drop a number of old packets which are equal to a number of added packets from the new RSU. Based on this scheme, we find an adaptive solution with the traffic load diversity in an urban area.

6.2. Siimulations. Evaluating the performance of a proposed scheme will be done by developing NS-2 [17] simulator in this section. Implementing the realistic traffic models is performed by SUMO [12]. Vehicles enter the road from one end with interarrival times drawn using instances of exponential distribution with parameter λ_s. In order to compare our scheme with DMRC, we also considered 50 points as the positions of RSUs along the road. We use the transmission range R as the unit of distance in our simulations. We focus on a collector vehicle that departs from one end of the road and travels along it until it reaches the other end. The number of vehicles in each road is determined by (6) and (7). Table 1 shows the parameters used in simulations.

Table 1: Simulation parameters.

Parameters	Value
Simulation time	1600 seconds
Communication range (R)	200 m
Distance between consecutive RSUs (d)	400 m
Simulation road length	24000 m
Broadcast interval	100/second
Buffer size	300
Required number of packet for decoding the message ($\mathbb{1}$)	800 packets

Table 2: The values of m_0.

Vehicle velocity	m_0
20 (m/s)	11
30 (m/s)	8
40 (m/s)	4

As the first step, we investigate the influence of vehicle velocity and interarrival time on determining the number of stored packets in the buffer of carrier corresponding to each RSU (m_0). Primarily, we fix the value of 0.2 vehicle/sec for interarrival time and 2800 m for DD*. By setting the vehicle velocity and using (12), we can find the values of m_0 corresponding to each source. These values related to each velocity are presented in Table 2.

We perform simulations with value determined in Table 2. At this point, we consider another performance metric to compare the result. P_{success} is the probability that a random message is generated at a (random) source ϕ_i is available at node v before it enters the communication range of ϕ_i. We measure P_{success} as a function of distance to the source. The presented graphs are the average of P_{success} over all active sources.

Figure 2 presents P_{success} for various vehicle velocities in the road.

Now, in order to see the influence of interarrival time of vehicles, we change it based on the presented values in Table 3 and calculate the value of m_0 for sources.

Figure 3 shows the changes in P_{success} for different values of λ_t.

In order to implement our scheme, we consider a 24000 meters road with 2 intersections. The first segment is regarded as the first 6000 meters distance of the road. The second segment is set from 6000 meters till 12000 meters of the road and after 12000 meters is the last segment. Each

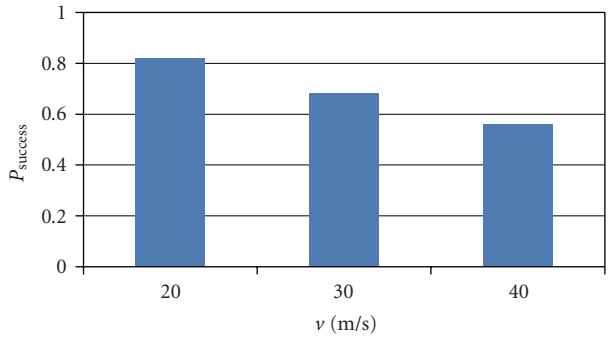

Figure 2: $P_{success}$ for different velocity.

Table 3: The values of m_0.

Interarrival time	m_0
0.1 (vehicle/sec)	9
0.3 (vehicle/sec)	11
0.4 (vehicle/sec)	10
0.5 (vehicle/sec)	9

Table 4: Road parameters.

Segment	Road parameters	Value
0–6000 m	Interarrival of vehicles (λ_1)	0.2 veh/sec
	Average velocity (V_1)	38 m/s
6000–12000 m	Interarrival of vehicles (λ_2)	0.6 veh/sec
	Average velocity (V_2)	28 m/s
12000–24000 m	Interarrival of vehicles (λ_3)	0.4 veh/sec
	Average velocity (V_3)	35 m/s

Table 5: The vaiues of m_0 for all sources.

$m_{050} - m_{030}$	18
$m_{029} - m_{027}$	20
$m_{026} - m_{023}$	19
$m_{022} - m_{020}$	21
$m_{019} - m_{016}$	16
$m_{015} - m_{013}$	17
$m_{012} - m_{010}$	18
$m_{09} - m_{08}$	16
$m_{07} - m_{01}$	10

segment is characterized with interarrival of vehicles and the average velocity of vehicles in that segment. Parameters related to each segment are presented in Table 4.

In order to meet the optimal distribution of m_{0i}, the value of DD* is set to 2800 m. the value of m_{0i} corresponding to the sources of the last segment of the road would be calculated by using $N = B/m_{0i}$ in the (12). Therefore, The value of m_{0i} for the last 20 sources is equal. Then, we used (13) to adjust the value for 29th source. Considering the value of DD*, we can find the segments in which the collector should collect the packets of specific RSU. The value of m_{0i} corresponding to each source is presented in Table 5.

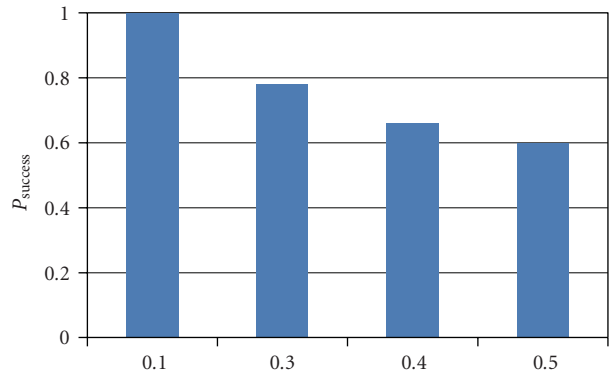

Figure 3: $P_{success}$ for different λ_t.

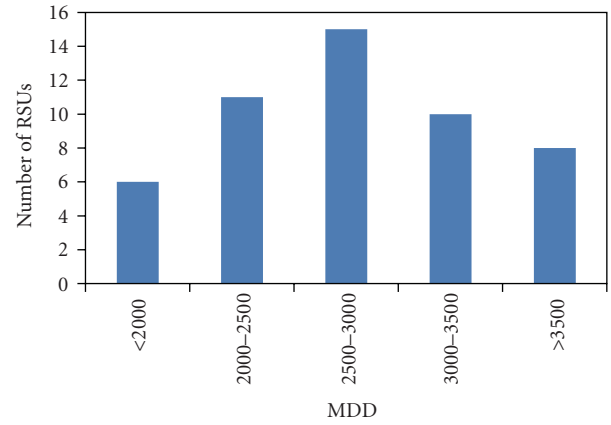

Figure 4: Dispersal of MDD around 2800 m for scheme B.

By considering the value of $N = 10$ in DMRC scheme, the value of MDD for vehicle velocity between 20–40 (m/s) is between 3500–2000 m. Therefore, we approximately could mention the average of 2800 m as decoding distance for these velocities. We compare our scheme (scheme A) with two other schemes. The first is DMRC scheme with $N = 10$. The second one is the scheme which uses the average velocity of V_i as the velocity and average λ_i in these three segments as the intervehicle spacing and set these values in (12) to obtain equal value for m_{0i} corresponding to all sources (scheme B). Based on the determined parameters in Table 2, we have $\overline{v} = 33.66$ $\overline{\lambda} = 0.4$. By using (13) and $N = B/m_{0i}$, we obtain 18 packets as the number of stored packets from every RSU in the road. We first perform the simulation for our proposed scheme.

Figure 4 shows the dispersal of MDD for all sources in the entire road.

Figure 5 shows the dispersal of MDD for all sources in the entire road for the scheme using the average of values in Table 2.

As presented in Figure 4, messages of 15 RSUs are decoded approximately in 2800 m but in Figure 5, this value is 9. Also the average decoding distance for all RSUs in scheme A is equal to 2814 m with standard deviation of 770, but in the scheme B, MDD is equal to 3011 with standard deviation of 1181. Although the larger MDD is the better

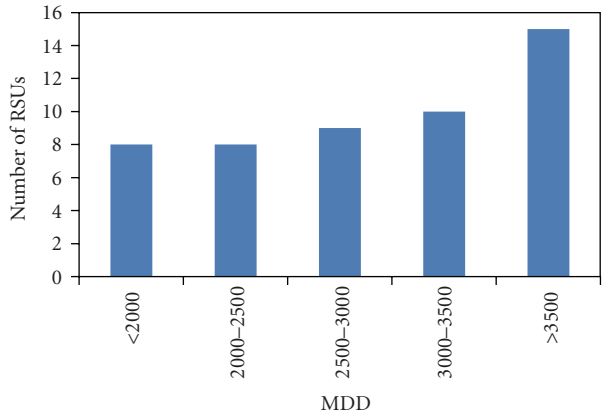

Figure 5: Dispersal of MDD around 2800 m for scheme B.

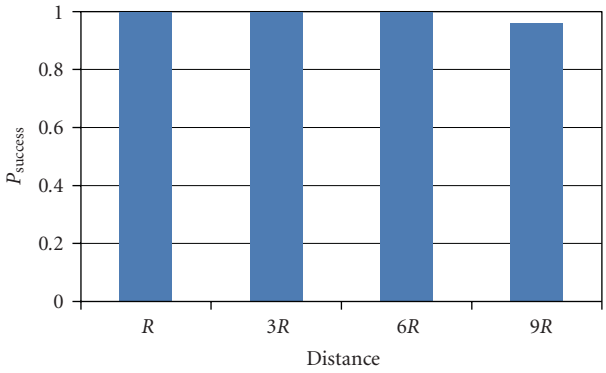

Figure 6: $P_{success}$ for variouse distances (in multiple of R) in scheme A.

result, it was expected to find the value of 2800 for MDD. Therefore, our scheme is working better.

In order to evaluate scheme A and DMRC, The value of $P_{success}$ is compared for both schemes and $P_{success}$ versus distance is plotted for scheme A and DMRC with $N = 10$ in Figures 6 and 7, respectively.

As presented in Figures 6 and 7, $P_{success}$ in the scheme A has the better results.

7. Conclusion

In this work, a new scheme based on rateless codes for collaborative content distribution from road side units to vehicular networks in an urban area is presented. Using the advantage of DMRC, an adaptive model which is compatible with the characteristics of the road was introduced. The proposed scheme can seamlessly handle both sparse and dense scenarios. Our simulations are performed in an urban area without any traffic lights, and by considering some sideways streets, the traffic loads in the road would be changed. The future researches are to introduce more realistic traffic models for urban areas with traffic lights where the exponential assumptions for interarrival time are not valid. Further, adapting the analysis for such scenarios and finding the optimal distribution for buffer allocation are our immediate goals.

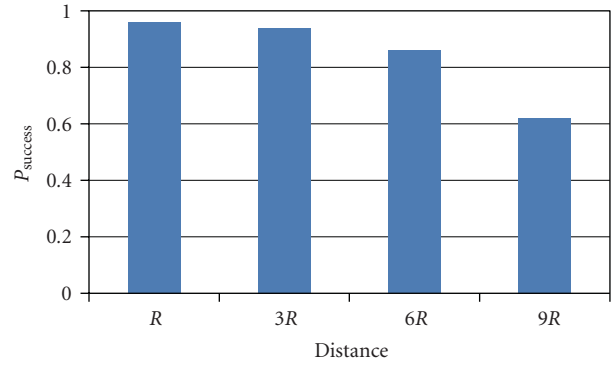

Figure 7: $P_{success}$ for variouse distances (in multiple of R) in DMRC ($N = 10$).

References

[1] J. A. Davis, A. H. Fagg, and B. N. Levine, "Wearable computers as packet transport mechanisms in highly-partitioned ad-hoc networks," in *Proceedings of the 5th International Symposium on Wearable Computers (ISWC 2001)*, pp. 141–148, October 2001.

[2] L. Wischhof, A. Ebner, and H. Rohling, "Information dissemination in self-organizing intervehicle networks," *IEEE Transactions on Intelligent Transportation Systems*, vol. 6, no. 1, pp. 90–101, 2005.

[3] J. Zhao and G. Cao, "VADD: vehicle-assisted data delivery in vehicular ad hoc networks," in *Proceedings of the 25th IEEE International Conference on Computer Communications (INFOCOM '06)*, April 2006.

[4] ASTM E2213-03, "Standard specification for telecommunication and information exchange between roadside and vehicle systems—5 GHz band dedicated short range communications (DSRC) medium access control (MAC) and physical layer (PHY) specificifications," ASTM Int'l, July, 2003.

[5] J. Yin, T. Elbatt, G. Yeung et al., "Performance evaluation of safety applications over DSRC vehicular ad hoc networks," in *Proceedings of the 1st ACM International Workshop on Vehicular Ad Hoc Networks (VANET '04)*, pp. 1–9, October 2004.

[6] S. B. Lee, G. Pan, J. S. Park, M. Gerla, and S. Lu, "Secure incentives for commercial ad dissemination in vehicular networks," in *Proceedings of the 8th ACM International Symposium on Mobile Ad Hoc Networking and Computing (MobiHoc '07)*, pp. 150–159, New York, NY, USA, September 2007.

[7] M. Sardari, F. Hendessi, and F. Fekri, "DMRC: dissemination of multimedia in vehicular networks using rateless codes," in *Proceedings of the IEEE International Conference on Computer Communications (INFOCOM '09)*, pp. 1–6, April 2009.

[8] V. Namboodiri, M. Agarwal, and L. Gao, "A study on the feasibility of mobile gateways for vehicular ad-hoc networks," in *Proceedings of the 1st ACM International Workshop on Vehicular Ad Hoc Networks (VANET '04)*, pp. 66–75, October 2004.

[9] H. Wu, R. Fujimoto, R. Guensler, and M. Hunter, "MDDV: a mobility-centric data dissemination algorithm for vehicular

networks," in *Proceedings of the 1st ACM International Workshop on Vehicular Ad Hoc Networks (VANET '04)*, pp. 47–56, October 2004.

[10] Z. D. Chen, H. T. Kung, and D. Vlah, "Ad hoc relay wireless networks over moving vehicles on highways," in *Proceedings of the ACM International Symposium on Mobile Ad Hoc Networking and Computing (MobiHoc '01)*, pp. 247–250, October 2001.

[11] N. Wisitpongphan, F. Bai, P. Mudalige, V. Sadekar, and O. Tonguz, "Routing in sparse vehicular ad hoc wireless networks," *IEEE Journal on Selected Areas in Communications*, vol. 25, no. 8, pp. 1538–1556, 2007.

[12] "Simulation of urban mobility," http://sumo.sourceforge.net/.

[13] N. Abramson, "The Aloha System: another alternative for computer communications," in *Proceedings of the Fall Joint Computer Conference (AFIPS '70)*, pp. 281–285, Montvale, NJ, USA, 1970.

[14] M. Luby, "LT codes," in *Proceedings of the 34rd Annual IEEE Symposium on Foundations of Computer Science*, pp. 271–280, 2002.

[15] Y. Wang, S. Jain, M. Martonosi, and K. Fall, "Erasure-coding based routing for apportunistic networks," in *Proceeding of the ACM SIGCOMM Workshop on Delay-Tolerant Networking (WDTN '05)*, pp. 229–236, New York, NY, USA, 2005.

[16] M. Sardari, F. Hendessi, and F. Fekri, "Infocast: a new paradigm for collaborative content distribution from roadside units to vehicular networks," in *Proceedings of the 6th Annual IEEE Communications Society Conference on Sensor, Mesh and Ad Hoc Communications and Networks (SECON '09)*, June 2009.

[17] "The Network Simulator NS-2," http://www.isi.edu/nsnam/ns/.

Hindawi Publishing Corporation
International Journal of Vehicular Technology
Volume 2011, Article ID 653542, 11 pages
doi:10.1155/2011/653542

Research Article

The Effect of IntelliDrive on the Efficiency of Highway Transportation Systems

Mohammad Nekoui,[1] Hossein Pishro-Nik,[1] and Daiheng Ni[2]

[1] *Department of Electrical and Computer Engineering, University of Massachusetts, Amherst MA 01003, USA*
[2] *Department of Civil and Environmental Engineering, University of Massachusetts, Amherst MA 01003, USA*

Correspondence should be addressed to Mohammad Nekoui, nekoui@ecs.umass.edu

Received 15 August 2010; Accepted 6 December 2010

Academic Editor: Zainab Zaidi

Recently, the IntelliDrive initiative has been proposed by the US Department of Transportation (USDOT) to enhance on-road safety and efficiency. In this study, we provide a mathematical framework which predicts the effect of such technologies on the efficiency of multilane highway systems prior to their real-life deployment. Our study shall encompass mixed traffic conditions in which a variety of assisted, automated and unequipped vehicles coexist. We show that intervehicular communications improves the flow of vehicles by reducing the perception-reaction (P-R) times of drivers and, in some cases, allowing for more efficient lane-changing operations. As we shall see, unlike the latter, the former effect of IntelliDrive on driver P-R time is always there, regardless of the specific traffic conditions.

1. Introduction

With the ever increasing production of vehicles and their inevitable role in everyday life, transportation systems are drawing the attention of industry and academia more than any other time. Despite the undeniable beneficial aspects of transportation systems, there are numerous factors by which they impair our everyday life. Without any doubt, many of us have experienced being trapped in heavy traffic, wasting our time and energy resources. Traffic congestion wastes 40 percent of travel time on average, unnecessarily consumes about 2.3 billion gallons of fuel per year, and adversely impact the environment [1]. More importantly, traffic accidents are held responsible for a good portion of death causes. Annually, more than 40,000 people are killed and much more injured in highway traffic accidents in the United States alone [2]. IntelliDrive [3]—formerly known as Vehicle Infrastructure Integration (VII)—a major initiative at the United States Department of Transportation (USDOT), proposes to use Dedicated Short Range Communications (DSRCs) to establish vehicle-vehicle and vehicle-roadside communications to deliver timely information to save lives, reduce congestion, and improve quality of life. The network of communicating vehicles forms a Vehicular Ad-Hoc Network (VANET) on roads. VANET is an emerging area, and due to the potentially dramatic improvements it renders in terms of safety, highway efficiency, and driver convenience, has attracted attention from both academia and industry in the US, EU, and Japan. The most important feature of VANETs is their ability to extend the horizon of drivers and on-board devices and thus to improve road traffic safety, efficiency, and comfort. VANET will enable a wide range of novel applications such as accident avoidance messaging, congestion sensing, ramp metering, and general information services [4–6]. The allocation of 75 MHz in the 5.9 GHz band for DSRC may also enable future delivery of rich media content to vehicles at short to medium ranges via both intervehicle and roadside-vehicle communications.

In the near future, a traffic stream may consist of mixed vehicles operated under different driving modes: a vehicle may be operated without IntelliDrive assistance "unequipped", by a human driver with IntelliDrive assistance "assisted" or by an IntelliDrive-enabled automated system which is itself in charge of driving "automated". The

IntelliDrive Initiative envisions that each future vehicle will be equipped with an On-Board Equipment (OBE) which includes a DSRC transceiver, a Global Positioning System (GPS) receiver, a processing unit, and possibly appropriate sensing accessories. Also equipped with similar devices, RoadSide Equipment (RSE) will be deployed at selected roadside locations. Therefore, vehicles will be able to communicate with each other and with the roadside by means of DSRC. As a result, assisted drivers will be able to respond to their driving environment earlier, that is, shorter Perception-Reaction (P-R) times than drivers without IntelliDrive assistance. Here, relevant information of a vehicle such as its location, speed, and acceleration are transmitted via its DSRC radio to its surrounding vehicles. The payload size of such a status packet is in the order of a (few) hundred bytes for ordinary safety applications [5]. This packet is sent with a frequency equivalent to the GPS update rate (1–10 Hz). However, the packet throughput relies on the total number of nodes and the physical characteristics of the wireless channel. With this setting, a vehicle that has a sufficient amount of information regarding its surroundings is typically informed about a specific traffic condition much sooner. Hence, it takes it less time to perceive its leader vehicle's sudden braking when that happens. Also, as the attention of assisted drivers has already been drawn to the condition before the driver is needed to react, the variance in his or her perception time (and hence the variance of P-R time) is much lower than drivers of unequipped vehicles. The above observation is supported by [7] which notes that the most important variable that affects driver P-R time is driver expectation which can affect the P-R time by a factor of 2. There, the author concludes that an unexpected event can increase both the perception and reaction time of the driver. In addition, evidence in the psychology literature indicates that P-R time strongly depends on the type and intensity of stimulus [8]. Since IntelliDrive-enabled systems constitute a new type of stimulus with high intensity that help increase driver expectation, such systems are likely to shorten drivers' P-R times. In addition to assisted vehicles, partially or fully automated driving systems will be devised to further reduce the P-R time and hence the variation in responses. Here, as a control unit within the vehicle is in charge of the driving task, the variance in P-R time is essentially zero. This is because there is no human factor involved in this case. The mean of P-R time, however, is at its worst equal to the interval between the reception of two subsequent status packets from neighboring vehicles. Hence, the mean is dependent on the communications capacity within the network of vehicles and relies on different factors such as the number of nodes but is in general much less than the mean of the P-R time of assisted vehicles in the vast majority of traffic scenarios. As we shall see, lower P-R time would enable the assisted and automated vehicles to decrease their distance with their leaders without decreasing their speeds. This would lead to more compact clusters which consequently means higher flow of vehicles on the highway. IntelliDrive could also be utilized to help a vehicle perform more efficient lane-changing maneuvers. As we shall see, a lane change, which might at first seem unlikely for a driver, could be made possible with the help of IntelliDrive. However, unlike its effect on driver P-R time, the effect of IntelliDrive on lane-changing is highly dependent on the specific traffic conditions.

In this paper, we propose a mathematical framework which can be used to foresee the effect of the gradual deployment of IntelliDrive-enabled vehicles on the efficiency of transportation systems. As a first step, we develop an appropriate mobility model which shall serve our analysis throughout the paper. For the base case of a single-lane highway, mathematical modeling of vehicle clusters is provided. To make the analysis more realistic, the modeling is generalized to multilane highways next. Appropriate lane-changing mechanisms are also discussed in the framework. With the mobility model in hand, we then proceed to derive mathematical expressions to address the effect of IntelliDrive on vehicular flow under mixed traffic conditions.

2. Related Work

The current literature on the safety and efficiency of vehicular networks contains studies conducted within both wireless communications and transportation societies. It has long been established that car clustering (platooning) in automated highways increases the highway capacity [9]. This is accomplished by automated vehicles following each other very closely at highway speeds and without increasing the risk of a collision [10, 11]. Real-world experiments in this prospect have validated the increase in capacity [12]. However, stable clusters are viable only under a certain degree of intervehicle communications [13]. The safety and efficiency of manual and automated highways have been compared in [14]. There, automated highways with different levels of cooperation between individual vehicles and also platoon-based systems have been considered. Currently, due to practical and deployment cost considerations, the trend has moved from fully automated to driver-assisted vehicles. USDOT's IntelliDrive initiative is a pioneer in this prospect. The effect of driver-assisting technologies such as cruise control on vehicular traffic flow has been addressed in [15, 16]. In Adaptive Cruise Control (ACC) systems, the main objective is to safely increase driver comfort rather than improving highway capacity. The global impact of ACC on the safety of highways is studied in [17]. In that study, the effect of ACC on traffic flow capacity is considered a secondary issue. In [18], Tampere et al. prove that the time gap and driver relaxation times have the greatest effect on traffic stability. Based on this, they propose that any driver assistance system that intends to improve traffic stability should aim at influencing these parameters. Despite all this, there is a lack of a study that specifically addresses the effect of IntelliDrive on traffic flow efficiency.

Within the wireless communications society, specific characteristics of VANETs such as its highly dynamic topology, delay-sensitive applications, and constrained deployment region have led to the outgrowth of an abundant number of VANET-specific physical, MAC, and routing layer schemes [4, 19, 20]. The authors have also addressed MAC and network layer issues for urban deployments of VANETs

[21]. The goal in most of these schemes is to establish reliable point-to-point communications between vehicles to achieve safety goals such as intersection collision warning. To the best of the authors' knowledge, there has little been done, if any, to study the effect of communications on traffic flow capacity and stability.

3. System Modelling and Preliminaries

3.1. Mobility Model: Vehicle Clustering. In this section, we study how vehicle clusters form and evolve in a multi-lane highway. Within a cluster, vehicles follow their leaders according to a car-following model elaborated in the next subsection. Furthermore, we shall see that the intervehicle spacings within a cluster ought to be enough to ensure a safe maneuver for the follower in case of the leaders abrupt braking. This spacing is a function of driver P-R time which is itself dependent on the level of IntelliDrive market penetration rate. Here, we first show, through a probabilistic analysis, how clusters are formed in a single lane highway. The analysis is then extended to account for multilane highways. As we shall later see, the beneficial effect of IntelliDrive on the capacity of multi-lane highways is not only because of its potential in reducing intervehicle spacings, but also due to the advantages it renders in terms of allowing for more efficient lane-changing operations.

3.1.1. Vehicle Clustering on a Single Lane. Consider a group of N vehicles on a single-lane highway. Typically, each driver has a desired speed which it chooses from a (truncated) normal distribution [22, 23] within the range $[V_{\min} V_{\max}]$. Clearly, if a vehicle's desired speed is higher than at least one of the cars preceding it, it will join the cluster ahead; otherwise, it will trail back and form a new cluster. Hence, if the vehicles are numbered from 1 to N from the beginning to the end of the road, the ith vehicle would form a new cluster with probability $1/i$ and join the cluster ahead with probability $(i-1)/i$. In what follows, we shall denote the initial randomly chosen speed of vehicle i by v_i and its ultimate speed within cluster j by V_j. Note that all vehicles within a cluster move with the same speed. Within a cluster, a vehicle would leave a safety distance with its leader, proactively avoiding collisions.

Figure 1 shows the clustering probabilities for up to 5 vehicles. The numbers on the branches separated by commas show the length of the clusters, and the number in the circle to which the branch ends is the probability of having that specific clustering configuration. For example, the branch labeled as (2, 2, and 1) represents the configuration of having 2, 2 and 1 vehicles in the 1st, 2nd, and 3rd clusters, respectively. As can be seen from the tree, this happens with the probability of 1/40. The following example illustrates how these probabilities are derived. Assume that we have a (2,2) configuration. The 5th vehicle either joins the cluster ahead with probability 4/5, hence arriving at a (2,3) arrangement with probability $3/24 \times 4/5 = 1/10$, or trails back with probability 1/5, resulting in the (2,2,1) configuration with probability $3/24 \times 1/5 = 1/40$ (see dotted section of Figure 1). By extending this tree for an arbitrary number of vehicles, one can derive all the clustering probabilities. In this sense, each cluster can be seen as a kinematic wave [24] moving with the speed of its leader.

In what follows, we shall compute the average number of the clusters. Let us define X_i as

$$X_i = \begin{cases} 1 & \text{if the } i\text{th vehicle is a clusterhead,} \\ 0 & \text{otherwise.} \end{cases} \tag{1}$$

With this definition, it can be seen that if C denotes the mean number of clusters

$$\begin{aligned} C &= E\left[\sum_{i=1}^{N} X_i\right] = \sum_{i=1}^{N} E[X_i] \\ &= \sum_{i=1}^{N} p_i = \sum_{i=1}^{N} \frac{1}{i} = 1 + \ln(N)(1 + o(1)), \end{aligned} \tag{2}$$

where $p_i = P(X_i = 1)$ and $o(1) \to 0$ as $N \to \infty$, where N is the number of vehicles on the road.

3.1.2. Multilane Highway System. Here, we study the extension of the above scenario to multi-lane highways. Multi-lane highways typically allow for a more dynamic environment where vehicles with a high desired speed that are "stuck" in a low-speed cluster of vehicles are allowed to change lanes and join a higher-speed cluster on the other lane. As mentioned before, a vehicle on a specific lane either moves with its own desired speed (as a cluster head) or with the speed of its predecessor, whichever is lower. However, in this case, if the current speed of a vehicle within a cluster is lower than its desired speed, it might have the chance to overtake this cluster of vehicles and join a higher-speed one on the lane to its left. To this end, assume vehicle i with the desired speed v_i resides in cluster m (and hence has speed V_m) when cluster n on the lane to its left with speed V_n comes cruising by. Here, vehicle i decides to make a lane change and join cluster n if $v_i \geq V_n > V_m$. Once such a vehicle has made a lane-change decision, it seeks an opportunity to merge into the higher-speed lane by searching for a sizeable gap. Such a gap-acceptance model works as follows. Consider cluster $n+1$ to immediately follow cluster n on the left lane. We assume that in equilibrium conditions, the speed of a leading cluster is larger than the trailing one (because otherwise they would ultimately merge into a single cluster) in each lane. This fact is well anticipated by our clustering model proposed in Section 3.1.1. At the same time, we also assume that the left lane clusters have higher speeds than all the ones on the right lane. Hence, under these conditions, we have $V_m < V_{n+1} < V_n$. A valid gap-acceptance model should determine the circumstances under which vehicle i is able to make a lane change and join cluster n such that it collides with neither the vehicles of cluster n nor those of cluster $n+1$. Note that after making a lane change and with an initial speed of V_m, vehicle i would accelerate to reach its final speed, V_n. Since $V_m < V_{n+1}$, it is during this period of time that the trailing cluster $n+1$ could collide with vehicle i. Assuming the worst

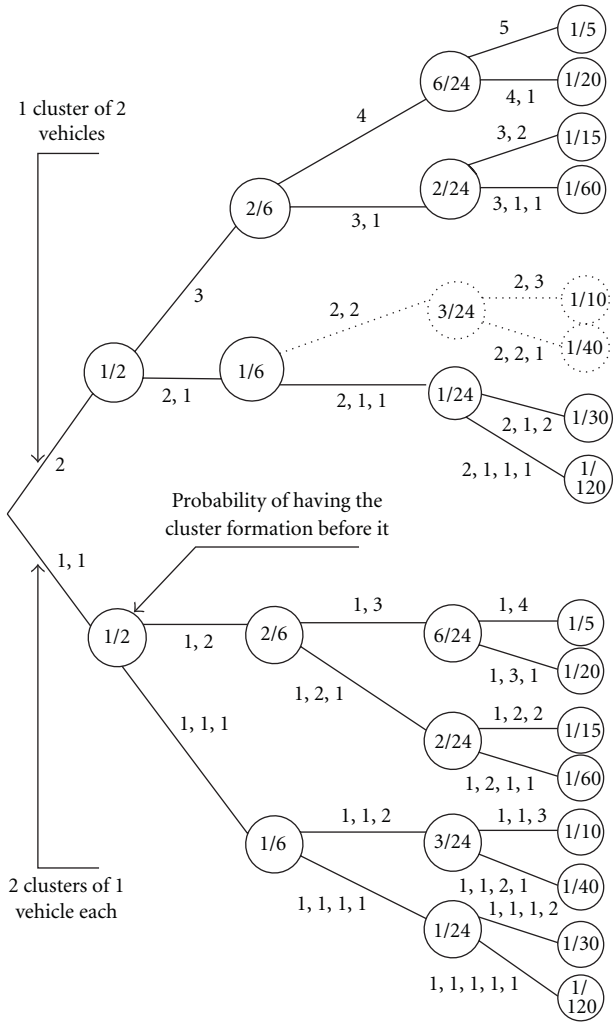

Figure 1: Decision tree demonstrating clustering probabilities.

case where the vehicles in cluster $n+1$ do not decelerate (and hence continue cruising with their previous speeds) upon observing a leading lane changing vehicle, it can be verified that the following condition ensures a safe lane-changing maneuver for vehicle i:

$$s_{n,n+1} > \frac{(V_{n+1} - V_m)^2 - (V_n - V_{n+1})^2}{2a_i}, \tag{3}$$

where $s_{n,n+1}$ is the spacing between clusters n and $n+1$ at the intended time of the lane change and a_i denotes vehicle i comfortable acceleration rate. The derivation of (3) is elaborated in Appendix A.

A driver of a unequipped vehicle has to rely on his own visual eyesight and estimate of the speed and spacing in order to make a lane-change decision. Moreover, in the case where it cannot see a possible trailing vehicle in the other lane in its rear or side mirrors (e.g., when there is curvature in highway trajectory or fluctuations in its elevation), it should account for the worst case when a high-speed vehicle rapidly closes up onto it once the lane change has been made. An IntelliDrive-enabled vehicle, on the other hand, typically knows the exact location and speed of a trailing vehicle on the destination lane in case the latter is also assisted. Hence, the driver does not have to assume for the worst case scenario and further would not suffer from estimation deficiencies to miss a potential lane-change opportunity. Here, we want to study the effect of IntelliDrive on the average number of vehicles that leave cluster m for the higher speed cluster n. In general, this value is dependent on the relative speeds and the distance between the leading and trailing clusters on the destined lane, that is, even if all the vehicles in cluster m were IntelliDrive-enabled, none of them could perform a lane change when $s_{n,n+1}$ does not satisfy (3). Hence, the effect of IntelliDrive on the lane-change maneuvers entirely depends on the real-time traffic conditions. Moreover, cluster m could belong to one of the following categories with respect to cluster n:

(1) neither the equipped nor the unequipped vehicles within it are able to join cluster n,

(2) only the equipped vehicles, based on the real time information that they obtain, are able to join cluster n,

(3) all vehicles, whether equipped or not, can complete the lane-change maneuver and join cluster n.

The road topology along with the gap-acceptance equation (3) determines to which of the above classes does cluster m belong. For an equipped vehicle, equation (3) suffices to indicate whether a lane change is possible. For unequipped vehicles, road topology plays a role as well, that is, if the road topology is such that any trailing cluster is visible to the lane-changing vehicle, it would deploy (3) to estimate whether it could perform the lane change or not. If not, it should assume that the trailing cluster has speed $V_{n+1} = V_{\max}$ and resides at the furthest visible point from cluster n. For future analysis, let $Y_{mn} = j$ if cluster m is category $j \in \{1, 2, 3\}$ with respect to cluster n.

To see how many vehicles leave cluster m for cluster n, we define $X_{mn}(i)$ as

$$X_{mn}(i) = \begin{cases} 1 & \text{vehicle } i \text{ in cluster } m \text{ leaves for cluster } n, \\ 0 & \text{otherwise.} \end{cases} \tag{4}$$

Note that $X_{mn}(i) = 1$ if $v_i \geq V_n$ and otherwise vehicle i stays in cluster m. With the above definition, $X_{mn} = \sum_{i=1}^{N_m} X_{mn}(i)$ denotes the total number of departures from cluster m for cluster n where N_m is the number of vehicles within cluster m.

3.2. Mobility Model: Car Following. The spacing between vehicles within a cluster should allow for a safe and comfortable declaration of the follower in case of the leader's sudden braking. As we shall see, this spacing is highly dependent on the driver's P-R time which is assumed to be a function of IntelliDrive market penetration rate. Car following models have long been studied by transportation engineers. Models such as Pipes [25], General Motors (GM) [26, 27], and Gipps [28] account for different car following behaviors.

Our analysis adopts a variation of the Gipps' model which is rather conservative. In this model, vehicles allow for a safety distance between themselves and their leading vehicle. The safety distance should be such that in the event when the leader (vehicle $i-1$) applies a sudden brake and slows down with maximum deceleration B_{i-1}, the follower (vehicle i) should be able to safely stop behind it after going through a P-R process and a deceleration process at a comfortable rate b_i ($|b_i| < |B_i|$). If we denote by x_i and v_i the position and speed of the ith vehicle, and by x_{i-1}^* and x_i^* the stopping position of the leader and follower, respectively, we shall have

$$x_{i-1}^* = x_{i-1}(t) - \frac{v_{i-1}^2(t)}{2B_{i-1}}, \tag{5}$$

$$x_i^* = x_i(t) + v_i\tau_i - \frac{v_i^2(t)}{2b_i}, \tag{6}$$

where τ_i is driver i's P-R time. Equation (6) is true because the follower would go through a P-R time before applying the brakes. To ensure safety, we must have $x_{i-1}^* - L_{i-1} \geq x_i^*$ where L_{i-1} is the length of the $(i-1)$th vehicle. Within a cluster, where the two vehicles have the same speed $v = v_i = v_{i-1}$, we have for the intervehicle spacing, S_i

$$S_i = x_{i-1} - x_i \geq \tau_i v + Gv^2 + L, \tag{7}$$

where $G = 1/2B - 1/2b$ and the subscripts for B, b, and L have been dropped for simplicity. As evident from (7), the stochastic properties of the intervehicle spacing is solely dependent on the stochastic properties of driver P-R time. As discussed before, a driver of an unequipped vehicle on average goes through a longer P-R time in case of an unexpected situation in comparison to an assisted vehicle where the driver has been alerted (and hence his or her P-R time reduced) via timely warning messages. In [7], the author emphasizes that driver attention is a graded function. Hence, the above two cases represent a graded continuum rather than a dichotomy. Based on this and prior discussions, we propose that the mean and the variance of drivers' P-R time is a decreasing linear function of IntelliDrive market penetration rate, that is, the more the percentage of assisted vehicles within a cluster, the lower is the mean and variance of its drivers' P-R times. Note that the linear relation is considered for the convenience to expedite the mathematical analysis and that other decreasing functions would yield similar results of this paper. Moreover, if α denotes the market penetration rate of assisted vehicles, we assume that the driver P-R time, $\tau(\alpha)$ has a truncated normal distribution with (The normal distribution for driver P-R time is justified in [7], noting that in reality it is mostly skewed towards larger values.)

$$\mu_{\tau(\alpha)} = \alpha\left(\mu_{\tau(\alpha=1)} - \mu_{\tau(\alpha=0)}\right) + \mu_{\tau(\alpha=0)}, \tag{8}$$

$$\sigma_{\tau(\alpha)}^2 = \alpha\left(\sigma_{\tau(\alpha=1)}^2 - \sigma_{\tau(\alpha=0)}^2\right) + \sigma_{\tau(\alpha=0)}^2, \tag{9}$$

where μ and σ are the mean and variance of driver P-R time with $\mu_{\tau(\alpha=1)} \leq \mu_{\tau(\alpha=0)}$ and $\sigma_{\tau(\alpha=1)}^2 \leq \sigma_{\tau(\alpha=0)}^2$. This way, the spacing between an assisted vehicle and its leader also follows a truncated normal distribution with the same variance as in (9) and mean an appropriately scaled and shifted version of (8). The P-R time of unequipped vehicles is the same as when $\alpha = 0$ for assisted vehicles and the P-R time for automated vehicles is deterministic (and equal to $\mu_{\tau(\beta)}$) as discussed before. Figure 2 shows how the probability distributions of driver's P-R time varies with IntelliDrive market penetration. As we shall see in the next section, the mean values for driver P-R times suffice to compute the lower bounds on the expected value of vehicular flow.

4. Effect of IntelliDrive on Highway Efficiency

In this section, we quantify the enhancements IntelliDrive renders in terms of traffic flow efficiency. Moreover, we mathematically explore the extent at which IntelliDrive can increase the flow of vehicles on roads without increasing the risk of collisions. As mentioned before, this is a result of the drivers' reduced P-R time which lets them maintain their speed while reducing their spacing with the leading vehicle. We shall also study how IntelliDrive can enhance lane-change maneuvers in multilane highways. In what follows, the term flow shall denote the number of vehicles that pass an arbitrary point of the highway in unit time. In equilibrium conditions, the following relation exists between traffic flow characteristics, flow (q), density (k), and speed (v) [29]:

$$q = kv. \tag{10}$$

As vehicles within a cluster move with the same speed, equation (10) can be used as follows to derive the flow within cluster i as:

$$q_i = \frac{N_i V_i}{\sum_{j=1}^{N_i} S_{ij}}, \tag{11}$$

where V_i, N_i, and S_{ij} are the speed, number of vehicles, and intervehicle spacings in cluster i. Note that here, flow is a probabilistic value as a result of the intervehicle spacings being probabilistic due to (7). The following theorem addresses its expected value.

Theorem 1. *For a single cluster of N_i vehicles all moving with the same speed V_i, the following holds for the flow of the cluster when each vehicle within it is assisted with probability α and automated with probability β:*

$$E[q_i] \geq \frac{V_i}{c + a\beta + b\alpha^2(1-\beta)}, \tag{12}$$

where $a = V_i(\mu_{\tau(\beta)} - \mu_{\tau(\alpha=0)})$, $b = V_i(\mu_{\tau(\alpha=1)} - \mu_{\tau(\alpha=0)})$, and $c = GV_i^2 + \mu_{\tau(\alpha=0)}V_i + L$.

Proof. See Appendix B. □

Notice that the lower bound is independent of the number of vehicles within the cluster, N_i. We shall later see that the lower bound is also quite tight. Figure 3 depicts the enhancement in flow due to IntelliDrive. The values used to evaluate (12) are gathered in Table 1. First, notice that, as

Table 1: Parameter values.

$\mu_{\tau(\alpha=0)}$	2 s	B	$-6\frac{m}{s^2}$	$\overline{\alpha}_1^r$	27.3%	$\overline{\beta}_1^r$	9.1%	N_1^r	30	$E[\overline{N}_1^r]$	28.3
$\mu_{\tau(\alpha=1)}$	1 s	b	$-3\frac{m}{s^2}$	$\overline{\alpha}_1^l$	36.6%	$\overline{\beta}_1^l$	12.2%	N_1^l	10	$E[\overline{N}_1^l]$	11.7
$\mu_{\tau(\beta)}$	0.1 s	α	30%	$\overline{\alpha}_2^l$	30%	$\overline{\beta}_2^l$	10%	N_2^l	15	$E[\overline{N}_2^l]$	15
L	5 m	β	10%	$\overline{\alpha}_3^l$	29%	$\overline{\beta}_3^l$	9.7%	N_3^l	20	$E[\overline{N}_3^l]$	31.8

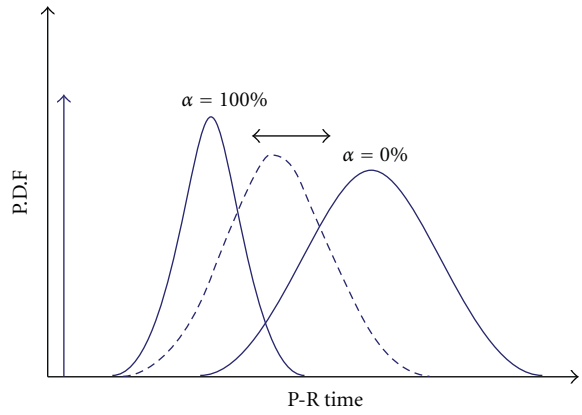

Figure 2: Perception-Reaction times for different classes of vehicles. The normal distributions correspond to the P-R times of assisted vehicles for various market penetration rates. P-R time of unequipped vehicles is the same as when $\alpha = 0$. The delta function represents the P-R time of an automated vehicle.

seen in Figure 3(a), the flow-speed relation in a cluster of vehicles moving with the same speed follows closely the trend of a typical macroscopic flow-speed relation in a highway [29]. The only difference is that the speed at which the peak flow occurs is somewhat lower which is due to the rather conservative car following model we have used in our analysis. Hence, our results also provide a good insight on the effect of IntelliDrive on the macroscopic behaviors of general highway systems. Figure 3(a) also shows the effect of IntelliDrive on the speed-flow curve for various penetration rates of assisted and automated vehicles. Further, by looking at Figure 3(c), one can see that for a fixed β, flow increases by increasing α. The same is true when β is increased for a fixed α (see Figure 3(d)). However, the augmentation in throughput obtained by increasing β is greater than the one achieved by increasing α. This is seemingly right since automated vehicles have lower P-R times than assisted vehicles. Moreover, when all vehicles are automated, flow can increase by up to 65%, whereas when they are all just assisted, the increase in flow is by about 25%. As a final remark, in Figure 3(d), we have compared the exact value of flow against the lower bound in (12). As can be seen, with an accuracy of about 99.9%, the lower bound serves as a perfect approximation for the exact value.

For a two-lane highway, consider an instance where N^r and N^l vehicles initially reside on the right and left lanes, respectively, $(N^r + N^l = N)$. We number the clusters from 1 through C^r and 1 through C^l on the right and left lanes, from the beginning to the end of each lane. Hence, $N^r = \sum_{i=1}^{C_r} N_i^r$ and $N^l = \sum_{i=1}^{C_l} N_i^l$, where N_i^r (N_i^l) is the number of vehicles in cluster i on the right (left) lane. Here, we address the average traffic flow after a group of high-speed clusters on the left lane overtake a group of lower speed ones on the right lane, during which lane-changing maneuvers can happen when needed and allowed based on the discussion in Section 3.1.2. As we shall see, the effect of IntelliDrive on traffic flow is due to its role in the lane-changing maneuvers as well as the lowering of driver P-R times. Note that if $C = C^r + C^l$, then according to (2) we would have $C = O(\ln N)$. Hence, the effect of the bounded inter-cluster spacings on the total flow would be negligible as N grows arbitrarily large, and a weighted average of the per-cluster flows would serve as a fine approximation of the total flow. The total flow after the overtakings take place can be stated as (the superscripts have been dropped for simplicity)

$$q = \frac{\sum_{i=1}^{C} N_i q_i}{N}. \tag{13}$$

Hence,

$$\begin{aligned} E[q] &= \frac{\sum_{i=1}^{C} E[N_i q_i]}{N} \\ &= \frac{1}{N}\sum_{i=1}^{C}\sum_{n_i=1}^{N} n_i E[q_i \mid N_i = n_i] P(N_i = n_i) \\ &\overset{(1)}{\geq} \frac{1}{N}\sum_{i=1}^{C} E[q_i] \sum_{n_i=1}^{N} n_i P(N_i = n_i) \\ &= \frac{1}{N}\sum_{i=1}^{C} E[q_i] E[N_i], \end{aligned} \tag{14}$$

where (1) is due to Theorem 1 which implies that the lower bound on the expected flow of a cluster is independent of the number of vehicles within it.

In what follows, we aim at comparing the value of $E[q_i]$ after the overtakings take place with and without the utilization of IntelliDrive. When IntelliDrive is available, we assume that the penetration rate of assisted and automated vehicles in each cluster is initially α and β before the overtakings take place. In order to compute (14), we need to have the ultimate values for $E[q_i]$'s and $E[N_i]$'s after the overtakings take place. For $E[q_i]$, note that, according to (12), the only influential parameters on flow that change during the course of the overtakings are the percentage of equipped vehicles in each cluster. Here, we study their evolution over time.

For an arbitrary cluster m on the right and n on the left lane, let $n'_m = \max_{Y_{mi}\in\{2,3\}} i \in \{1,\ldots,n-1\}$ and $n''_m =$

$\max_{Y_{mi}=3} i \in \{1,\ldots,n-1\}$ where again, $Y_{mn} = j$ if cluster m is category $j \in \{1,2,3\}$ with respect to cluster n. This way, $V^l_{n'_m}$ is the speed of the nearest leading cluster n'_m which the equipped vehicles in cluster m have had the chance to join (hence m is category 2 or 3 with respect to n'_m). If no such cluster exists, then $V^l_{n'} = V_{\max}$. On the other hand, $V^l_{n''_m}$ is the speed of the nearest leading cluster n''_m which all vehicles in cluster m, whether equipped or not, have had the chance to join. Again, if no such cluster exists, we have $V^l_{n''_m} = V_{\max}$. Note that essentially $V^l_{n'_m} \le V^l_{n''_m}$. With this setting, if $\alpha^r_{m_{n+1}}$ denotes the probability that a vehicle within cluster m on the right lane is assisted, right before being overtaken by cluster $n+1$ on the left lane, we have, starting with $\alpha^r_{m_1} = \alpha$

$$\alpha^r_{m_{n+1}} = \begin{cases} \alpha^r_{m_n}, & Y_{mn} = 1, \\ \dfrac{\alpha^r_{m_n} P\left(v < V^l_n \mid V^l_m \le v < V^l_{n'_m}\right)}{1-\left(\alpha^r_{m_n}+\beta^r_{m_n}\right)\left(1-P\left(v < V^l_n \mid V^r_m \le v < V^l_{n'_m}\right)\right)}, & Y_{mn}=2, \\ \dfrac{\alpha^r_{m_n} P\left(V^r_m \le v < V^l_{n''_m}\right)}{\left(\alpha^r_{m_n}+\beta^r_{m_n}\right)P\left(V^l_{n'_m} \le v < V^l_{n''_m}\right)+P\left(V^r_m \le v < V^l_{n'_m}\right)}, & Y_{mn} = 3. \end{cases} \tag{15}$$

The derivation of (15) is provided in Appendices A and B. Through (15), the ultimate probability that a vehicle in cluster m on the right lane is assisted, $\overline{\alpha}^r_m$, can be derived by computing $\alpha^r_{m_{C_{l+1}}}$. The same as above holds for automated vehicles by only replacing β for α in (15). With the ultimate values of α and β in hand, the new values of $E[q_i]$'s can be derived from (12).

Let us now consider the evolution of the $E[N_i]$'s. For that, we compute the expected number of vehicles that leave a cluster for another. Note that for an arbitrary cluster m on the right lane, one of the following is true with respect to an arbitrary cluster n on the left lane. (Here, we assume that a vehicle surely performs the lane-change maneuver once it knows it is safe to do so. In the general case for assisted drivers, human uncertainty can be accounted for by incorporating an appropriate probability function based on which the assisted driver makes a lane-change decision.)

(1) When neither the equipped nor the unequipped vehicles leave cluster m for cluster n we have $X_{mn} = 0$.

(2) When just the equipped vehicles in m can join cluster n

$$E[X_{mn}(i)] \overset{(1)}{=} P(X_{mn}(i) = 1) = \left(\beta^r_{m_n} + \alpha^r_{m_n}\right)P\left(v_i \ge V^l_n \mid V^l_{n'_m} \ge v_i \ge V^r_m\right), \tag{16}$$

where (1) is due to (4). Let us elaborate on the condition of the probability. Note that for vehicle i in cluster m we already know $v_i \ge V_m$. Also, if it is equipped and still resides in cluster m at the the time it encounters cluster n on the left lane, we know that $v_i \le V^l_{n'_m}$.

(3) When equipped and unequipped vehicles can merge from m into n, we have:

$$\begin{aligned} &E[X_{mn}(i)] \\ &= \left(\beta^r_{m_n} + \alpha^r_{m_n}\right)P\left(v_i \ge V^l_n \mid V^l_{n'_m} \ge v_i \ge V^r_m\right) \\ &\quad + \left(1-\beta^r_{m_n} - \alpha^r_{m_n}\right)P\left(v_i \ge V^l_n \mid V^l_{n''_m} \ge v_i \ge V^r_m\right). \end{aligned} \tag{17}$$

Here, at the time vehicle i in cluster m encounters cluster n on the left lane it has $v_i \le V^l_{n'_m}$ if it is equipped and has $v_i \le V^l_{n''_m}$ if it is unequipped.

For all the above scenarios, we have

$$\begin{aligned} E[X_{mn}] &= E\left[\sum_{i=1}^{N^r_{m_n}} X_{mn}(i)\right] \\ &= E\left[N^r_{m_n}\right]E[X_{mn}(i)], \end{aligned} \tag{18}$$

where $N^r_{m_n}$ is the number of vehicles within cluster m on the right lane, just before the nth cluster on the left lane reaches it. Here,

$$E\left[N^r_{m_n}\right] = E[N^r_m] - \sum_{i=1}^{n-1} E[X_{mi}], \tag{19}$$

where $N^r_m = N^r_{m_1}$. Note that (18) follows from Wald's equation. (Wald's equation states that $E[\sum_{i=1}^{T} X_i] = E[T]E[X]$ where the X_i's are i.i.d, and independent from T and $E[T], E[x] < \infty$.) The use of the latter equation needs independent and identically distributed (i.i.d) $X_{mn}(i)$'s which is true as the desired speed of a vehicle and the chances of it being equipped are independent of any other. The other conditions that need to be true in order to let us use the Wald's equation is for $N^r_{m_n}$ and $X_{mn}(i)$ to have finite mean values and also to be independent which all clearly hold in our case.

Finally, (16) or (17) are used along with (18) and (19) to give us the expected number of vehicles that leave a cluster for another and consequently the ultimate number of vehicles within each cluster. The final percentage of assisted vehicles for cluster n on the left lane is obtained as

$$\overline{\alpha}^l_n = \frac{\alpha N^l_n + \sum_{m:Y_{mn}=3} \alpha^r_{m_n} X_{mn} + \sum_{m:Y_{mn}=2} \left(\alpha^r_{m_n}/\left(\alpha^r_{m_n}+\beta^r_{m_n}\right)\right) X_{mn}}{N^l_n + \sum_m X_{mn}}. \tag{20}$$

The numerator shows the expected number of assisted vehicles. Here, αN^l_n is the initial number of assisted vehicles cluster n contains before the overtakings take place. The second and third terms represent the contribution of category 2 and 3 clusters during the course of the overtakings. Also, the denominator is the total number of vehicles in cluster n upon the completion of the overtakings. A similar equation is true for $\overline{\beta}^l_n$ by just replacing β for α.

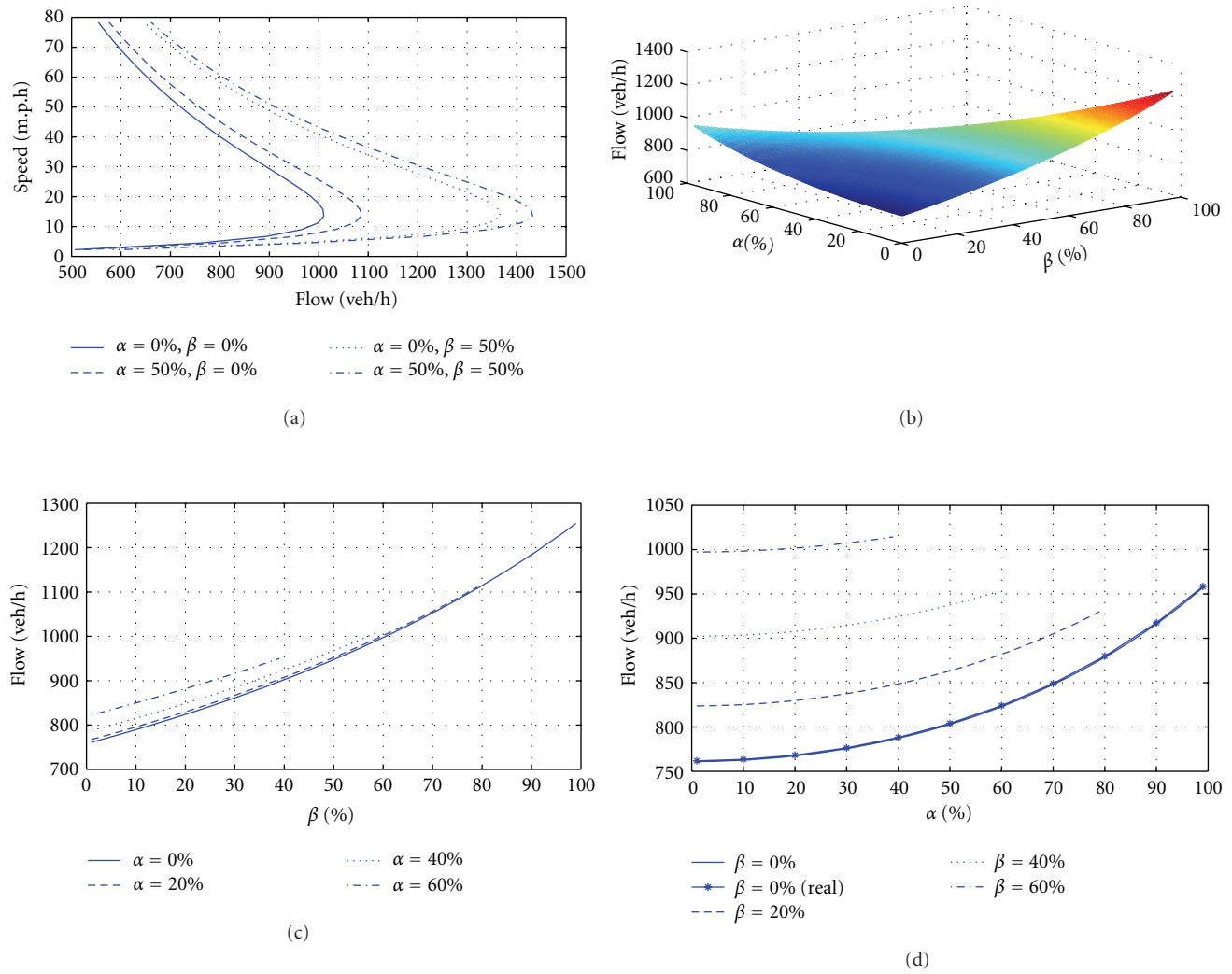

FIGURE 3: (a) The effect of IntelliDrive on the flow-speed curve. (b) Traffic flow variation with the penetration of automated and assisted vehicles into the market. (c) Flow enhancement for a fixed penetration of assisted vehicles. (d) Flow enhancement for a fixed penetration of automated vehicles. $V = 44.8$ m.p.h. in (b), (c), and (d).

To clarify the concept, here we consider an example scenario of a two-lane highway depicted in Figure 4, where three clusters on the left lane overtake a lower speed one on the right lane. As can be seen from Figure 4(b), the cluster on the right lane is category 2 with respect to the first cluster on the left lane, that is, $Y_{11} = 2$. This is because if vehicle i on the right lane that has made a lane-change decision (since $v_i \geq V_1^l$) is equipped, then it is able to figure out that the current gap between the first and second clusters on the left lane, that is, s_{12}, is more than the minimum required (100 m) anticipated by the gap-acceptance equation (3). Hence, it is able to safely make a lane change. However, if it is not equipped, it goes on to assume that the second cluster resides at the furthest point which has line of sight to the first and has virtually the same speed as V_1^l. According to (3), this requires a gap more than 150 m. But since the furthest line-of-sight point is only 80 meters away, lane-changing cannot be performed by an unequipped vehicle. By (15) and letting $m = 1$ and $n = 1$, $\alpha_{1_2}^r$ can be computed by noting that $\alpha_{1_1}^r = \alpha$ and $V_{1_{1'}}^l = V_{\max}$. Further, we have according to (18) and (16) that $E[X_{11}] = N_1^r(\alpha + \beta)P(v_i \geq V_1^l \mid V_{\max} \geq v_i \geq V_1^r)$ and hence according to (19), $E[N_{1_2}^r] = N_1^r - E[X_{11}]$.

Following on, note that the cluster on the right lane is category 1 with respect to the second cluster on the left lane hence, $\alpha_{1_3}^r = \alpha_{1_2}^r$ and $X_{12} = 0$. Thus the market penetration of the equipped vehicles and the total number of vehicles within the second cluster remain unchanged when it overtakes the cluster on the right lane.

Finally, as we have $Y_{13} = 3$, the ultimate penetration rate of the equipped vehicles in the cluster on the right lane can be obtained by letting $m = 1$ and $n = 3$ in (15) which results in $\overline{\alpha}_1^r = \alpha_{1_4}^r = \alpha_{1_3}^r$ since $V_{3_1''}^l = V_{3_1'}^l = V_1^l$. The ultimate number of vehicles in this cluster is then $N_1^r - E[X_{11}] - E[X_{13}]$, where $E[X_{13}] = N_{1_3}^r P(v_i \geq V_3^l \mid V_1^l \geq v_i \geq V_1^r)$ due to (17) and further (18). Also, for the ultimate penetration rate of equipped vehicles on the left lane, we have due to (20) that $\overline{\alpha}_1^l = (\alpha N_1^l + (\alpha/(\alpha + \beta))E[X_{11}])/(N_1^l + E[X_{11}])$, $\overline{\alpha}_2^l = \alpha$ and $\overline{\alpha}_2^l = \alpha N_3^l + \alpha_{1_3}^r E[X_{13}]/N_3^l + E[X_{13}]$.

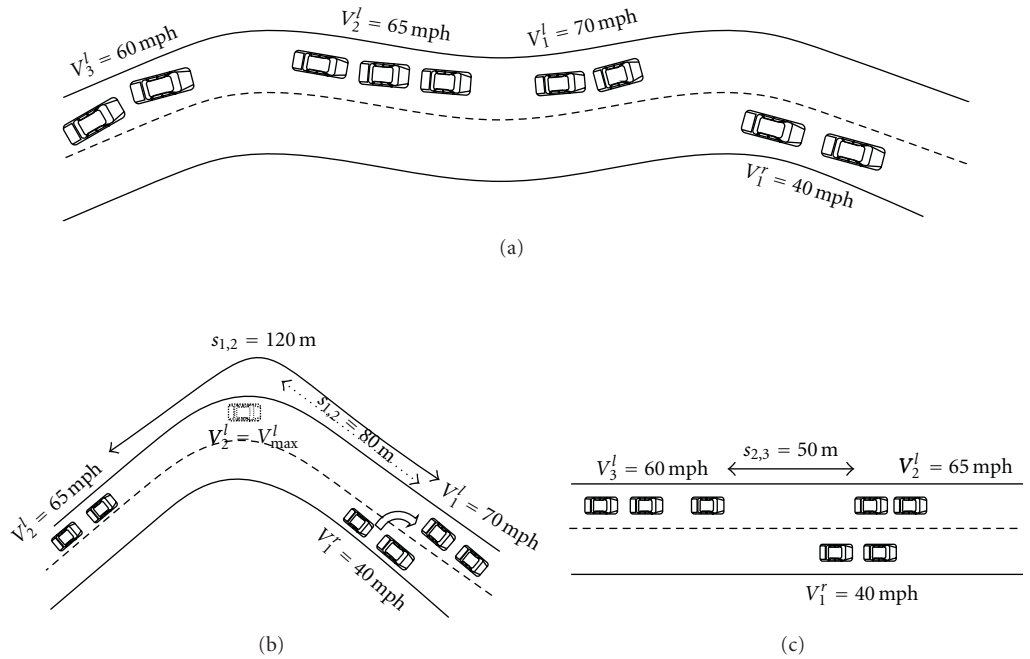

Figure 4: (a) Two-lane highway. The distribution of the desired speed of the vehicles is truncated normal with $\mu = 60$, $\sigma = 8$ within the [40–80] m.p.h range. (b) Cluster on the right lane is category 2 with respect to the first cluster on the left. (c) Cluster on the right lane is category 1 with respect to the second cluster on the left.

Table 1 exhibits the ultimate values of IntelliDrive market penetration rates and the number of vehicles within each cluster. These values are used in conjunction with (12) to evaluate the average flow over all clusters in (14). When there is no IntelliDrive, we have $X_{11} = X_{12} = 0$ and $E[X_{13}] = N_1^r P(v_i \geq V_3^l \mid V_{\max} \geq v_i \geq V_1^r)$. For our example scenario (with the IntelliDrive market penetration rates of $\alpha = 30\%$ and $\beta = 10\%$), the total flow after the overtakings take place is higher than when there is no IntelliDrive deployment (702 as opposed to 672 veh/h).

Notice that the effect of IntelliDrive on the flow of a multi-lane highway is due to two main factors. One, as before, is by lowering the P-R time of drivers which leads to a higher per-cluster flow. The other means by which IntelliDrive can affect flow is by letting the equipped vehicles make lane changes that are not typically allowed for the unequipped vehicles. Notice that this does not necessarily increase the total flow even if the lane-changing vehicle joins a higher-speed cluster than its own. This is evident from the flow-speed curve in Figure 3 which implies that higher speed does not necessarily correspond to higher flow. Hence, to assess the effect of IntelliDrive on the total flow, the following should be determined. If there is no category 2 cluster on the right lane, the effect of IntelliDrive on flow is always constructive. For any category 2 cluster, on the other hand, we should check whether the flow corresponding to its speed is higher or lower than the flow of the cluster to which the lane-changing vehicles merges into. If lower, IntelliDrive again enhances flow. However, if the flow of the destined cluster is lower, the total flow increases only when the constructive effect of the reduced P-R time of drivers is able to compensate for the loss in flow due to the lane-changing maneuver, the case held in our example scenario above. Finally, even if the total flow was seen to reduce when using IntelliDrive, the total travel time of drivers is enhanced by letting them join higher-speed clusters.

5. Conclusion

In this paper, we investigated the effect of IntelliDrive on the efficiency of multi-lane highway systems. We studied how the gradual introduction of IntelliDrive-enabled vehicles can enhance the efficiency of traffic flow. Towards this goal, we developed a mobility model where vehicles moved in clusters inside which they constantly maintained a safety car-following distance with their leaders. Having justified the fact that IntelliDrive would reduce the perception-reaction time of drivers, traffic flow was seen to increase due to the lower lead spacing of the equipped vehicles. A tight lower bound for the flow of a cluster of a mixed variety of vehicles was also derived. This bound was shown to be independent of the number of vehicles inside the cluster. A weighted average of the per-cluster flows was then used as a metric to represent the flow over all clusters. Lane-changing mechanisms where incorporated into the model for multi-lane highways. In some cases, IntelliDrive could be utilized to help make lane changes which are otherwise not possible without such help. We argued that such assisted lane changes, although might not always increase the overall flow, would in any case decrease the travel time of the drivers.

Appendices

A. Derivation of the Gap-Acceptance Equation (3)

Let vehicle j be the leader vehicle in cluster $n+1$ which is therefore moving with the constant speed V_{n+1}. Then, its location evolves with time as $x_j(t) = x_j + V_{n+1}t$, where x_j is vehicle j's location at the time vehicle i wants to make a lane-change. Moreover, as vehicle i, after making the lane-change, accelerates with the rate a_i to reach the speed V_n, its location evolves as $x_i(t) = 0.5a_it^2 + V_mt + x_i$ for $t \in [0 \ \ (V_n - V_m)/a_i]$, where x_i is its initial location on the left lane (which is equal to the location of the last vehicle in cluster n). Note that here we have assumed that it takes vehicle i zero time to carry out the lane-changing. To have no collision between cluster $n+1$ and vehicle i, we should have $x_i(t) - x_j(t) \geq Lt \in [0 \ \ (V_n - V_m)/a_i]$. The latter is a degree 2 function which is positive before its first root. Hence, by letting the first root being greater than $(V_n - V_m)/a_i$ and some manipulations, (3) is obtained.

B. Proof of Theorem 1

Given that vehicles are assisted or automated with probability α and β, respectively, (corresponding to $100\alpha\%$ and $100\beta\%$ market penetration rates for the assisted and automated vehicles), the number of assisted and automated vehicles within cluster i (N_i^α and N_i^β) would follow a binomial distribution, hence,

$$
\begin{aligned}
E[q_i] &= V_i \sum_{r=0}^{N_i} \sum_{s=0}^{N_i - r} E\left[\frac{N_i}{\sum_{j=1}^{N_i} S_{ij}} \mid N_i^\beta = r, N_i^\alpha = s \right] \\
&\quad \times p\left(N_i^\alpha = s \mid N_i^\beta = r\right) p\left(N_i^\beta = r\right) \\
&= V_i N_i \sum_{r=0}^{N_i} \sum_{s=0}^{N_i - r} E\left[\frac{\binom{N_i - r}{s} \alpha^s (1-\alpha)^{N_i - r - s}}{\sum_{j=1}^{N_i} S_{ij}} \mid N_i^\beta = r, N_i^\alpha = s \right] \\
&\quad \times p\left(N_i^\beta = r\right) \\
&\overset{(1)}{\geq} V_i N_i \sum_{r=0}^{N_i} \sum_{s=0}^{N_i - r} \frac{\binom{N_i - r}{s} \alpha^s (1-\alpha)^{N_i - r - s}}{E\left[\sum_{j=1}^{N_i} S_{ij} \mid N_i^\beta = r, N_i^\alpha = s\right]} p\left(N_i^\beta = r\right) \\
&\overset{(2)}{=} V_i N_i \sum_{r=0}^{N_i} \sum_{s=0}^{N_i - r} \frac{\binom{N_i - r}{s} \alpha^s (1-\alpha)^{N_i - r - s}}{ar + b\alpha s + cN_i} p\left(N_i^\beta = r\right) \\
&\overset{(3)}{\geq} V_i N_i \sum_{r=0}^{N_i} \frac{p\left(N_i^\beta = r\right)}{ar + b\alpha(\alpha(N_i - r)) + cN_i} \\
&= V_i N_i \sum_{r=0}^{N_i} \frac{\binom{N_i}{r} \beta^r (1-\beta)^{N_i - r}}{(a - b\alpha^2)r + (c + b\alpha^2)n} \\
&\overset{(4)}{\geq} \frac{V_i N_i}{(a - b\alpha^2)\beta N_i + (c + b\alpha^2)N_i} \\
&= \frac{V_i}{c + a\beta + b\alpha^2(1-\beta)},
\end{aligned}
\tag{B.1}
$$

where (2) is because according to the car-following spacing (7), we have

$$
\begin{aligned}
&E\left[\sum_{j=1}^{N_i} S_{ij} \mid N_i^\beta = r, \, N_i^\alpha = s \right] \\
&\quad = r\left(GV_i^2 + \mu_{\tau(\beta)} V_i + L\right) + s\left(GV_i^2 + \mu_{\tau(\alpha)} V_i + L\right) \\
&\qquad + (N_i - r - s)\left(GV_i^2 + \mu_{\tau(\alpha=0)} V_i + L\right).
\end{aligned}
\tag{B.2}
$$

which results in (2) when $a = V_i(\mu_{\tau(\beta)} - \mu_{\tau(\alpha=0)})$, $b = V_i(\mu_{\tau(\alpha=1)} - \mu_{\tau(\alpha=0)})$, $c = GV_i^2 + \mu_{\tau(\alpha=0)} V_i + L$. Note that all (1), (3) and (4) are due to Jensen's inequality. (Jensen's inequality states that $E[f(x)] \geq f(E[x])$ when f is a convex function.) The use of Jensen's inequality in (3) is as follows:

$$
\begin{aligned}
&\sum_{s=0}^{N_i - r} \frac{\binom{N_i - r}{s} \alpha^s (1-\alpha)^{N_i - r - s}}{ar + b\alpha s + cN_i} \\
&\quad = E_s\left[\frac{1}{ar + b\alpha s + cN_i} \right] \\
&\quad \geq \frac{1}{ar + b\alpha E[s] + cN_i} \\
&\quad = \frac{1}{ar + b\alpha(\alpha(N_i - r)) + cN_i}.
\end{aligned}
\tag{B.3}
$$

The expectation in the first equality is with respect to random variable s which is drawn from a set of size $N_i - r$ according to a binomial distribution with parameter α. This way the expected value of s would be $\alpha(N_i - r)$ which is used to achieve the last equality. (4) is a result of applying the same ideas as above for the automated vehicles.

C. Derivation of Equation (15)

When $Y_{mn} = 1$, according to definition, no vehicle from cluster m can join cluster n hence $\alpha^r_{m_{n+1}} = \alpha^r_{m_n}$. For the case where $Y_{mn=2}$, multiply both the numerator and the denominator by $N^r_{m_n}$, the number of vehicles in cluster m at the time of encountering cluster n. Notice that here only the equipped vehicles could make the lane change. Thus, the numerator shows the expected number of assisted vehicles and the denominator the expected total number of vehicles that remain in cluster m after being overtaken by cluster n. For the case where $Y_{mn} = 3$, we define the following events. Let $A = \{V^r_m \leq v < V^l_n\}$, $B = \{V^r_m \leq v < V^l_{n'_m}\}$, and

$C = \{V_m^r \le v < V_{n''_m}^l\}$. As $A \subseteq B \subseteq C$, we have $P(A \mid B) = P(A)/P(B)$ and $P(A \mid C) = P(A)/P(C)$. Hence:

$$\begin{aligned}
&\alpha_{m_{n+1}}^r \\
&= \frac{\alpha_{m_n}^r P(A \mid B) N_{m_n}^r}{\left(\alpha_{m_n}^r + \beta_{m_n}^r\right) P(A \mid B) N_{m_n}^r + \left(1 - \alpha_{m_n}^r - \beta_{m_n}^r\right) P(A \mid C) N_{m_n}^r} \\
&= \frac{\alpha_{m_n}^r P(C)}{\left(\alpha_{m_n}^r + \beta_{m_n}^r\right) P(C - B) + P(B)}
\end{aligned} \tag{C.1}$$

which yields the result.

References

[1] T. T. Institute, "2005 urban mobility report," 2005, http://.mobility.tamu.edu/ums/report/.

[2] BTS, "National transportation statistics 2006," 2006, http://www.bts.gov/publications/national_transportation_statistics/2006/index.html.

[3] ITS, "Intellidrive," http://www.its.dot.gov/intellidrive/.

[4] D. Jiang, V. Taliwal, A. Meier, W. Holfelder, and R. Herrtwich, "Design of 5.9 GHz DSRC-based vehicular safety communication," *IEEE Wireless Communications*, vol. 13, no. 5, pp. 36–43, 2006.

[5] Q. Xu, T. Mak, J. Ko, and R. Sengupta, "Vehicle-to-vehicle safety messaging in DSRC," in *Proceedings of the 1st ACM International Workshop on Vehicular Ad Hoc Networks (VANET '04)*, pp. 19–28, Philadelphia, Pa, USA, October 2004.

[6] T. K. Mak, K. P. Laberteaux, and R. Sengupta, "A multi-channel VANET providing concurrent safety and commercial services," in *Proceedings of the 2nd ACM International Workshop on Vehicular Ad Hoc Networks (VANET '05)*, pp. 1–9, September 2005.

[7] M. Green, "How long does it take to stop? Methodological analysis of driver perception-brake times," *Transportation Human Factors*, vol. 2, no. 3, pp. 195–216, 2000.

[8] R. D. Luce, *Response Times: Their Role in Inferring Elementary Mental Organization*, Oxford University Press, New York, NY, USA, 1986.

[9] A. Vahidi and A. Eskandarian, "Research advances in intelligent collision avoidance and adaptive cruise control," *IEEE Transactions on Intelligent Transportation Systems*, vol. 4, no. 3, pp. 132–153, 2003.

[10] F. Michaud, P. Lepage, P. Frenette, D. Létourneau, and N. Gaubert, "Coordinated maneuvering of automated vehicles in platoons," *IEEE Transactions on Intelligent Transportation Systems*, vol. 7, no. 4, pp. 437–446, 2006.

[11] S. Darbha and K. R. Rajagopal, "Intelligent cruise control systems and traffic flow stability," *Transportation Research Part C*, vol. 7, no. 6, pp. 329–352, 1999.

[12] H.-S. Tan, R. Rajamani, and W.-B. Zhang, "Demonstration of an automated highway platoon system," in *Proceedings of the American Control Conference*, pp. 1823–1827, June 1998.

[13] D. Swaroop, J. Hedrick, C. C. Chien, and P. Ioannou, "Comparison of spacing and headway control laws for automatically controlled vehicles," *Vehicle System Dynamics*, vol. 23, no. 1, pp. 597–625, 1994.

[14] J. Carbaugh, D. N. Godbole, and R. Sengupta, "Safety and capacity analysis of automated and manual highway systems," *Transportation Research Part C*, vol. 6, no. 1-2, pp. 69–99, 1998.

[15] J. Zhou and H. Peng, "Range policy of adaptive cruise control vehicles for improved flow stability and string stability," *IEEE Transactions on Intelligent Transportation Systems*, vol. 6, no. 2, pp. 229–237, 2005.

[16] B. S. Y. Rao and P. Varaiya, "Flow benefits of autonomous intelligent cruise control in mixed manual and automated traffic," *Transportation Research Board*, vol. 1408, pp. 36–43, 1993.

[17] A. Touran, M. A. Brackstone, and M. McDonald, "A collision model for safety evaluation of autonomous intelligent cruise control," *Accident Analysis and Prevention*, vol. 31, no. 5, pp. 567–578, 1999.

[18] C. Tampere, S. Hoogendoorn, and B. van Arem, "A behavioural approach to instability, stop and go waves, wide jams and capacity drop," in *Proceedings of the 16th International Symposium on Transportation and Traffic Theory*.

[19] Q. Xu, T. Mak, J. Ko, and R. Sengupta, "Medium access control protocol design for vehicle—vehicle safety messages," *IEEE Transactions on Vehicular Technology*, vol. 56, no. 2, pp. 499–518, 2007.

[20] F. Li and Y. Wang, "Routing in vehicular ad hoc networks: a survey," *IEEE Vehicular Technology Magazine*, vol. 2, no. 2, pp. 12–22, 2007.

[21] M. Nekoui and H. Pishro-Nik, "Reliable inter-vehicle communications for vehicular ad hoc networks," in *Proceedings of the 4th Annual International Wireless Internet Conference (WICON '08)*, 2008.

[22] D. Helbing, A. Hennecke, V. Shvetsov, and M. Treiber, "Micro- and macro-simulation of freeway traffic," *Mathematical and Computer Modelling*, vol. 35, no. 5-6, pp. 517–547, 2002.

[23] S. P. Hoogendoorn and P. H. L. Bovy, "Continuum modeling of multiclass traffic flow," *Transportation Research Part B*, vol. 34, no. 2, pp. 123–146, 2000.

[24] W. L. Jin, *Kinematic wave models of network vehicular traffic*, Ph.D. thesis, University of California, Davis, Calif, USA, 2003, http://arxiv.org/abs/math.DS/0309060.

[25] L. A. Pipes, "Car following models and the fundamental diagram of road traffic," *Transportation Research*, vol. 1, no. 1, pp. 21–29, 1967.

[26] R. Chandler, R. Herman, and E. Montroll, "Traffic dynamics: studies in car following," *Operations Research*, vol. 6, no. 2, pp. 165–184, 1958.

[27] D. C. Gazis, R. Herman, and R. W. Rothery, "Non-linear follow the leader models of traffic flow," *Operations Research*, vol. 9, pp. 545–567, 1961.

[28] P. G. Gipps, "A behavioural car-following model for computer simulation," *Transportation Research Part B*, vol. 15, no. 2, pp. 105–111, 1981.

[29] A. D. May, "Traffic flow fundamentals," in *Microscopic Density Characteristics*, pp. 162–177, Prentice Hall, 1990.

Hindawi Publishing Corporation
International Journal of Vehicular Technology
Volume 2011, Article ID 853948, 14 pages
doi:10.1155/2011/853948

Research Article

Heterogeneous Wireless Sensor Network for Transportation System Applications

K. Selvarajah,[1] C. Shooter,[2] L. Liotti,[3] and A. Tully[1]

[1] *School of Computing Science, Newcastle University, Newcastle NE1 7RU, UK*
[2] *TRW Conekt, Stratford Road, Solihull B90 4AX, UK*
[3] *Process Research, Centro Ricerche FIAT, Strada Torino, 50, 10043 Orbassano (TO), Italy*

Correspondence should be addressed to K. Selvarajah, k.selvarajah@ncl.ac.uk

Received 6 August 2010; Accepted 2 March 2011

Academic Editor: Syed R. Rizvi

The important innovations in wireless and digital electronics will support many applications in the areas of safety, environmental and emissions control, driving assistance, diagnostics, and maintenance in the transport domain. The last few years have seen the emergence of many new technologies that can potentially have major impacts on transportation systems. One of these technologies is Wireless Sensor Networks. A wireless sensor device is typically composed of a processing unit, memory, and a radio chip which allows it to communicate wirelessly with other devices within range. The Embedded Middleware in Mobility Applications (EMMA) project delivers a middleware that aims to facilitate the interaction between sensing technologies in transportation systems. This paper outlines our experience in the EMMA project and provides an illustration of the important role that wireless sensor technology can play in future transportation system. The paper discusses our experience of using heterogeneous sensors to develop transportation system applications in the EMMA project and focuses on how cooperation between vehicle and infrastructure can be addressed. It also presents encouraging results obtained from the experiments in investigating the feasibility of utilising wireless sensor in vehicle and vehicle-to-infrastructure communication in real transportation applications.

1. Introduction

A recent study by the UK Government's Office of Science and Innovation, which examined how future intelligent infrastructure would evolve to support transportation over the next 50 years, looked at a range of new technologies, systems, and services that may emerge over that period [1, 2]. One key class of technology that was identified as having a significant role in delivering future intelligence to the transport sector is Wireless Sensor Networks (WSN) and in particular the fusion of fixed and mobile networks to help deliver a safe, sustainable, and robust future transport system based on the better collection of data, its processing and dissemination, and the intelligent use of the data in a fully connected environment. As future intelligent infrastructure will bring together and connect individuals, vehicles and infrastructure through wireless communications, it is critical that robust communication protocols are developed.

Mobile wireless ad-hoc networks (MANETs) are self-organising networks where nodes exchange data without the need for an underlying infrastructure [3]. MANETs have attracted extraordinary attention from the research community in recent years including in real transport applications. In the road transport domain, schemes which are fully infrastructureless and those which use a combination of fixed (infrastructure) devices and mobile devices fitted to vehicles and other moving objects are of significant interest to the transport community as they have the potential to deliver a "connected environment" where individuals, vehicles, and infrastructure can coexist and cooperate, thus delivering more knowledge about the transport environment, the state of the network, and who indeed is travelling or wishes to travel [4]. This may offer benefits in terms of real-time management, optimisation of transport systems, intelligent design, and the use of such systems for innovative road charging and possibly carbon trading schemes as well as through the CVHS (Cooperative Vehicle and Highway Systems) for safety and control applications. Within the vehicle, the devices may provide wireless connection to various Information and Communications Technologies (ICT)

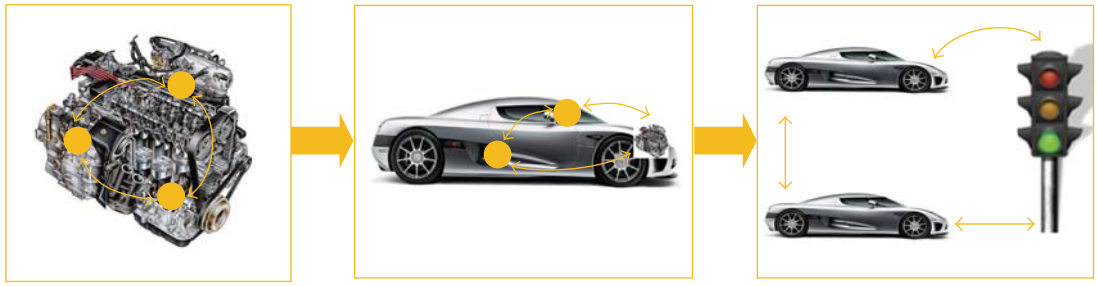

Figure 1: EMMA hierarchical network.

components in the vehicle and connect with sensors and other devices within the engine management system [5]. Advances in wireless sensor networking techniques which offer tiny, low power and MEMS (Micro-Electro Mechanical Systems) integrated devices for sensing and networking will exploit the possibility of vehicle-to-vehicle and vehicle-to-infrastructure communications [6].

In this paper, wireless sensor network applications in the transport systems and using middleware to integrate heterogeneous Wireless Cooperative Objects (WICOs) are discussed. Section 2 describes the EMMA project and its hierarchical approach and communication technologies. An overview of wireless sensor networks middleware and components of the EMMA middleware is presented in Section 3. Section 4 describes the different hardware platforms which are used as wireless cooperating objects in the prototype applications. Three applications for each hierarchical level and an inter-hierarchical level application are given in Section 5. Section 5 also presents encouraging results obtained from the experiments in investigating the feasibility of utilising EMMA middleware in real transport system applications. Conclusions are then presented in Section 6.

2. The EMMA Project

The EMMA project (Embedded Middleware in Mobility Applications project) is partly funded by the European Commission under the Information Society Technologies (IST) Priority of the 6th Framework Programme. The EMMA project was committed to deliver a middleware platform and a development environment which facilitates the design and implementation of embedded software for cooperative sensing objects [7, 8]. The EMMA network architecture (Figure 1) can be considered at three levels: within an engine level, at a vehicle level, and at the supra-vehicle level. Recently, many wireless sensor network applications have been developed for a variety of applications including transport monitoring and control. However, there are still numerous challenges to be overcome if wireless sensor devices are to communicate with each other in an intelligent, cost-effective, and reliable way.

EMMA communication networks at the supra-vehicle level can be considered as mobile wireless sensor networks while vehicle level networks and engine level networks can be considered as static wireless sensor networks. The current wireless sensor networks employ conventional technologies to interact with other devices in the network, and many companies and organizations are developing various wireless communication interface and protocols for sensors. Bluetooth is currently the most widely used automotive wireless technology for in-vehicle communication and Wi-Fi is used for vehicle to vehicle communication by several pilot research projects such as the Car2Car consortium [9]. ZigBee technology is able to provide the interconnection of low power wireless sensors within vehicles and vehicle to infrastructure. The ZigBee standard has evolved since its original release in 2004 and it is a low cost low power wireless networking standard for sensors and control devices. ZigBee provides network speed of up to 250 kbps and is expected to be largely used in typical wireless sensor network applications where high data rates are not required [10, 11].

The EMMA project needed to discover which communication technologies are more suitable and how the networks are formed by WICOs from different levels. ZigBee, Bluetooth and Wi-Fi have been designed for short-range wireless applications with low power solutions and could be used at the EMMA infrastructure level. ZigBee can accommodate larger numbers of devices than Bluetooth. On the other hand, Bluetooth offers high bandwidth with relatively high throughput. EMMA network applications do not require high data rate communication technology as it is based on data exchange. ZigBee provides 250 kbps data rate and is expected to be enough for the EMMA sensor network applications. Notably, ZigBee uses low overhead data transmission and requires low system resources which are vitally important factors for embedded wireless sensor networks. Also mesh networking features in ZigBee technology allow devices to extend coverage and optimize radio resources. These features show that ZigBee is a suitable communication technology for the EMMA project applications.

3. Middleware for Wireless Sensor Networks

The term middleware refers to the software layer between the operating system and the applications. A middleware layer seeks primarily to hide the underlying network environment complexity by insulating applications from explicit

protocol handling, disjoint memories, data replication, network faults, and parallelism. Further middleware masks the heterogeneity of computer architectures, operating systems, and communication technologies to facilitate application programming and management [12]. The design and development of a successful middleware should address many challenges in WSN such as scarcity of resources, mobility, heterogeneity, data aggregation, quality of services, and security. Several middleware systems have been proposed for WSN but each addresses a different part of the problem space. Notable middleware for sensor networks are Impala, Mate, TinyDB, TinyCubus, TinyLime, and MiLAN [13]. Most of these middleware are built on top of TinyOS [14] which is an open source operating system mainly designed for wireless sensor networks. The middleware can be classified as service-centric middleware and data-centric middleware. Service centric middleware is driven by commands while data centric middleware is driven by data.

Service-centric middleware is described as a well-defined and self-contained function that does not depend on the context or the state of other services. Such a service is executed by explicitly calling it. After the completion of the service, a response is returned. This type of middleware is the principally used paradigm in traditional distributed systems, either with a procedural abstraction or based on object-orientation. Data-centric middleware is mostly concerned with the communication of data and provides a small general purpose API to send and receive data. There is no client-server relationship but there is a distinction between data providers and data consumers. The data-centric approach is mainly followed in the area of sensor networks where the naming and type of data play a more important role than the specific device responsible for its processing.

The EMMA Embedded Middleware Platform (EM2P) is designed to support a range of applications running on different WICOs. EM2P is designed in a modular fashion. The communication adapters form the interface between the communication module and the actual hardware drivers. The communication module has a generic part and two specialised parts for message and data-centric communication. The security add-on is configurable via the middleware API, but is actually used in the communication module. The same applies for the data connector. Installation and the configuration and monitoring module use message communication and are, therefore, built on top of the message communication. A general communication abstraction is used by the synchronisation module. The main components of the EM2P is shown in Figure 2.

The middleware abstracts from the underlying communication technology by providing a high-level addressing mechanism and the communication functions do not imply a specific communication technology. The middleware converts the local representation of a data value to its network representation and vice versa when sending or receiving data. Messages can be sent directly to a specific WICO by knowing only its EMMA WICO address. An application can register for the reception of messages. A call back function is called when a message is received. The content of a message is completely controlled by the application and no data conversion is done by the middleware. Therefore, the application has to assure that the receiver understands the message contents. EM2P uses publish/subscribe communication, request/response communication, and data connector functionalities.

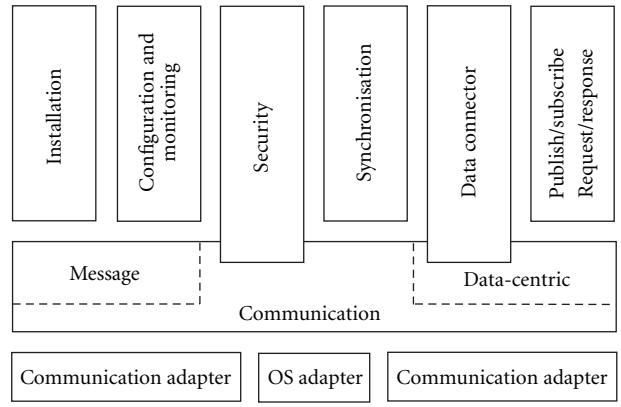

Figure 2: Components of EMMA Middleware.

4. EMMA Wireless Cooperative Objects

The following sections explain three different platforms which are used in EMMA project prototype applications: Commercially available Crossbow MicaZ and TelosB and an off-the-shelf Xilinx ML403 FPGA board. C-based multi-threaded NanoQplus [15] operating system is used in MicaZ and TelosB motes while a Linux-based Qplus [15] operating system is used in Xilinx ML403 FPGA. These devices with sensors, actuators, and related software are called WIreless Cooperating Objects (WICOs) which may be heterogeneous, but nevertheless able to cooperate together to achieve specific goals [8].

4.1. Supra-Vehicle Level WICO. Smartdust (or mote) is a new concept for wireless sensor networks which offers tiny, low-power, and MEMS integrated devices for sensing and networking. It is interesting for the low-power sensing technologies and also the low-power communication and networking capability which it has demonstrated. Fundamentally, it provides a convenient and economic means of gathering and disseminating environmental and other useful information in the transport domain. The existence of a ZigBee-based networking capability between the motes and other devices will benefit many applications in the transportation domain. The motes have sensors attached to them to monitor the physical environment in some way. These sensors can be built directly onto the mote or can come as daughter boards which can be connected in to the motes main mother board. Initial studies suggest environmental monitoring, vehicle-to-vehicle, vehicle-to-infrastructure, and infrastructure to infrastructure applications may exist for motes in the transportation domain. The vital application of the devices is beginning to be tested in the road vehicle environment. Even though a range of mote platforms are

Figure 3: MicaZ WICO.

available in the market, Crossbow MicaZ [16] family motes had been chosen for EMMA project as it features sensing and networking capabilities with low-power consumption using ZigBee as communication protocol. Figure 3 shows a Crossbow MicaZ mote.

The MicaZ is a family of the Crossbow Mica motes where the radio transceiver uses the Chipcon CC2420 IEEE 802.15.4 (ZigBee) compliant chipset. This allows the MicaZ to communicate with other ZigBee compliant equipment. The software stack includes a MicaZ mote-specific layer with ZigBee support and platform device drivers, as well as a network layer for topology establishment and single/multihop routing features. It is mainly used for research and development of low power wireless sensor network applications. The MicaZ mote platform is built around the Atmel AtMega128L processor which is capable of running at 7.37 MHz. The MicaZ motes have 128 Kbytes of program memory, 512 Kbytes of flash data logger memory, and 4 Kbytes of SRAM. Power is provided by two AA batteries, and the devices have a battery life of roughly one year depending on the application (very low duty cycle assumed). Sensor boards can be attached through a surface mount 51 pin connector, Inter-IC (I2C), Digital Input Output (DIO), Universal Asynchronous Receiver Transmitter (UART), and a multiplexed address/data bus.

4.2. Engine Level WICO. In the Engine level application, the Crossbow TelosB [16] mote platform was chosen for the EMMA project prototype applications. Compared to the MicaZ mote, the TelosB mote has higher processing power which is required to implement with a multitasking approach applications: to run several threads of the middleware, the acquisition task, and keeping low latencies in the communication among the Engine WICOs. The high ADC resolution is necessary to satisfy one of the needs of the engine application that is the acquisition of an accurate analogue signal. Less important but good features are the presence of a USB connection, the on board sensors, and LEDs for demonstration and development purposes.

The Crossbow TelosB (Figure 4) mote is a commercially available mote platform with Chipcon CC2420 IEEE

Figure 4: TelosB WICO.

802.15.4 (ZigBee) compliant chipset with integrated onboard antenna. This allows the TelosB mote to communicate with other ZigBee compliant equipment such as MicaZ. It is also mainly used for research and development of low-power wireless sensor network applications. The TelosB mote platform is built around the TI MSP430 (a 16-bit microcontroller) which is capable of running at 8 MHz. The TelosB mote has 48 Kbytes of program memory, 1024 Kbytes of flash data logger memory, and 10 Kbytes of SRAM. Power is provided by two AA batteries, and the devices have a battery life of roughly 1 year depending on the application (very low duty cycle assumed). The TelosB mote has 12 bit ADC resolution, while the MicaZ mote has 10 bit resolution. Sensor boards can be attached through Inter-IC (I2C), Digital Input Output (DIO), Universal Asynchronous Receiver Transmitter (UART), and SPI.

4.3. Vehicle Level WICO. At the vehicle level, there is a need for introducing wireless communication to existing sensing technologies. In addition, it may be necessary to increase the processing power and memory space in order to ensure the EMMA middleware runs seamlessly without compromising the performance of each sensor. It is important to keep the low-power communications available in the other hardware alternatives used but it may be necessary for the units themselves to be capable of running much more complex algorithms. The hardware chosen for EMMA project for this level of WICO, therefore, reflects that extra processing power needed. The vehicle level WICO consists of two elements. Firstly, an off-the-shelf Xilinx ML403 FPGA [17] board is used as the foundation of the system. This FPGA contains a powerful Power PC microprocessor. Secondly, the functionality in this board is extended using a custom, built daughter board. This daughter board contains a number of different hardware devices required by the project including a 12 V automotive power supply, a CAN [18] port for interfacing to automotive ECUs and 2 further RS232 ports which are used to send and receive data over ZigBee and from the other devices as appropriate (e.g., GPS). Figure 5 shows Xilinx ML403 FPGA with TRW Conekt interface board.

5. Prototype Applications

This section provides four different prototype applications, their implementation, and related experiments. The applications are developed here not only to evaluate the overall

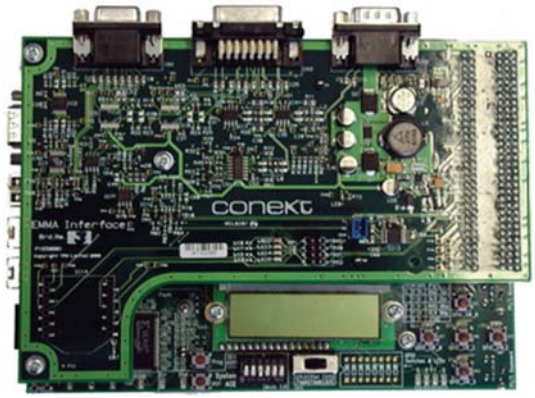

Figure 5: Xilinx processor board with TRW Conekt interface board mounted on top.

results of the project, but also to demonstrate the validity of the EMMA approach and its potential applications of heterogeneous wireless networks in transport systems.

5.1. Engine Level Application. The application proposed in the EMMA project is a solution for new engine control architecture (Figure 6), characterised by the integration of new sensors (in-cylinder pressure, oil pressure, and valve lift, not available on current engines) without redesigning the ECU engine. The engine network (Figure 7), wirelessly connected with the ZigBee technology, is so composed:

(i) 4 Cylinder WICOs, sampling the two sensors (a pressure sensor and a valve lift sensor) on each cylinder,

(ii) oil pressure WICO, sampling by a sensor for the measurement of the oil pressure in the oil delivery head,

(iii) ECU WICO, composed by a wireless node connected to the ECU (Electronic Control Unit).

The role of the four Cylinder WICOs is to sample the two analogue channels (connected to the valve lift and the in-cylinder pressure sensors) and calculate the maximum value for the first and the integral over a whole engine cycle for the second. The oil pressure sensor is responsible for sampling the oil pressure sensor. Upon a request from the ECU (simulated by a LabVIEW software on a Laptop), the ECU WICO queries the other engine WICOs, collects the received messages, calculates their latency and validity, and returns the data to the ECU.

5.1.1. Implementation. The Engine WICO consists of two main components: a TelosB mote and hardware adaptation module, necessary to properly interface the connection available on the board to the required conditioning electronics required by the engine sensors. The application has been evaluated by an ad-hoc test bench, where the values acquired from the real sensors are reproduced on the analogue outputs of an acquisition board, reading them from a set of measurement previously acquired from a real Multijet engine. The ECU is implemented by the software running on a Laptop.

All the WICO applications have been programmed by the EM2P (EMMA middleware) functionalities. Several set of experiments have been carried out for data centric paradigm (request/response).

5.1.2. Experimental Results. This engine application has been validated in three different scenarios: the whole test bench has been tested in the laboratory environment and in the environmental chamber, while the engine nodes (without the acquisition board) have been tested directly on a real engine. A set of tests have been performed for the three different environments based on EMMA request/response mechanism (*data-centric*), and for several values of RPM (from 1000 rpm to 6000 rpm). For each test, a set of log files (registering latencies, packet loss, and other WSN-related data) have been collected for offline analysis of the application performance.

Laboratory Environment. The laboratory tests were carried out on a test bench using an engine simulator for the six different rpm values (1000 to 6000 rpm, step 1000). Table 1 summarises the results of each log file generated from each test run. The average and standard deviation of each cylinder's latency has been calculated using only complete packets, that is, where all cylinder WICOs returned a packet flag of 0.

Figure 8 shows that the average latency of all Cylinder WICOs increases slightly in-line with the rpm, whilst the standard deviations are consistent throughout all rpm. These results suggest that it is also possible to make a *data-centric* measurement of the engine sensors for a single engine cycle by simply performing a request with the necessary advance. Packet loss is under 2% for all rpm values, which demonstrates good communication stability for the *data-centric* paradigm.

Engine Environment. The engine environment tests were conducted as before, using a petrol engine to measure the influence of electromagnetic noise and the presence of metal objects in close proximity to the WICOs, in order to model the effects of "real world" conditions. The tests were carried out using an engine simulator for four different rpm values (1000, 2000, 3000, and 6000 rpm), all with the engine switched on. Table 2 summarises the results of each log file generated from each test run. The average and standard deviation of each cylinder's latency has been calculated using only complete packets, that is, where all cylinder WICOs returned a packet flag of 0.

Figure 9 shows that the average WICO latency increases in-line with the rpm for Cylinder 1 WICO, Cylinder 3 WICO, and Cylinder 4 WICO. Although the average latency of Cylinder 2 WICO actually decreases slightly at rpm value 2000 it increases for higher rpm values. The standard deviations of all Cylinder WICO latencies are consistent at all rpm. This further supports the notion that for *data-centric* communication, it is possible to make a measurement of the engine sensors for a single engine cycle by simply performing a request with the necessary advance. Packet loss

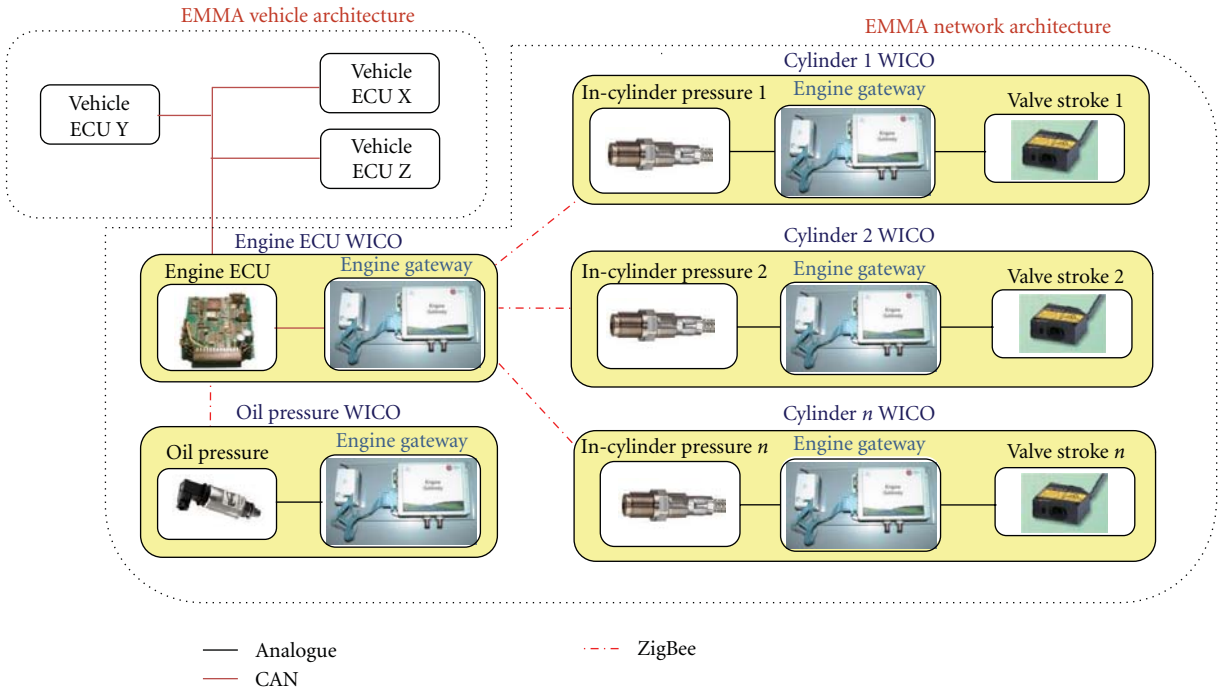

Figure 6: Engine level application diagram.

Figure 7: Engine WICOs experimental setup: acquisition board, 6 WICOs and ECU implemented on a Laptop.

Table 1: Summary of test results for laboratory environment.

rpm	Number of enquiries	Lost engine data* (n, %)	Cylinder WICO latency average (ms), standard deviation (ms)				Serial latency average (ms), standard deviation (ms)
			Cyl. WICO1	Cyl. WICO2	Cyl. WICO3	Cyl. WICO4	
1000	5717	88, 1.5	27, 3	4, 2	20, 3	16, 3	119, 7
2000	2603	12, 0.5	33, 3	11, 2	27, 3	23, 4	125, 6
3000	2952	36, 1.2	35, 2	13, 2	29, 3	25, 3	128, 3
4000	7445	72, 1.0	37, 2	15, 2	30, 2	26, 3	128, 6
5000	2631	24, 0.9	37, 2	15, 2	31, 2	27, 3	128, 3
6000	2024	12, 0.6	38, 3	16, 2	31, 3	27, 3	130, 4

*Excluding lost packets from Oil WICO.

Table 2: Summary of test results for engine environment.

rpm	Number of enquiries	Lost engine data* (n, %)	Cylinder WICO latency average (ms), standard deviation (ms)				Serial latency average (ms), standard deviation (ms)
			Cyl. WICO1	Cyl. WICO2	Cyl. WICO3	Cyl. WICO4	
1000	1810	16, 0.9	10, 2	26, 3	3, 2	19, 2	124, 5
2000	3731	30, 0.8	11, 2	19, 3	33, 3	28, 3	132, 6
3000	1644	12, 0.7	13, 2	21, 2	35, 2	31, 3	132, 5
4000	—	—	—	—	—	—	—
5000	—	—	—	—	—	—	—
6000	1967	24, 1.2	15, 3	23, 2	37, 3	33, 3	133, 3

*Excluding lost packets from Oil WICO.

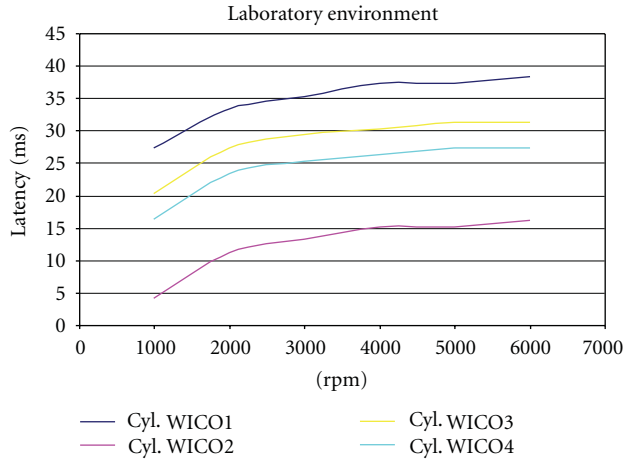

Figure 8: Cylinder WICOs latencies in laboratory environment.

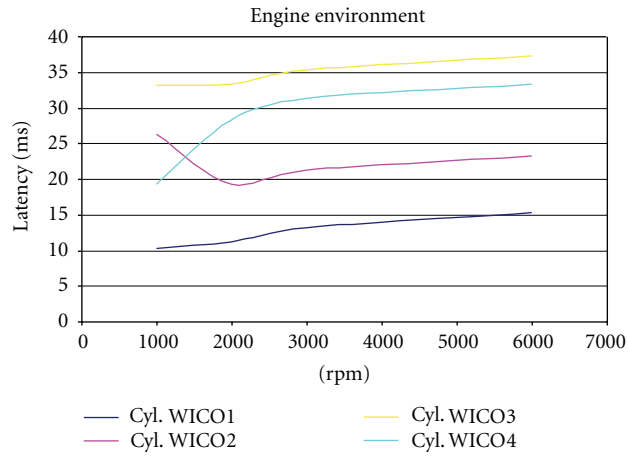

Figure 9: Cylinder WICOs latencies in engine environment.

in the engine environment is low, around 1% for all rpm, demonstrating good communication stability for the *data-centric* paradigm.

Environmental Chamber. Tests were carried out using an environmental chamber to control temperature and humidity conditions. The Cylinder 1 and Cylinder 2 WICOs were placed inside the chamber and the internal temperature varied for each test, whilst the remaining WICOs were placed outside the chamber during each test. Test runs were conducted using constant temperatures of −10, 10, 30, 50, and 80°C but unlike the laboratory and engine tests, these tests were only undertaken at two different rpm, 1000 and 3000, so the main variable investigated here was the effect on the WICO performance of the temperature inside the chamber. Tables 3 and 4 summarise these tests.

The results of the *data-centric* environmental chamber tests indicate that there is an effect of higher temperatures on the performance of the WICOs. To confirm this finding, the constant temperature tests were followed by a further variable temperature test. This applied a positive temperature ramp to the WICOs in the environmental chamber from -30 to 90°C using an rpm of 1000.

Table 5 presents the results of the variable temperature test which further illustrates the effects of temperature on the WICO latency values. The WICOs inside the chamber (Cylinder 1 and Cylinder 2) have higher standard deviations than those outside and overall packet loss is also slightly higher than in the other tests, at 3%. Figure 10 illustrates how the latencies of each WICO changed as the temperature ramp was applied, and clearly demonstrates the effect of increasing temperature on the WICO latency.

For the laboratory and engine environments, the latency standard deviations of all Cylinder WICOs were remarkably consistent, which demonstrates robust data communication stability across both environments for the *data-centric* paradigms. For the Environmental Chamber tests, an increase in the average latency of the Cylinder WICOs within the chamber was observed along with an increase in the standard deviations, which indicates a slight loss in communication stability for the *data-centric* paradigms.

The results of the environmental chamber tests clearly illustrate the impact of higher temperatures on WICO latency performance and the packet loss rate. The impact on latency performance is particularly noticeable in the Environmental Chamber tests where the differences in individual

Table 3: Summary of test results for environmental chamber at 1000 rpm.

Temp °C	Number of enquiries	Lost engine data*(n, %)	Cylinder WICO latency average(ms), standard deviation (ms)				Serial latency average (ms), standard deviation (ms)
			Cyl. WICO1	Cyl. WICO2	Cyl. WICO3	Cyl. WICO4	
−10	2295	44, 1.9	28, 3	5, 2	22, 3	17, 3	123, 6
10	1529	8, 0.5	9, 3	16, 3	26, 2	5, 2	119, 6
30	1868	16, 0.9	19, 2	30, 5	27, 3	6, 5	122, 7
50	1359	8, 0.6	2, 4	1, 7	8, 6	17, 5	92, 5
80	5652	68, 1.2	45, 4	39, 4	13, 5	6, 5	123, 6

*Excluding lost packets from Oil WICO.

Table 4: Summary of test results for environmental chamber at 3000 rpm.

Temp °C	Number of enquiries	Lost engine data*(n, %)	Cylinder WICO latency average (ms), standard deviation (ms)				Serial latency average (ms), standard deviation (ms)
			Cyl. WICO1	Cyl. WICO2	Cyl. WICO3	Cyl. WICO4	
−10	2354	48, 2.0	36, 2	14, 2	30, 2	25, 3	128, 3
10	1608	28, 1.7	19, 2	26, 3	35, 2	14, 2	127, 2
30	2147	24, 1.1	23, 2	32, 4	35, 3	17, 3	127, 2
50	1350	8, 0.6	35, 3	34, 7	26, 6	17, 5	122, 6
80	2236	23, 1.0	28, 3	40, 4	36, 3	14, 3	127, 4

*Excluding lost packets from Oil WICO.

Table 5: Summary of test results for temperature ramp within the environmental chamber.

Ramp	Number of enquiries	Lost engine data* (n, %)	WICO latency average (ms), standard deviation (ms)				Serial latency average (ms), standard deviation (ms)
			Cyl. WICO1	Cyl. WICO2	Cyl. WICO3	Cyl. WICO4	
+ve	2225	67, 3.0	34, 15	32, 13	7, 5	14, 5	122, 8

*Excluding lost packets from Oil WICO.

WICO latencies are primarily due to the experimental setup of the tests performed.

During these tests, two Cylinder WICOs were placed in the Environmental Chamber (Cylinder 1 and 2 WICOs) while the others (ECU WICO and Cylinder 3 and 4 WICOs) were placed outside. As the temperature increases, the time to perform the channel sampling and the calculation increases for the TelosB in the Environmental Chamber. For this reason, both the operations are completed first for the Cylinder WICOs 3 and 4, and then for the Cylinder WICOs 1 and 2 at higher temperatures, not in the serial order as expected.

As an example, where the bit rate of the ZigBee channel is around 40 kbps, if the answer length of each Cylinder WICO is around 800 bits, each answer will keep the ZigBee channel busy for at least 800 b/40000 bps (=20 ms). With the overhead of the ZigBee and the overhead introduced by the EMMA middleware, a difference between the latency values of two contiguous Cylinder WICOs of about 40 ms is understandable. This explains why the latency increases for the Cylinder WICOs 1 and 2 in the Environmental Chamber, and therefore the reason why they are the last in the answer message queue.

The reasons for the increase in the loss rate can be attributed to the fact that all electronic devices have an operating point at which they can operate normally. As the temperature increases, I/V (current-voltage) characteristic of a device changes and the behaviour of the device can be different from what would be expected under "normal" conditions. For the WICOs, this change in I/V characteristics means that there is a possibility that a ZigBee transmitter chip behaves erroneously, which in turn produces corrupted data at the chip level. If an error does occur, repeated retransmission occurs on a chip as well as at the MAC level.

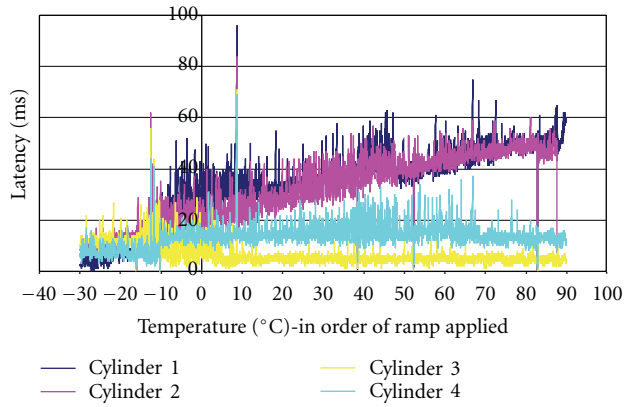

Figure 10: Cylinder WICO Latencies, positive temperature ramp applied.

The experimental results of all tests performed on the three scenarios have highlighted some key findings and issues.

(1) The latencies are quite stable with the RPM, but they increase when the temperature reaches 50–60 degrees: this suggests that the TelosB mote requires further hardware design development for an automotive engine level application.

(2) For the message centric version of the application, a loss packet rate lower than the data centric version has been observed: this suggest that in the two paradigms there is a different call-back implementation, or in the thread management in the OS.

(3) For high values of RPM, ZigBee was unable to manage synchronously the connection between the ECU WICO and the 4 Cylinder WICOs: in fact the amount of data transmitted by each Cylinder WICO keep the RF channel busy for a number of millisecond comparable with the engine period, and this does not allow the ECU WICO to collect the data from the Cylinder WICO at the same time.

5.2. Vehicle Level Application. Figure 11 shows the example application that was developed to test the EMMA system. The overall purpose of the vehicle WICO was to provide the absolute position of targets being tracked by the radar. This was achieved by combining the absolute position of the vehicle (based on GPS & vehicle dynamics data) and the relative position of the detected target (using automotive ACC radar).

NMEA 0183 format data was used to transmit the GPS and vehicle data to the Radar WICO within the system. This standardised format was selected to ensure maximum interoperability of the individual WICOs in future setups.

5.2.1. Implementation. All implementations on the Xilinx ML403 FPGA board follow the generic architecture layout described below in Figure 12. Creation of the applications was carried out utilising the Qplus [15] operating system, which is based on Linux and the EMMA middleware.

Table 6: Summary of latency results for vehicle-level request/response.

Metric (in ms)	Run 1	Run 2	Run 3
Minimum	66	58	54
Maximum	475	436	452
Average	267	267	273
Standard deviation	400	483	566

GPS WICO. The interface to the Radar WICO was implemented using the publish/subscribe EM2P functionality to send the required GPS NMEA sentences to the main Radar WICO when they have been correctly received from the GPS unit. During development of the host vehicle tracking algorithm, it was discovered that only the GPGGA NMEA sentence was required for the application so all other sentences were filtered out by the GPS WICO.

Vehicle Dynamics WICO. The interface to the Radar WICO was implemented using the request/response EM2P functionality to send the latest vehicle dynamics data to the main Radar WICO when requested. The WICO buffers the received data from the individual sensors and sends the latest full update when requested. The NMEA sentence received from the digital compass was modified to filter out all data except the required heading data. The integrity of all of the data received was checked before it is passed on to the Radar WICO.

Radar WICO. The interfaces to the other two WICOs are defined above and attempt to test as many of the EM2P interface options as possible. The overall scheduling of the application was implemented so that the tracking algorithm runs after a full update of radar data has been received from the ACC radar. The request to the vehicle dynamics data was sent after the algorithm has run so that the next run of the algorithm has the latest vehicle dynamics and radar data. The GPS data was published from the GPS WICO totally asynchronous to the rest of the application.

The host vehicle's GPS position was calculated in the Radar WICO using a Kalman filter algorithm that fuses GPS and Vehicle Dynamics data in order to update position at higher rate and overcome synchronism issues between the sensor WICOs. All of the targets reported from the ACC radar were in relative coordinates relative to the centre of the radar. These coordinates are then converted to the full GPS coordinate system and referenced to the tracked host vehicle position. This data was then available for fusing with other on board sensor data using the GPS co-ordinate system or for passing to the infrastructure for use in traffic management.

5.2.2. Experimental Results. To validate the WICOs in a "real-world" environment for this application it was decided that a test bench environment (Figure 13) would be used to playback a variety of recorded scenarios using data from the Radar, GPS, and Vehicle Dynamics devices to ensure consistency. Three runs of the same data were undertaken,

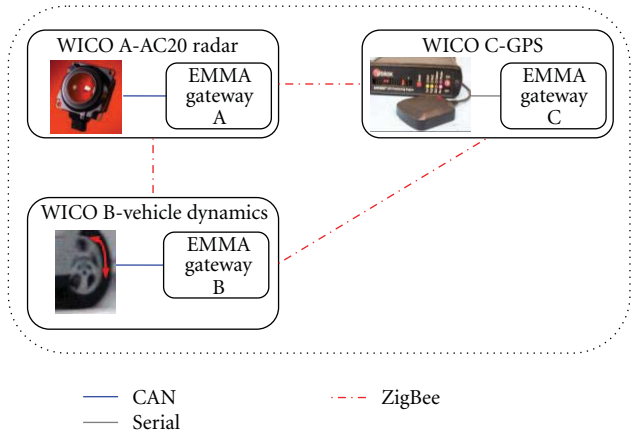

Figure 11: Vehicle level application diagram.

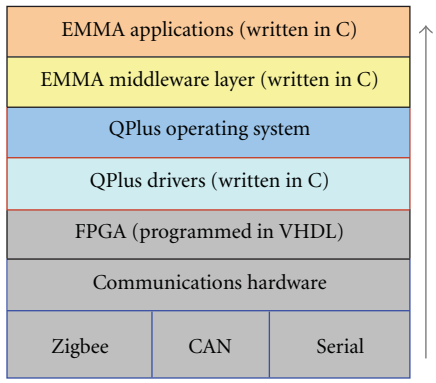

Figure 12: Application architecture on Xilinx board.

Figure 13: Three WICOs as tested in lab and in vehicle demonstration.

which would allow for the relevant metrics (message latency and lost messages) to be evaluated.

(a) Message Latency

Publish/Subscribe. It was only possible to check the timing of the publish/subscribe mechanism using a timestamp recorded in a log file. This was only set up to record to a one-second level of precision, and the GPS messages were only updated every second anyway. There was very little evidence of latency except in the third run where there was evidence some messages were delayed by one second.

Table 7: Summary of lost message results for car-level communications.

WICO-WICO interaction	Missing messages		
	Run 1 (n, %)	Run 2 (n, %)	Run 3 (n, %)
GPS-Radar	15, 12.6	36, 28.1	16, 13.6
VehDyn-Radar	7, 1.2	9, 1.4	6, 1.0

Request/Response. The request/response time was measured internally in microseconds and reported in the log file. The results as shown in Table 6.

(b) Lost WICO to WICO Messages. The results showed in Table 7 a small message loss (around the 1% level for all runs) between the Vehicle Dynamics WICO and the Radar WICO, whereas there was a much higher message loss between the GPS WICO and the Radar, as high as 28.1% during Run 2.

There was minimal message loss between the Vehicle Dynamics WICO and the Radar WICO. It is supposed that these missed messages could have been caused by the Radar WICO simultaneously receiving a successful GPS message. However, comparison of log files proved inconclusive as all records of a missing Vehicle Dynamic message in the Radar logs coincided with a missing GPS message, which suggest a temporary total loss of communications between all WICOs. The only exception to this could be found in 4 records from all the Radar logs which had a missing Vehicle Dynamics message followed one second later by a successful GPS message, but these occurrences were not cyclical in the log files.

For the missing GPS messages, the causes for the higher loss rate were again not clear. A small number of messages in the GPS log files had a fault code which indicates that ZigBee communications were not allowed due to the system not acknowledging that the previous message had successfully

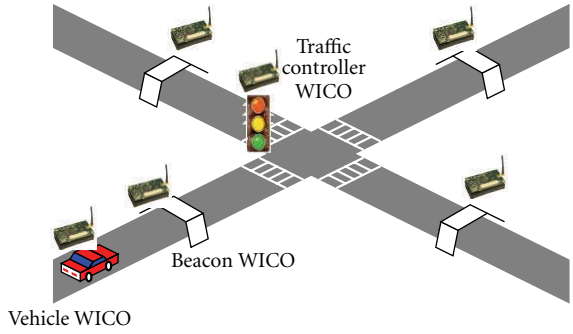

Figure 14: Giving priorities for emergency vehicle.

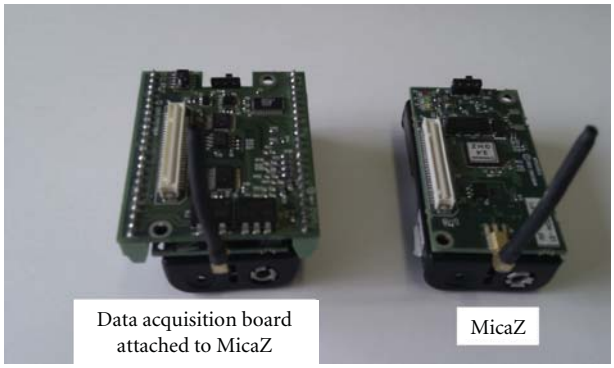

Figure 15: Micaz and MDA300.

been sent. Further investigation of these results is required to improve message lost between the Radar and GPS WICOs.

5.3. Supra-Vehicle Level Application. An application was developed in order to demonstrate the benefits of the middleware in priority to emergency vehicles. For that purpose, an emergency vehicle (ambulance, fire engine or police car, etc) would be equipped with a MicaZ WICO which would broadcast a beacon message if it was on an emergency mission (Figure 14). For example, in a busy intersection controlled by traffic lights, emergency vehicles are detected and given priority by regulating the state of the traffic lights.

5.3.1. Implementation. The implementation consists of two elements. The first element consists of a MicaZ WICO. The second element consists of a CITY traffic controller, manufactured by ETRA I+D, Spain. The CITY traffic controller is a well-proven controller that implements advanced capabilities for traffic management and control. A Cross-bow commercial data acquisition board MDA 300 (Figure 15) is used to provide as an interface between MicaZ WICO and CITY traffic controller with a small electric signal adaption stage.

In the demonstration, a MicaZ WICO was connected to a CITY traffic controller (Figure 16) that acted directly by providing information to the regulator about an emergency situation. Another MicaZ WICO was placed in the infrastructure to relay this message to the traffic light regulator.

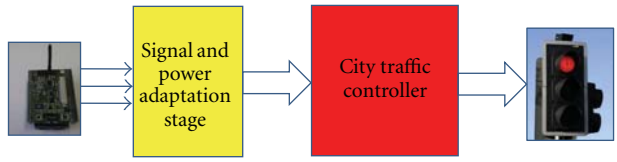

Figure 16: MicaZ to CITY Traffic Controller Interface.

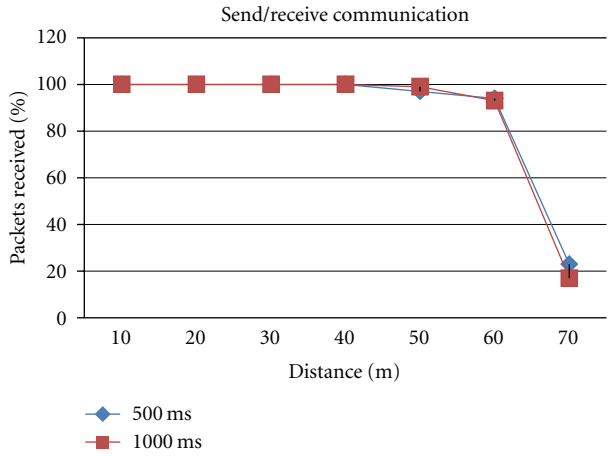

Figure 17: Urban environment packets received.

It was placed so far as needed in order to give time to the traffic regulator to change its status taking into account the time lost due to communication mechanisms (publish/subscribe) and other time periods the traffic regulator needs in order to guarantee safety first. The traffic regulator has been programmed to attend to the trigger signal provided by the mote activating an emergency control sequence. The demonstration was successfully carried out in a real road environment in Valencia, Spain.

5.3.2. Experimental Results. Several sets of experiments were carried out with EMMA middleware to evaluate possible use of the MicaZ WICO in the supra-vehicle level application. These experiments evaluated the use of MicaZ WICO with EMMA middleware for the application scenario at the supra-vehicle level. Two MicaZ WICOs (EMMA middleware running on them) were used for data-centric (request/response) and message-centric (send/receive) communication both in urban environment and mobile environment.

(a) Send/Receive Communication

Urban Environment Experiment. This experiment was carried out on Claremont Road, a busy road near Newcastle University. In each scenario, 100 packets were sent for every 500 ms, 1000 ms and those packets were received with another WICO which was connected to a Laptop via MIB 520 programming board. Both WICOs were placed at 1m above the ground. The MicaZ WICO's power level was set to default (NanoQplus power level 31). Each scenario was repeated three times, and calculations were performed offline to determine how many messages were lost at each distance and average values reported in Figure 17.

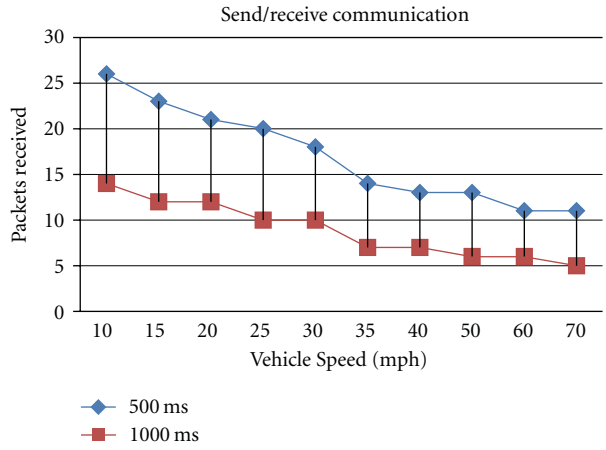

Figure 18: Mobile environment packets received.

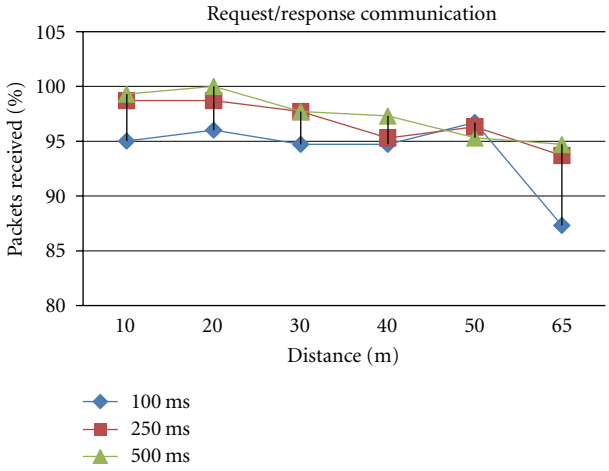

Figure 19: Urban environment packets received.

Mobile Environment Experiment. This experiment was carried out on Claremont Road up to 40 mph and on a Motorway near to the Newcastle Airport for higher speeds. The first MicaZ WICO was placed on a roadside stand 1 m from the ground, and the second MicaZ WICO was placed on the middle of the dashboard of a vehicle and connected to a Laptop via MIB 520 programming board. The MicaZ WICO at the road side sent messages periodically (500 ms, 1000 ms) which were received by the MicaZ WICO in the vehicle. Each scenario was repeated three times, and calculations were performed offline to determine how many messages were lost at each distance and average values reported in Figure 18.

In the mobile environment experiment, the received packets decreased with an increase in speed as the WICO is in range for a shorter period of time. This means that communication time window decreased with the increase in vehicle speed. At 70 mph speed, the WICO in the roadside received 5 and 11 packets for sending intervals 1000 ms, 500 ms, respectively. There were no packets lost between the first packet and the last packet received. This Experiment demonstrated that

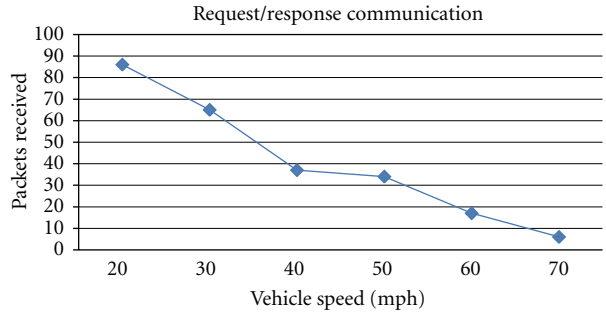

Figure 20: Mobile environment packets received.

MicaZ WICO can be used with EMMA middleware communication methods between a fixed infrastructure WICO and also fast moving vehicle-based WICO application. This is an important finding which proves that MicaZ WICOs do not suffer from any Doppler effects at normal motorway (70 mph) speeds.

(b) Request/Response Communication

Urban Environment Experiment. This experiment was carried out on Claremont Road, a busy road near to Newcastle University. Two WICOs were used for request/response communication with a request message transmitted every 100 ms, 250 ms, and 500 ms for different WICO-WICO separations from 10 m to 65 m. In each scenario, response packets were received and recorded. Both WICOs were placed at 1m above the ground. The MicaZ WICOs power level was set to default (NanoQplus power level 31). Each scenario was repeated three times, and calculations were performed offline to determine how many messages were lost at each distance and average values reported in Figure 19.

Mobile Environment Experiment. This experiment was carried out on Claremont Road up to 40 mph and on a Motorway near to Newcastle airport for higher speeds. The first MicaZ WICO was placed on a road side stand 1m from the ground and the second MicaZ WICO was placed on the middle of the dashboard of a vehicle and connected to a Laptop via MIB520 programming board. The MicaZ WICO at the roadside sent messages periodically which were received by the MicaZ WICO in the vehicle. Due to limited access to public roads and for safety reasons, the experiment was conducted only at a packet transmission interval of 100 ms. The experiment was repeated three times, and calculations were performed offline to determine how many messages were received at each distance and average values reported in Figure 20.

The urban environment experiment shows that packets can be received without any packet lost up to 45 m distance. The percentage of packets lost increases above 45 m distance in both cases. In the mobile environment experiment, the received packets decrease with the speed increases as the WICO is in range for a shorter period of time. This means that communication time window is decreasing with the

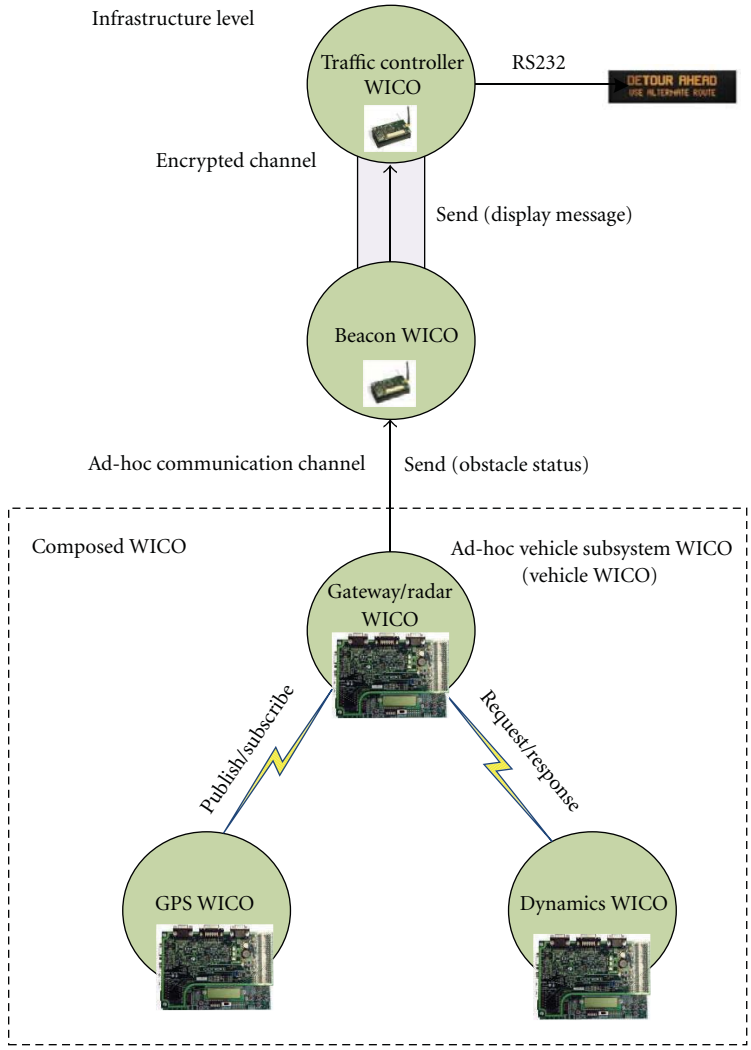

Figure 21: Deployment of WICOs in the inter-hierarchical demonstrator.

vehicle speed. At the 70 mph speed, The WICO in the roadside received 5 and 11 packets for sending intervals 1000 ms, 500 ms, respectively. And interestingly, there were no packets lost between the first packet and the last packet received. This experiment demonstrated that MicaZ WICO can be used with EMMA middleware communication methods between a fixed infrastructure WICO and also fast moving vehicle-based WICO applications. This is an important finding which proves that the MicaZ WICOs do not suffer from any Doppler effects at normal motorway (70 mph) speeds.

5.4. Inter-Hierarchical Level Application. One of the main objectives of the project was to achieve a middleware able to abstract complex subsystems formed by different kinds of WICOs into simpler elements (composed WICOs) that behave in the upper level system as a single unit. This way, complex applications could be built with a hierarchical shape, each group of WICOs working together on the same functionality appearing a unique element providing certain types of data to the remaining. In addition, the possibility to form ad-hoc WICOs (i.e., to discover previously unknown elements on the system), and to propagate published data through the different abstraction layers, allowing their transformation and combination as it crosses certain points of the hierarchies, does really enhance the achievable possibilities of applications built on EMMA Middleware.

An inter-hierarchical application, integrating different hierarchical levels developed in the project: the car level and the supra-vehicle level, demonstrated how heterogeneity issues could be solved by developing middleware such as EMMA. In order to demonstrate the inter-hierarchical collaboration of the WICOs developed on the project, the application consisted of transforming the information provided by the vehicles at both automotive and vehicle subsystem levels into specific traffic control actions at infrastructure (i.e., supra-vehicle) level.

The inter-hierarchical demonstration made use of the WICOs at the vehicle level and supra-vehicle level. This demonstration aimed to provide advanced warning to a vehicle behind that there is an obstacle ahead. As can be seen

in Figure 21 the inter-hierarchical demonstrator made use of all communications mechanisms in the EM2P middleware and exercised most of the functionality of the middleware. In this demonstrator, inter-hierarchical collaboration of the WICOs developed on the project consisted of transforming the information provided by the vehicles at vehicle level (GPS, Vehicle Dynamics and Radar sensors based on Xilinx ML 403 platform with TRW Conekt daughter board) into specific traffic control actions at infrastructure (to MicaZ) level. In the infrastructure level, two MicaZ WICOs were used. First MicaZ WICO was used as beacon WICO to relay any message received by ad-hoc vehicle subsystem WICO to the second MicaZ WICO which was connected to a portable VMS panel to display the information sent by the vehicle level WICO. This application was successfully demonstrated for the EMMA project final review in a real road environment in London.

6. Conclusions

It is clear that the next generation of vehicles will be required to have increased safety, lower emissions, and more entertainment with higher performance than those of today. The innovations in wireless sensor devices will enable novel automotive applications which will become very common in future transportation applications. The challenges such as integrating heterogeneous wireless devices for specific transportation application can be met by developing middleware technologies such as in EMMA. This paper has presented the EMMA project that has been undertaken to investigate the suitability of using heterogeneous wireless sensors in transportation system applications. The validation of the prototype applications shows that wireless sensor networking technologies can be used at the engine level, vehicle level, and supra-vehicle level. The ability to communicate between vehicle and roadside illustrates that wireless sensor networks will enable efficient and discrete communications between vehicle and roadside.

Acknowledgments

Authors would like to thank Alberto Zambrano Galbis (ETRA I+D) for his contribution to the supra-vehicle level and inter-hierarchical level application. The work presented here was sponsored by EC under FP6 programme (IST-2005-5-034097) and authors also would like to thank all the project partners for their contributions.

References

[1] The Eddington Transport Study, UK Department of Transport, May 2011, http://webarchive.nationalarchives.gov.uk/+/http:/www.dft.gov.uk/about/strategy/transportstrategy/eddingtonstudy/.

[2] A. Tully, "Pervasive tagging, sensors and data collection: a science and technology review for the foresight project on intelligent infrastructure systems," *IEE Proceedings Intelligent Transport Systems*, vol. 153, no. 2, pp. 129–146, 2006.

[3] F. Li and Y. Wang, "Routing in vehicular ad hoc networks: a survey," *IEEE Vehicular Technology Magazine*, vol. 2, no. 2, pp. 12–22, 2007.

[4] N. Navet, Y. Song, F. Simonot-Lion, and C. Wilwert, "Trends in automotive communication systems," *Proceedings of the IEEE*, vol. 93, no. 6, pp. 1204–1223, 2005.

[5] X. Li, W. Shu, M. Li, H. Y. Huang, P. E. Luo, and M. Y. Wu, "Performance evaluation of vehicle-based mobile sensor networks for traffic monitoring," *IEEE Transactions on Vehicular Technology*, vol. 58, no. 4, pp. 1647–1653, 2009.

[6] H. Cai and Y. Lin, "A roadside ITS data bus prototype for intelligent highways," *IEEE Transactions on Intelligent Transportation Systems*, vol. 9, no. 2, pp. 344–348, 2008.

[7] K. Selvarajah, A. Tully, and P. T. Blythe, "Integrating Smartdust into the Embedded Middleware in Mobility Applications (EMMA) Project," in *4th IET International Conference on Intelligent Environments, IE08*, Seattle USA, 21-22 July 2008.

[8] T. Kosch, I. Kulp, M. Bechler, M. Strassberger, B. Weyl, and R. Lasowski, "Communication architecture for cooperative systems in Europe," *IEEE Communications Magazine*, vol. 47, no. 5, pp. 116–125, 2009.

[9] CAR 2 CAR Communication Consortium, July 2010, http://www.car-to-car.org/.

[10] Zigbee Alliance, July 2010, http://zigbee.org/.

[11] G. Cena, A. Valenzano, and S. Vitturi, "Advances in automotive digital communications," *Computer Standards and Interfaces*, vol. 27, no. 6, pp. 665–678, 2005.

[12] K. Geihs, "Middleware challenges ahead," *Computer*, vol. 34, no. 6, pp. 24–31, 2001.

[13] S. Hadim and N. Mohamed, "Middleware: middleware challenges and approaches for wireless sensor networks," *IEEE Distributed Systems Online*, vol. 7, no. 3, pp. 1–23, 2006.

[14] TinyOS, July 2010, http://www.tinyos.net.

[15] NanoQplus and Qplus, July 2010, http://www.qplus.or.kr.

[16] Crossbow Technology: "MPR/MIB User's Manual", May 2011, http://www.memsic.com/products/wireless-sensor-networks/wireless-modules.html.

[17] Xilinx, December 2010, http://www.xilinx.com/.

[18] M. Peller and N. Berwanger, "Road vehicle Controller area Network (CAN)—part 4: time-triggered communication," ISO IS 11898.

Hindawi Publishing Corporation
International Journal of Vehicular Technology
Volume 2011, Article ID 730895, 13 pages
doi:10.1155/2011/730895

Research Article

Evaluation of Selective Broadcast Algorithms for Safety Applications in Vehicular Ad Hoc Networks

Kaan Bür and Maria Kihl

Department of Electrical and Information Technology, Lund University, P.O. Box 118, 221 00 Lund, Sweden

Correspondence should be addressed to Kaan Bür, kaan.bur@eit.lth.se

Received 15 September 2010; Revised 17 December 2010; Accepted 8 February 2011

Academic Editor: Syed R. Rizvi

Just as wireless communications develop further to achieve higher performance, new application areas emerge to challenge the limits. Vehicular ad hoc networks are one of these areas, and emergency situation warning is one of their most popular applications since traffic safety is a concern for everyone. Due to the life-critical nature of emergency applications, however, it is extremely important to ensure the solutions proposed meet the standards required, such as reliable and timely delivery of the safety warning in a situation like car collision avoidance. In order to put the candidate solutions to the test and evaluate their feasibility, we adopt the approach of computer simulation. We implement four different selective broadcast algorithms used for information dissemination in vehicular ad hoc networks, and compare their performance under identical realistic simulation conditions. Our goal is to provide an evaluation focussing on the performance with respect to safety, rather than to network aspects like throughput, loss, and delay. We define four new performance criteria to address the effectiveness, efficiency, timeliness, and overhead of the broadcast algorithms in safety warning delivery. The results we obtain using these criteria help us to understand better the design requirements of a high-performance selective broadcast algorithm.

1. Introduction

In light of the average speeds and car following distances observed on today's highways, the drivers' reactions to unexpected road hazards are dangerously slow. Driver perception-response time, defined as the time from the first sighting of an obstacle on the road until the application of the brakes, is measured in various experiments, and the results presented in [1] indicate a reaction time of about 1.6 s for 95% of the human subjects. As shown in [2], this is not a time long enough to avoid collisions in many emergency cases, especially when the driver violates the safety distance rule or the road and weather conditions limit the ability of the driver to spot the emergency event from a distance. Under these conditions, a collision avoidance strategy based solely on the tail brake lights of the cars ahead has a high probability of failure. What we need is an early warning system to inform the drivers on the emergency situation arising ahead of the road but still outside the driver's vision, triggering the driver's reaction well in advance so collision avoidance is possible even at a perception-response time as high as 1.6 s.

The developments in electronics as well as telecommunications, which led to handheld computers with mobile communication and environmental sensing capabilities, have also had a profound effect on the automobile industry. As discussed in [3], modern vehicles are becoming increasingly intelligent, already equipped with effective driver assistance and passive safety functions. The development of more complex, active safety functionality, on the other hand, requires accurate positioning and classification of objects around the vehicle. Today, this data is provided by in-vehicle sensors like radar and camera. However, in-vehicle sensors cannot detect out-of-sight objects around corners or behind summits, position objects accurately at large range, or detect all attributes like weight, tire-road friction, and intended direction. This information needs to be made available through a communication link. With the assistance of vehicular communication systems, active traffic safety applications like collision avoidance and notification can be developed, which can, in return, lower considerably the accident rates.

There are mainly two realistic ways to form a vehicular network [4–6]. First, the vehicles can organise themselves to form an ad hoc network, that is, a spontaneous, mobile network to operate without the help of an infrastructure and transmit data in a single- or multihop fashion. Roadside units can be included in the ad hoc network, providing the vehicles with Internet access and centralised services. Second, infrastructure-based communication technologies can be used, where vehicles transmit data to each other via a roadside base station. The vehicles do not need to be aware of each other, since the base stations have total control of the network. In this paper, we focus on the former alternative, known as vehicular ad hoc networks (VANET), where all communication is performed without any infrastructure.

Safety applications have stringent real-time operation and reliability requirements, typically represented by message frequency, delay, and loss [3]. Considering the mission-critical nature of the traffic safety applications, it is of extreme importance that, once the emergency situation arises, the warning reaches in a timely and reliable manner as many of the vehicles as possible, which are potentially endangered by the situation. Given the variable density of the vehicular network, the high speed of as well as big speed differences between its nodes, the possible coexistence of many wireless applications sharing the available bandwidth, and the unstable wireless channel conditions the network must operate under, the reliability and timeliness of the traffic safety application depends mainly on two factors at the network level: the method it uses for data dissemination and the network overhead it generates. An efficient data dissemination strategy has to ensure a high success rate regarding the timely delivery of the emergency message, while maintaining a low resource usage profile. This also reduces the probability of contention as well as packet loss in the network, yielding lower delays and, thus, helping the network to cope with the application's quality of service (QoS) requirements more easily.

The key to the successful dissemination of safety warnings is the decision mechanism employed for message delivery and repetition, that is, finding an intelligent way of deciding when and how a safety message should be delivered or repeated to maximise reliability while keeping the overhead low. Given the properties of safety applications and the limitations of vehicular communications, selective broadcast or multicast strategies (topology versus location based, reactive approaches) seem more applicable than both unicast routing (introducing more complexity and less redundancy) as well as flooding (generating a high overhead without increasing the success rate substantially) [4, 6, 7]. Several solution proposals have been made to introduce intelligence to the basic broadcast concept, in order to make it more selective and, thus, more efficient in its resource usage, while not jeopardising the high warning delivery rate required by the traffic safety application. Various selective broadcast algorithms have been developed as part of these proposals [2], which require careful examination under realistic test scenarios. Moreover, it is also necessary to compare these different algorithms within the framework of a unified methodology, that is, in a single environment and under the same conditions. In this paper, we present such an evaluation by way of simulation.

The rest of this paper is organised as follows. In Section 2, we summarise a selection of selective broadcast schemes and some of the research efforts directed at their evaluation. Section 3 presents our evaluation scenario, starting with a description of the algorithms under investigation, followed by the explanation of the simulation settings we chose for a realistic evaluation. In Section 4, we introduce our performance criteria and compare the algorithms according to these. Finally, Section 5 summarises our conclusions and gives some future research directions.

2. Related Work

Good surveys on VANET and intervehicle communication systems have been presented in the literature [4, 5, 8]. A good overview of recent research projects in this field is presented in [3], followed by a summary of the characteristics of standard wireless data links being integrated into vehicular systems, as well as a list of applications, their characteristics, and QoS requirements. A classification of vehicular applications, their requirements, characteristics, and related technical challenges are also presented in [9]. Several recent papers have discussed the challenges for the vehicle-to-vehicle wireless channel [10–12], which is very much affected by the high speed of cars, the vehicular traffic density, and obstacles like buildings.

A good tutorial on the IEEE standardisation activities in the field, mainly IEEE 802.11p and IEEE 1609.x, can be found in [13]. The system architecture, called Wireless Access in Vehicular Environments (WAVE), will support both traditional wireless communication using IPv6 as well as high-priority communication that uses a proprietary protocol called WAVE Short-Message Protocol (WSMP). IPv6 and WSMP communication is performed on two separate channels, where each unit supports multichannel operation. The European standardisation activities in the field, on the other hand, are described in [14]. The European ITS Communication Architecture supports three main vehicular application scenarios: traffic safety, traffic efficiency, and value-added services. The architecture supports both ad hoc communication with IEEE 802.11p and cellular communication with, for example, WiMAX or UMTS. There are two generic types of messages defined in the architecture. Cooperative Awareness Messages (CAM) provide the heartbeat, also called beaconing, information. Decentralised Environment Notification Messages (DENM) provide information about existing hazards in the defined area.

2.1. Selective Broadcast for Traffic Safety. Broadcasting techniques used in mobile and vehicular ad hoc networks are generally categorised as; (1) simple flooding, (2) probabilistic forwarding, (3) area based methods, and (4) methods using neighbour information [15]. In this section, we provide the reader with an overview of some of these protocols implemented in active traffic safety and emergency warning

applications. Among the papers we summarise here, the ideas presented in [2, 16] form the basis of our evaluation, as presented later in Section 3.1.

The authors of [17] claim the main driver for network performance to be connectivity, and state that collisions at the medium access control (MAC) layer have a negligible effect on service reliability. So, they lay special emphasis on keeping the network connected. They create a highway scenario, where the warning service triggered in an emergency employs multiple broadcast cycles to guarantee the desired lifetime for the safety area. The next node to take over the message delivery task is chosen probabilistically. The authors develop an analytical model to predict the reliability of a single broadcast cycle. Following this model, it is possible to calculate the average number of nodes in a node's neighbourhood and derive the distribution of the space to be covered by the next message, so the forwarding probability can be fine-tuned accordingly. The simulation results presented validate the authors' analysis. However, an error-free wireless channel and constant vehicle density are assumed in the simulations; and sparse networks are not considered in the scenario.

Enhanced multihop vehicular broadcast (MHVB) is a flooding algorithm with special characteristics based on the position and speed of the cars [18]. It employs a detection mechanism using sensors for car traffic congestion, and lets the cars at the edges of a congestion send messages more frequently than those in the middle do. It also contains a method to suppress unnecessary packets, which is called the backfire algorithm. The algorithm defines a backfire region to pick the right node to retransmit a warning, namely the node farthest away from the sender. The other nodes in the backfire region cancel their scheduled transmission upon hearing the retransmission. In original MHVB, this is a circular region. In the enhanced version, the region becomes sectoral within a circle, enabling a directional backfire. Finally, a dynamic scheduling algorithm ensures that nodes farther away from the sender are allowed to transmit earlier than those closer to it. Simulations show, in terms of the success rate, that the enhanced version achieves better results than the original version.

Smart broadcast is a position-based protocol aiming at the maximisation of the one-hop progress of the alert message and the minimisation of the re-broadcast delay [19]. It is accompanied by a mathematical model providing a means to set the protocol's parameters optimally. It employs a contention resolution method to determine the next relay node at each hop. According to this, the source sends a request-to-broadcast. The nodes behind the source (in the desired direction for message propagation) enter a relay election phase. The coverage area is divided into sectors; and each sector is assigned a different contention window, the farther away from the source, the smaller. Each node picks a random backoff value from it's respective sector's window. So, a node far away from the source gets a short backoff value and becomes the first one to reply to the source with a clear-to-broadcast. Upon hearing this message, the other nodes exit the contention phase. The source receives the reply, and sends the data. A comparison with 3 other broadcast protocols shows that smart broadcast has a competitive performance in terms of message propagation speed and one-hop progress.

Direction aware broadcast forwarding, a simple yet efficient method, is introduced [2] as an example of the communication protocols for cooperative collision avoidance in vehicle platoons. In their paper, the authors describe two versions of direction-aware broadcast. In naive broadcast, the vehicle detecting an emergency event starts sending warnings periodically. Upon receiving it, the other vehicles start sending their own periodical warnings if the message they received comes from their front. In intelligent broadcast with implicit acknowledgement, both the initiator as well as the repeaters cancel their periodical transmission when they hear the same warning coming from a node at their back. All receivers wait for a random time before starting to send their own warnings to see whether another node starts before them. If they do, they come to the conclusion that the warning has already propagated successfully, and do not start sending messages. The safety performance of these algorithms is evaluated through simulations; and the results show a significant improvement in terms of the success ratio under high background traffic and packet error rates when the intelligent version is used.

A simple selective broadcast algorithm, called edge-aware epidemic protocol, is introduced and evaluated [16]. According to this algorithm, only nodes at the boundary of a cluster of vehicles propagate messages, either instantly or in a store-and-forward fashion, thus keeping it alive when there is a disconnection in the network. Upon receiving a warning, nodes enter a random waiting period, the duration of which is inversely proportional with their distance to the sender of the message. During this period, they count the replicas they receive, in and against the desired flow of information separately, so they can use this information later to decide whether or not to forward the warning. This logic encourages those nodes closer to the edge of the sender's transmission range to relay the message, trying to increase the one-hop progress it makes. The author presents simulation results for three VANET scenarios with varying levels of connectivity. The channel model used in the simulations takes into account the effect of relative speed between two vehicles. The results confirm that the proposed protocol outperforms flooding in terms of successful information dissemination.

2.2. Comparative Studies on Broadcast Techniques. The performance of communication in VANET has been studied by a number of papers in the literature. In this section, we summarise some of these studies, covering various techniques like pure flooding, position-based flooding, position-based unicast, one-hop broadcast, and more general data dissemination.

Three techniques used for multihop message propagation in VANET are evaluated in [20]: simple flooding, direction-aware flooding, and multipoint relaying (MPR, which originates from optimised link state routing (OLSR)). The authors are mainly interested in emergency situations in the immediate aftermath of a car crash and the extension

of the safety area by information exchange between the cars. They design a scenario with a line of cars on a 1 km, 3-lane motorway and conduct 3 sets of simulations with varying background data rates, number of cars, and probability errors to see the effect of background data traffic, vehicle density, and packet errors, respectively, on the performance. Probability errors are used to represent wireless channel conditions. The performance criteria of the study are delay, interpacket delay, warning delivery ratio, and overhead. The results favour flooding despite its large overhead.

In their study of 3 data dissemination techniques, the authors of [21] use a working prototype of a system for data gathering, dissemination, and visualisation. The dissemination techniques under investigation are same direction, opposite direction, and both directions. In each of these tecniques, data are broadcast periodically and nonselectively apart from the direction of the cars involved. The evaluation is based on a mathematical analysis of the broadcast utilisation, which is defined as the percentage of the newly covered area—that is, not covered previously—by a broadcast message, and on simulation. In addition to broadcast utilisation, latency time, accuracy in position estimation, and percentage of known vehicles are also used as performance criteria. Simulation results show that using vehicles moving in the opposite direction significantly improves the system's overall performance.

An investigation of various radio propagation models' impact on different VANET routing protocols is presented in [22]. Two deterministic radio propagation models, two-ray ground reflection and line-of-sight differentiation, are implemented for this purpose. A third, detailed model, taking path loss, correlated shadowing, and multipath fading into consideration and simulating signal variability, is also implemented. These models are used to compare two unicast (greedy perimeter stateless routing, GPSR, and spatially aware routing (SAR)) and one broadcast (contention-based forwarding (CBF)) routing protocols, all multihop and position-based, through computer simulation in a Manhattan grid urban scenario with obstacles (buildings) under high car density. The main performance metric of the study is packet delivery, and it is shown that there are big differences between the different radio propagation models. Signal variability, in particular, reduces link reliability and, thus, needs to be taken into account in the simulations. The general conclusion to be drawn from this part of the study is that the broadcast protocol performs better than the unicast protocols. Analysing how the three protocols behave under different radio propagation models, the authors also come to the conclusion that protocol operation also changes significantly depending on the model used. Understanding these differences helps the prediction of the geographic packet distribution and, as a result, congestion control.

3. Evaluation Scenario

As we mentioned at the beginning of this paper, the purpose of this study is to evaluate a subset of selective broadcast algorithms in light of a realistic simulation environment, so we can observe and compare their performance with regard to mission-critical safety applications. The settings of such a simulation involve the selection of an appropriate mobility model, physical (PHY) and MAC layer, and scenario-related parameters like the number of nodes in the application's safety zone, the network density (as a representation of the application's penetration rate), node speed and the distance between nodes, the way the nodes enter and leave the network, the road length, the number of lanes, the direction of the vehicular traffic, the size and interval of the emergency messages, and the properties of the background data traffic. In the following sections, we first describe the broadcast algorithms as they are implemented in our simulations. Then, we summarise how we set our realistic scenario by carefully adjusting most of the parameters mentioned above.

3.1. Selective Broadcast under Inspection. In order to evaluate the efficiency of selective broadcast in vehicular safety applications, we implemented 4 algorithms, all with different heuristics. We call the first one *naive broadcast* (NB), and it is based on [2]. In this algorithm, upon encountering an emergency situation, the first vehicle initiates a periodic broadcast sequence and starts sending warning messages. Upon receiving a warning message, other vehicles start their own periodic broadcast sequence provided that the warning comes from a vehicle in front of them. Hence, they are called repeaters. There is no additional waiting time prior to the sending of the warnings and no termination condition for the periodic broadcast.

The second selective broadcast algorithm, also based on [2], is called *intelligent broadcast* (IB). In this more intelligent version, the first vehicle initiates its sequence as in naive broadcast, but it stops sending messages as soon as it overhears another vehicle at its back sending the same message, which is a sign showing that the warning has successfully propagated further down the road. The repeaters also start their sequence as in naive broadcast, but they, too, stop if they overhear others at their back repeating the warning. In addition to their periodic broadcast interval, the repeaters must also wait for a random duration t_{wait}, where $0 \leq t_{\text{wait}} \leq t_{\max}$ and $t_{\max}$ is the maximum waiting time, before sending their messages. If, while they are waiting, the stopping condition is satisfied, they cancel their sequence immediately since there is no need to repeat the warning any more.

For the third algorithm, we made a change, inspired by [23], to intelligent broadcast. So, we call it *modified intelligent broadcast* (MIB). In this version, we put some more intelligence to the waiting time t_{wait} introduced by the repeaters prior to sending their warnings. Instead of determining t_{wait} randomly, we made it inversely proportional to the distance between the repeater and the vehicle it has just received the message from. The new waiting time is formulated as

$$t_{\text{wait}} = t_{\max}\left(1 - \frac{d}{r_{\text{trans}}}\right). \tag{1}$$

In (1), r_{trans} is the maximum transmission range. Defining the waiting time like this gives priority to the vehicles

Table 1: Simulation parameters.

Description	Value
Number of vehicles (*variable*)	20 · · · 100
Wireless transmission range (*variable*)	100 m · · · 500 m
Emergency warning size	100 B
Emergency warning interval	100 ms
Background message size	800 B
Background message interval	500 ms
Wait-before-send time (*minimum* · · · *maximum*)	0 ms · · · 10 ms
Highway segment length	2 000 m
Highway width in one direction	14 m
Highway lane width	3.5 m
Vehicle speed (*minimum* · · · *maximum*)	60 km/h · · · 120 km/h
Deceleration rate	4 m/s^2
Reaction time	1.6 s

farther away from the sender over the ones closer to it, resulting in a probabilistically fuller exploitation of the wireless transmission range and, thus, in the full coverage of the emergency zone in fewer steps.

Our fourth algorithm, originally proposed in [16], can actually be considered another variant of the three above. It is called *epidemic broadcast* (EB). According to this algorithm, the initiator and the repeaters work as in modified intelligent broadcast. The waiting time t_{wait} is selected randomly between 0 and $t_{\max}$, where $t_{\max}$ is chosen by a formula exponentially biased towards vehicles farther away from the sender. We simplified that formula and redefined the waiting time as follows:

$$t_{\text{wait}} = t_{\max} \cdot \exp\left(-\frac{d}{r_{\text{trans}}}\right). \tag{2}$$

During each broadcast interval, extended by the waiting time, the repeaters count the duplicate messages they receive from their front and their back. At the end of the waiting time, they enter a decision process instead of immediately sending their warning message. So, the forwarding decision at the end of each interval is based on the difference between the counted messages that far. The vehicles with a bigger difference have a higher probability of keeping the message alive, denoted by P_{send} and formulated in our implementation as follows:

$$P_{\text{send}} = \exp\left(-\frac{w_{\text{back}}}{w_{\text{back}} + w_{\text{front}}}\right). \tag{3}$$

In (3), w_{back} and w_{front} are the number of duplicate messages received from the back and front, respectively. Thus, the decision process favours those nodes with an unbalanced message count, which means they are closer to the edge of the sender's transmission range.

As a benchmark for the algorithms above, we included a simple flooding algorithm (FL) to our evaluation. According to this algorithm, the initiator starts a periodic sequence, and the repeaters start their own as soon as they receive their first warning. Like in the naive broadcast algorithm, there is no termination condition for the sending of the periodic warnings.

Almost all broadcasting methods proposed so far use some sort of position information [7]. In our simulation study, we therefore also assume every node to be aware of its own position and able communicate that information to the others. Various other information, like a vehicle's own type, speed, direction, and destination, can be generally considered available as well. Although not used in our evaluation, this type of secondary information is quite useful for a number of vehicular applications. Finally, background traffic is generated by a simple application issuing periodic, single-hop broadcast messages with the parameters given in Table 1. The background application runs independently on each node of the vehicular network, and a node stops its background application as soon as it receives its first emergency warning.

Figure 1 demonstrates in a simplified manner how selective broadcast generally works. In order to keep the example uncomplicated, let us assume that the vehicles implement *intelligent broadcast* for the emergency warning application. The course of events differ, of course, when one of the other algorithms described above is employed; but it is easy to follow their logic using this example as well. (a) Vehicle 1 encounters an emergency, initiates its periodic warning sequence, and broadcasts a message. The packet is received by the other vehicles within transmission range, that is, vehicles 2, 3, and 4 in our example. Upon reception, vehicles 2, 3, and 4 all enter a waiting phase of random duration. The vehicle with the shortest waiting time starts its own periodic broadcast sequence once the waiting phase is over. In our example, this is vehicle 4. (b) As vehicle 4 broadcasts its message, vehicles 2 and 3 overhear the transmission and, realising that this is the same emergency warning they are about to send, they cancel their own transmission since it is not necessary anymore. Vehicle 1, the initiator of the emergency warning, also stops its periodic broadcast sequence upon overhearing the transmission, because this is an implicit acknowledgement showing that the warning has successfully propagated backwards, that is, in the desired direction. In the meantime, vehicles 5, 6, 7, and 8 receive the warning for the first time. (c) The same procedure applies for the next step, that is, vehicles 5, 6, 7, and 8 wait for a random duration before propagating the warning. In our example, it is vehicle 7 now which has the shortest random waiting time, so it starts its periodic broadcast sequence as the waiting time is up. Receiving the warning, vehicle 4 cancels its sequence since it now knows that the warning has propagated backwards, whereas vehicles 5, 6, and 8 decide not to start their respective sequences since another vehicle within their neighbourhood already did it for them.

3.2. Simulation Settings. As our tool for discrete event simulation, we have chosen ns-3 [24], which is developed as a free software licensed under GNU GPLv2 to replace

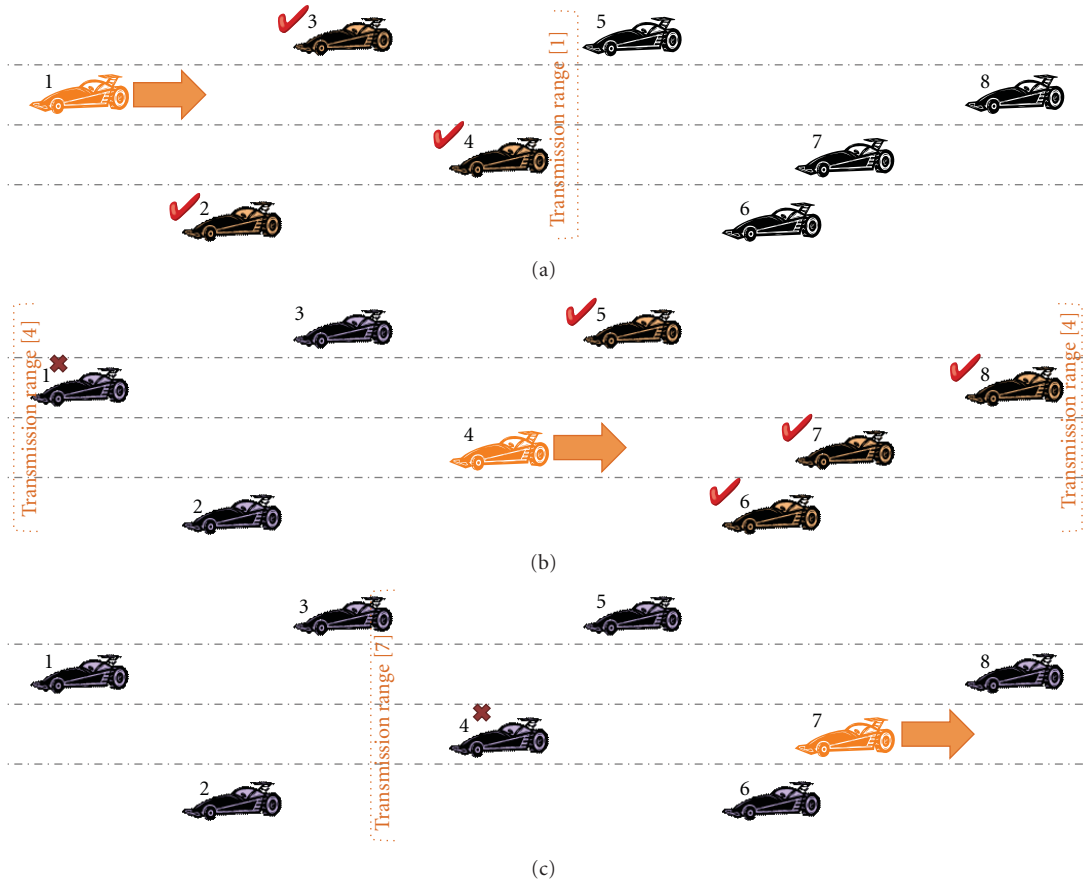

Figure 1: A demonstrative example showing three snapshots from a highway scenario with a 4-lane road segment and 8 cars: (a) periodical emergency warning broadcast is initiated by car 1. The warning is received by cars 2, 3, and 4. (b) Car 4 propagates the message. Car 1 overhears this and cancels its own broadcast sequence. Cars 5, 6, 7, and 8 receive the warning. (c) Car 7 propagates the message. Car 4 overhears it and cancels its own sequence.

eventually the very popular ns-2 [25]. ns-3 has already most of the models and functions of its predecessor and, like ns-2, is highly trusted among the network research community. Table 1 summarises the parameters and their values as we used them in our simulations.

The simulation parameters and additional settings we chose for our simulations are the result of a synthesis of various previous studies. For instance, the authors of [8] utilise periodic, one-hop broadcast for safety warnings with 10 messages per second, a maximum latency of 100 ms, and 150 m transmission range. They use IEEE 802.11p, orthogonal frequency-division multiplexing (OFDM), a 10 MHz channel, and a data rate of 3–27 Mbps. In [2], the authors define 50 vehicles moving at 32 m/s, packets of 64 B, a warning period of 100 ms, and 80–800 Kbps background traffic. They use 802.11a, prioritise the emergency communication, and introduce channel errors. Finally, the authors of [20] run simulations with 24, 45, and 60 nodes, all moving at 130 km/h, with an intervehicle distance of 130, 70, and 50 m, respectively. The emergency traffic is periodic with 10 messages per second, and the packet size is 100 B. They also generate single-hop, constant bit rate (CBR) background traffic at rates of 5, 10, and 20 packets per second with 1 KB packets. Their error probabilities are 0, 10, and 25%. Other parameters they use include a transmission range of 250 m, a carrier sense range of 550 m, a data rate of 11 Mbps, and 40 seconds of simulated time. Our target scenario represents a highway with n mobile nodes, that is, vehicles, configured as explained below.

3.2.1. Node Positioning. All vehicles are assigned a random x coordinate on the highway, chosen uniformly from the full length of the segment, as their initial position. They are also assigned a y coordinate; these, however, are chosen from integer multiples of the lane width and may not exceed the road width. The (x, y) coordinates thus put each vehicle precisely on a single lane along the highway segment. There are only two exceptions to this positioning strategy. The first one is the emergency initiator, that is, the first node to encounter the emergency situation and initiate the broadcast sequence. This node is placed on the first lane at the beginning of the highway segment. The second exception is one node put on the first lane at the very end of the highway segment, ensuring that the last node to receive a warning always has the same distance from the emergency initiator

and, thus, yielding a fairer comparison between the broadcast algorithms we evaluate. Obviously, it is very important to us to have a realistic node distribution on the road. With the highway segment and lane dimensions given in Table 1, the probabilistic average of the intervehicle distance is 80 m for 100 nodes. According to vehicular ad hoc routing studies like [26], this is a realistic value for sparse vehicular networks like the ones formed on a highway.

3.2.2. Mobility. Since, within the scope of this study, we are interested in the immediate aftermath of an emergency situation, spanning typically a few seconds, it is sufficient for our purposes to take a snapshot of the vehicular network as the warning message starts to propagate, rather than simulating the vehicular mobility in great detail. Furthermore, our work does not investigate the driver behaviour after having received the early warning message in an emergency situation, which means that the changes in mobility due to driver reactions do not need to be a part of the simulation. Thus, in our simulations, we employ a simple mobility model called *constant velocity*. In this model, a uniformly random individual speed between the minimum and maximum values given in Table 1, which does not change during the entire simulation, is assigned to each vehicle. There are also no changes in direction. It is, of course, possible to implement a more sophisticated vehicular mobility model and fine-tune further the simulation settings, such as minimum intervehicle distances or lane changing. Although interesting, these elements are currently out of scope for our study.

3.2.3. Wireless Module. Most PHY proposals are based on IEEE 802.11, and random access protocols (like carrier sense multiple access (CSMA)) are preferred to controlled access protocols (like time division multiple access (TDMA)) [4]. Furthermore, it is generally accepted that dedicated short-range communications (DSRC) may not be appropriate for all application types [15]. Therefore, we used the 802.11p standard with 5 GHz frequency range and 10 MHz data rate at 6 Mbps at the physical layer. As far as channel modelling is concerned, the current focus is on IEEE 802.11 DCF with one-hop broadcast as the basic communication type, by which MAC becomes simple CSMA. Packet reception is influenced by vehicle density, radio channel conditions, data rate, transmit power, and contention window size [8]. Two approaches can be distinguished in developing channel models. First, there are statistical models, which are faithful emulations of variations in channel behaviour in time. Second, there are deterministic models, doing exact estimations of the small scale channel fading characteristics at particular points in space and time [11]. For our purposes, we need a channel model adopting the first approach. Our wireless channel operates on the *constant speed* propagation delay model and *log-distance* propagation loss model available in ns-3. Finally, the MAC layer we chose has 4 application QoS classes with respective queues, where best effort is the default.

4. Simulation Results

In this section, we compare the performance of the four algorithms summarised above and of flooding, against a unified, realistic highway scenario. We first describe the performance criteria we consider important for the evaluation of a traffic safety application like collision avoidance. The results we achieved are presented and interpreted after that.

4.1. Performance Criteria. There are a number of performance metrics in the literature, such as packet error, loss, or delivery ratios, end-to-end delay, normalised network load, and packet duplication [27], which are typically more common for an evaluation from a pure network performance point of view. Nevertheless, we want to put more emphasis on the network's performance with respect to the mission-critical nature of the safety application running on top of it. Thus, we introduce four new performance criteria for our evaluation. We believe these will provide the reader with a clearer understanding of the various algorithms' success in fulfilling the stringent reliability requirements of the safety application. The criteria we are interested in are the following.

4.1.1. Warning Effectiveness. In an emergency situation like the possible collision of vehicles, it is of extreme importance that the application in charge of delivering the warning does the right thing. Thus, the effectiveness metric is defined as the percentage of the vehicles having received the collision warning in a timely manner at the end of the simulation. We measure this phenomenon by keeping track of the distance between the point where the emergency is initialised and the location of the vehicle as it receives the warning for the first time. Based on the emergency distance information we derive for the new recipient of the warning, and also given its speed, deceleration and driver reaction time as in [1, 2], we can determine whether a vehicle has received the warning before it is too late. Within the scope of our study, a timely delivery (i.e., before it is too late) of the emergency warning means that, by the time it receives the warning, the recipient's distance to the accident location is sufficient to stop in time.

4.1.2. Warning Efficiency. This metric is about evaluating the algorithms' ability to do things right. It is measured by observing two phenomena. The first one is the number of messages generated per vehicle until all reachable vehicles have been warned. If all the vehicles in the network can actually be reached before the simulation ends, this number gives us a per-vehicle average of the number of required warnings for a particular algorithm to cover completely the safety area. Otherwise, it gives us the average number of warnings to be sent by each vehicle to reach all the reachable vehicles. Depending on the different algorithm's heuristics, however, more messages may or may not be issued even after the last reachable vehicle has been informed on the emergency situation. This is represented by the second phenomenon we observe, that is, the total number of messages generated per vehicle until the end of the

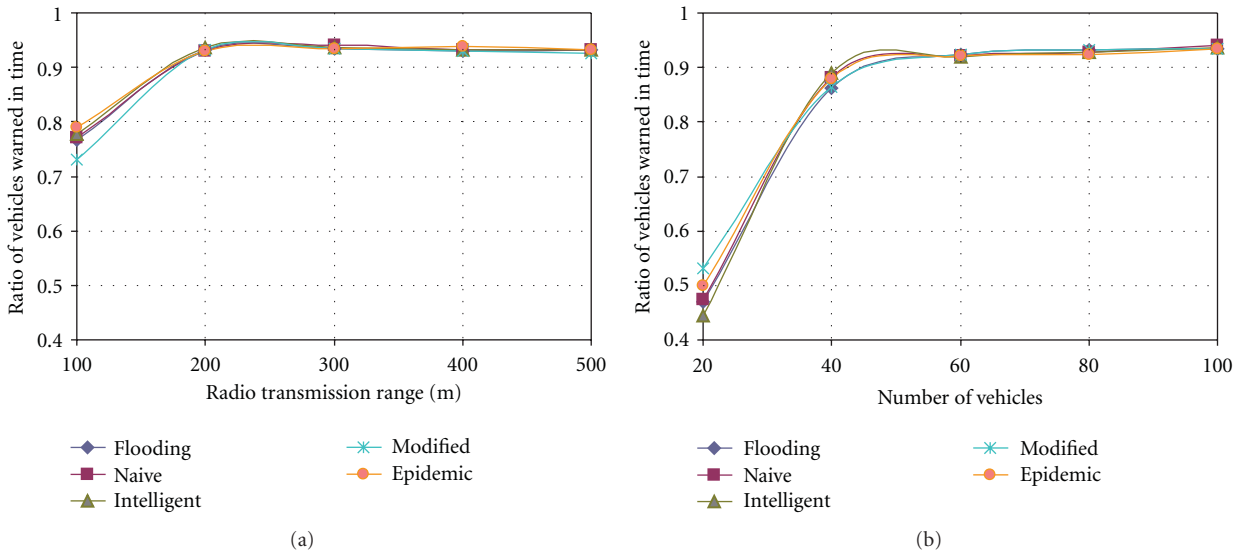

Figure 2: Warning effectiveness results, showing the algorithms' performance in terms of the ratio of vehicles warned in time as a function of (a) the transmission range for 100 vehicles and (b) the number of vehicles for 300 m transmission range.

simulation. Obviously, it is important to have a low value for the number of required messages; but it is also important to have a low value for the actual number of generated messages, which shows that the algorithm stops generating unnecessary data traffic soon enough after the last reachable vehicle has been warned.

4.1.3. Warning Propagation. The time required to reach all vehicles, or the last reachable vehicle in case not all are reachable, is the time for the algorithm to complete. So the propagation metric gives us an idea about how quickly the warning messages are disseminated throughout the vehicular network and, thus, how quickly the algorithm converges. It is easy to derive from this value the one-hop progress the packets make, which is another interesting value showing whether the algorithm can make full, or at least efficient, use of the nodes' wireless transmission range. The warning propagation time can be used as a criterion to see the effect of time of day and market penetration, both of which being represented by node density, on the success of the algorithms.

4.1.4. Warning Overhead. Based on the volume of the traffic generated by the broadcast algorithm, other network applications may be affected by the safety warning application in various levels. We observe this by generating background traffic, which represents those other applications, and measuring its packet delivery rate in the face of each of the broadcast algorithms it encounters. In our simulations, a packet is dropped at the wireless physical layer due to channel switching, collision, too small power, or random noise. The results give us an idea about the impact of our safety application on the rest of the network. The effect in the reverse direction, of course, is maybe even more important but, since our emergency message traffic is prioritised, this is beyond the scope of the study presented in this paper.

4.2. Comparison of Algorithms. In order to evaluate the algorithms we implemented, we conducted ns-3 simulations using the parameters set as shown in Table 1. We used the radio transmission range and the number of nodes in the network as our simulation variables. As we changed the transmission range between 100 m and 500 m, we fixed the number of nodes at 100. As we varied the number of nodes between 20 and 100, we set the transmission range to 300 m. This way, we were able to see the performance of the broadcast algorithms we implemented from two different perspectives, both of which we find important. We ran the simulations 100 times, all for 5 s with different random number seeds, for each algorithm described in Section 3.1 and each different value of the chosen variables. Each data point in the graphics is, thus, the average of 100 individual values, minimising the possibility of a biased result. In each simulation, background traffic starts immediately, whereas the first emergency warning is initiated 1 s into the simulation.

4.2.1. Warning Effectiveness. Figure 2 shows the performance of the algorithms in terms of warning effectiveness, described in Section 4.1, as we change (a) the transmission range, and (b) the number of nodes. Here, our criterion is the ratio of vehicles which receive the emergency warning in time, that is, when they still have a distance sufficient to stop before they collide with the car at the emergency site, taking into account the driver's reaction time as well as the car's deceleration rate.

According to Figure 2(a), all algorithms show a similar performance, especially for transmission ranges higher than 200 m. The ratio of cars they reach in time is above 0.90. The ongoing background communication between the nodes not yet received the warning causes some of the emergency packets to be dropped, and the low transmission range prevents the network from having the redundancy which

could enable the overall system to tolerate these losses. For transmission ranges as low as 100 m, all the algorithms suffer from too low network connectivity. From Figure 2(b) we can see the same trend. In sparse networks, all algorithms have a relatively low performance, that is, between 0.45 and 0.55; but they manage a success ratio as high as 0.90 as the network density increases.

4.2.2. Warning Efficiency. Figure 3 presents the results for warning efficiency, described in Section 4.1, as we change our two variables. This time, our criterion is the number of messages generated by each node in each algorithm in order to achieve the effectiveness shown in Figure 2, that is, the price paid for the above performance. Here, we see a clear distinction between the algorithms with and without selection criteria, that is, the ones incorporating a selective logic into their broadcast mechanism and the ones flooding the network. Typical values for the former group are around 1, whereas it is 39 for the latter. Here, it should also be noted that the algorithms with higher numbers of generated messages per node, that is, flooding and naive broadcast, also lack a stopping condition for their periodic broadcast, whereas the other two with very low numbers of generated messages per node, that is, intelligent and modified intelligent broadcast, benefit from their intelligent decision mechanisms for both when to broadcast a message and when to stop broadcasting. Epidemic broadcast, with its decision criterion based on the difference between the number of messages received from and against the direction of the desired warning flow, shows a mediocre performance in terms of efficiency. The main reason behind this performance is that, due to the small emergency messaging interval, the difference mentioned above is also quite small, resulting in an approximately 50% chance of relaying the warnings and increasing the number of messages per vehicle.

The number of generated warnings gives us a good idea about the cost of the broadcast algorithm's performance; but that is not all. In many cases, the number of warning messages really required to reach all reachable vehicles is less than those actually generated. In other words, the number of messages needed to warn all nodes about the emergency is usually smaller than what is shown in Figure 3. For the algorithms without a stopping condition, that is, flooding and naive broadcast, the reason for this is obvious: they just keep sending their periodical warnings. For the others, that is, intelligent, modified intelligent, and epidemic broadcast, we can say that it takes some time for the stopping condition to take action. Moreover, this condition is based on the re-reception of a warning by its sender as the message is relayed by the vehicles behind it. Thus, the condition is never met for the vehicles at the end of the vehicle cluster. Typically, the last vehicle in the safety zone defined in the simulation never stops sending periodic messages since it never overhears its own message relayed by another vehicle behind it. Thus, it is also a good idea to have a look at the difference between the number of generated and actually required (i.e., useful) messages to achieve the same warning performance.

Figure 4 shows the number of messages per vehicle actually required to cover the safety area, as we change (a) the transmission range and (b) the number of nodes. Like the results presented in the previous figure, there are three distinct groups, one with relatively high values, the other with low values, and the third with values in between. The higher values belong to flooding and naive broadcast, and it is interesting to see that, for transmission ranges higher than 200 m, the averages are around 2 messages per node, which are much lower than the averages in the previous figure. The lower values, on the other hand, belong to intelligent and modified intelligent broadcast, that is, those algorithms with stopping conditions, and the averages are very close to those in the previous figure. Epidemic broadcast, again, is placed between these two groups. The results show that a well-defined stopping condition can decrease significantly the actual cost of the emergency broadcast application by minimising the number of unnecessary warning repetition.

It is also interesting to see that, in Figure 4(b) and for flooding and naive broadcast, the number of useful warnings increases as the number of vehicles is increased from 20 to 60 and decreases again from 60 nodes to 100. The reason for that is that the network is largely disconnected when the network density is low; and the corresponding warning success rate is around 0.5, as can be seen from Figure 2(b). Due to the low number of nodes being successfully warned, the number of useful warnings also remains low. As the network becomes denser, the number of required warnings increases with the success rate. As the network becomes even denser, the success rate stabilises but it becomes possible to maintain the same rate with fewer messages due to the significant increase in the number of neighbours that can benefit from a single warning.

4.2.3. Warning Propagation. Figure 5 shows the time each algorithm requires to deliver the emergency warning to the last reachable vehicle in the safety area. As two of the algorithms we implemented, namely, modified intelligent and epidemic broadcast, try to maximise the one-hop propagation of the warning messages by setting waiting times inversely proportional to the distance between the relay node and its sender, it is particularly insightful to observe the results they achieved. According to the figure, flooding and naive broadcast do not perform as well as the other three algorithms. In other words, their average propagation time for transmission ranges higher than 200 m is around 1.2 s to 1.3 s, whereas epidemic broadcast ranks between 1.1 s and 1.2 s, and intelligent as well as modified intelligent broadcast have an average value well below 1.1 s. An interesting result in Figure 5 is that there is no significant difference in propagation time between intelligent and modified intelligent broadcasting, keeping in mind that the only difference between these algorithms is that the former defines a random waiting time prior to relaying a warning, whereas the latter employs a waiting time inversely proportional to distance.

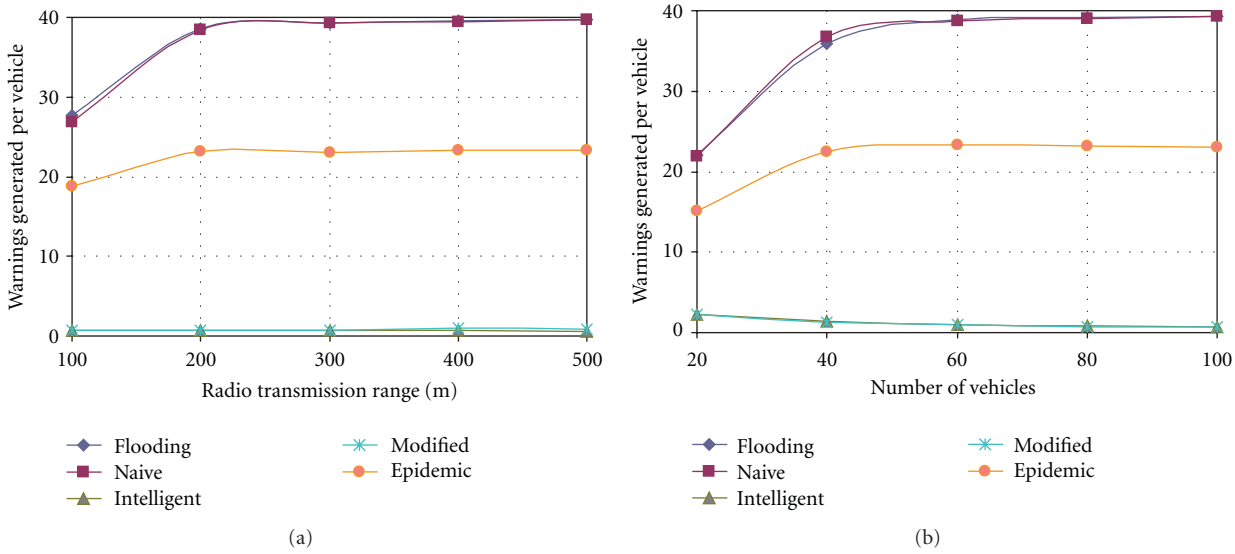

Figure 3: Warning efficiency results, showing the algorithms' performance in terms of the number of warnings generated per second by each vehicle as a function of (a) the transmission range for 100 vehicles and (b) the number of vehicles for 300 m transmission range.

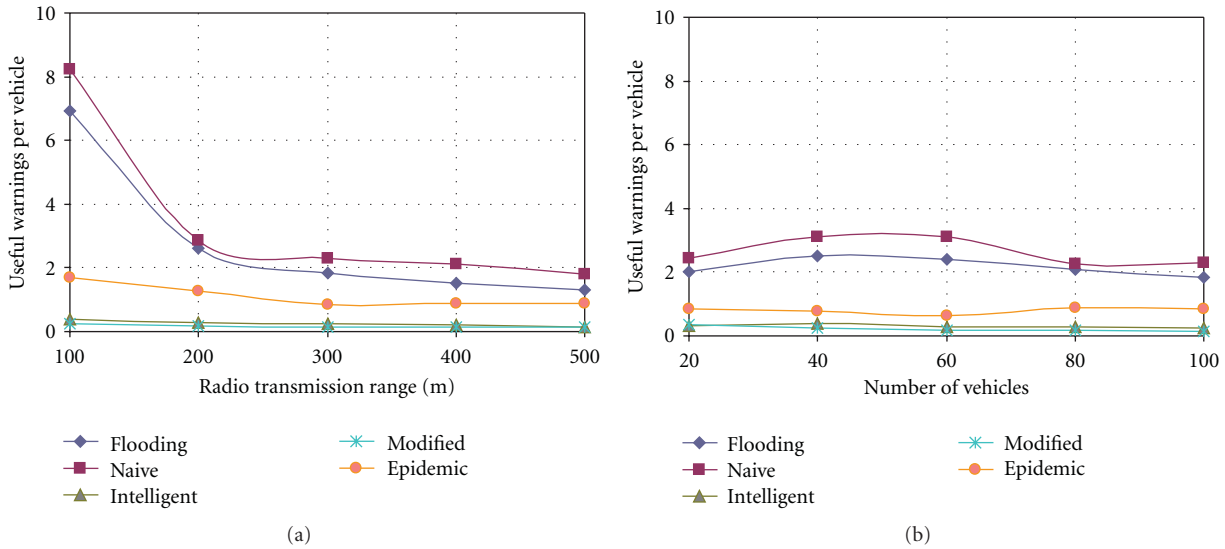

Figure 4: Warning efficiency results continued, showing the algorithms' performance in terms of the number of useful warnings (i.e., actually required to warn a new node) generated per second by each vehicle as a function of (a) the transmission range for 100 vehicles and (b) the number of vehicles for 300 m transmission range.

4.2.4. Warning Overhead. Finally, we observe the effect of the data traffic generated by the emergency warning application on other applications likely to be running in the network at the same time. Even though the emergency warning application has higher priority, that is, nodes are supposed to cease all other traffic as soon as they receive their first warning message, at any given time, there will be nodes in the network not having received the warning yet. Thus, these nodes' background data traffic is bound to be affected by the overhead created by the emergency application, and we need to evaluate this. Figure 6 shows the delivery ratio of the packets belonging to the background applications. The results show that all the emergency broadcast algorithms we tested have a similar impact on the background traffic, which seems counterintuitive. Given that they all incur different amounts of overhead on the network, as shown in Figure 3, one would expect to see a significant difference here. However, the frequency of the background traffic generation is much lower than that of the emergency application, and the propagation of the emergency warning is relatively fast, so that most of the background traffic is indeed ceased very quickly and regardless of the overhead of the emergency application. On the other hand, the background data's successful delivery rate decreases drastically as the

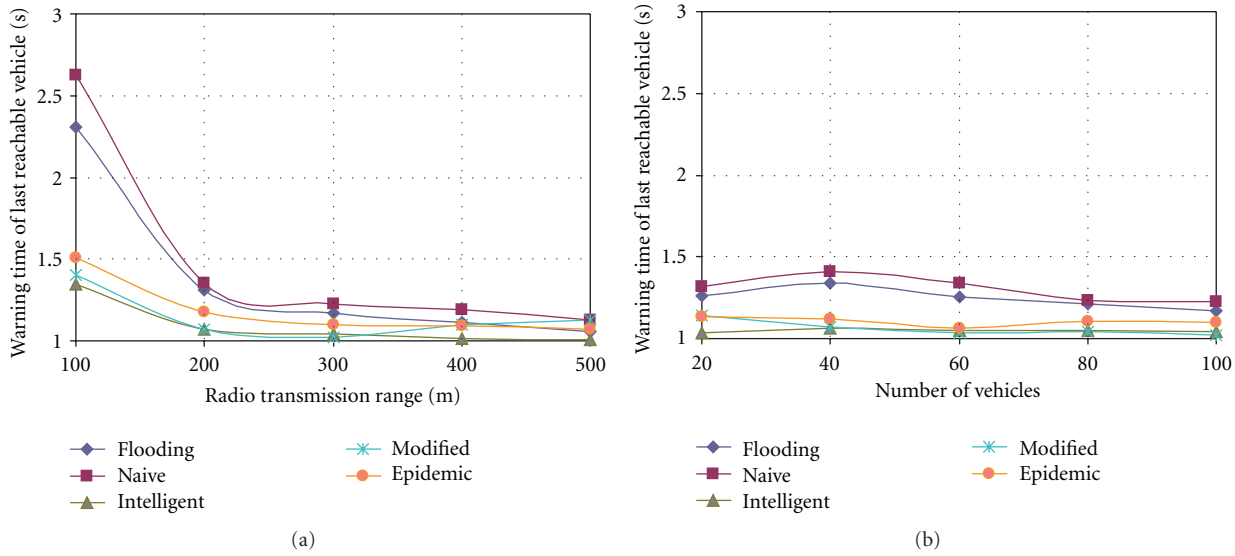

Figure 5: Warning propagation results, showing the algorithms' performance in terms of the time required to inform the last reachable vehicle as a function of (a) the transmission range for 100 vehicles, and (b) the number of vehicles for 300 m transmission range.

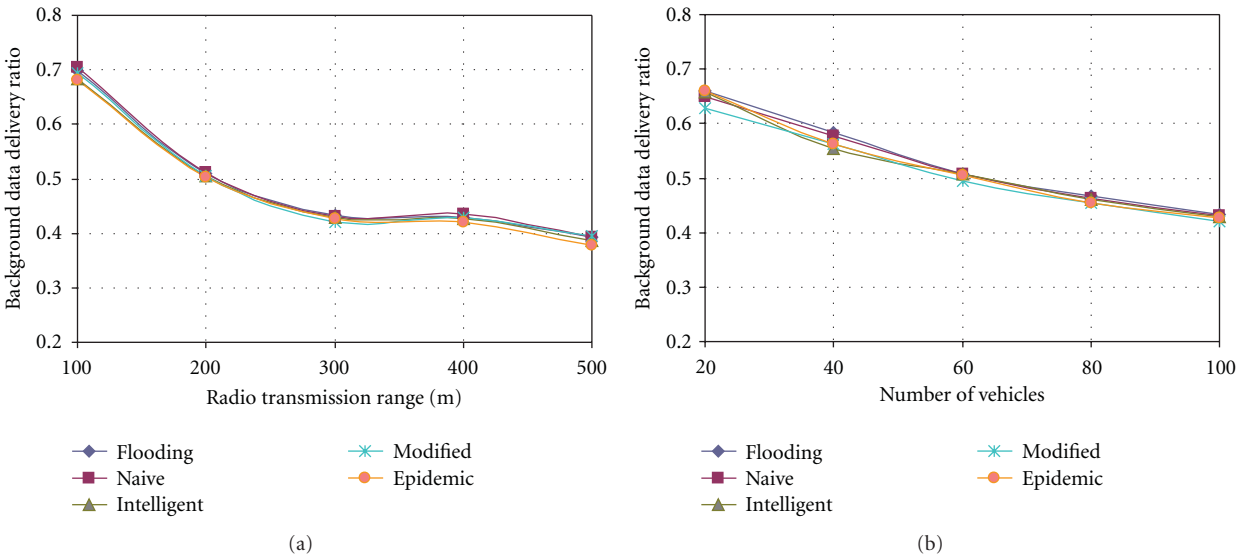

Figure 6: Warning overhead results, showing the algorithms' performance in terms of the ratio of background application data packets successfully delivered per vehicle as a function of (a) the transmission range for 100 vehicles and (b) the number of vehicles for 300 m transmission range.

transmission range increases from 100 m to 300 m or the number of nodes increases from 20 to 100, due to more nodes sharing the wireless spectrum.

5. Conclusion

Emergency warning applications using VANET have gained great interest as a powerful means of improving road safety. However, their time- and life-critical field of operation requires high QoS standards in terms of reliable, timely, and guaranteed message delivery. As mentioned in the introduction, the key to the successful dissemination of safety warnings is the mechanism to decide when to start and stop message relaying. The algorithms developed for information dissemination in VANET must meet these requirements so we can use them for these applications. In this paper, we compare the performance of a subset of selective broadcast algorithms in a unified simulation scenario, that is, under the same conditions, to see how well they cope with the criteria mentioned above.

For our evaluation, we use four new performance metrics to measure the effectiveness, efficiency, timeliness, and overhead of the algorithms. The results we obtain favour selective broadcast algorithms with intelligent decision mechanisms regarding their starting and stopping conditions. The results can be further interpreted as follows. First, periodicity improves significantly the success rate of the algorithm, due to the fact that, by creating redundancy, it helps the vehicular network to tolerate eventual packet losses. In an emergency scenario, especially when the transmission range is not high, it is simply too risky for a node to broadcast a warning only once. Second, it is more important to have some selection criteria (at all) about when to start relaying emergency messages than to employ the most sophisticated mechanism optimising the selection in question. A simple, random wait-before-send logic can achieve the same performance as a more complex, distance-based logic formulated by exponential functions, as confirmed by the fact that there is no significant difference in the performance of intelligent and modified intelligent broadcast. Finally, the stopping condition is not less important than the starting condition. If they employed stopping conditions, algorithms like flooding and naive broadcast would have better efficiency and overhead results.

The results we present show that much work remains to be done to realise safety applications with 100% reliability, so they can be widely and safely used in vehicles. Our evaluation is a contribution to the efforts in this direction; the results we obtain from our simulations help us to understand better the design requirements of a high-performance selective broadcast algorithm. It is necessary, on the other hand, to improve the simulation itself in order to achieve a platform which can evaluate the algorithms under investigation as fairly as possible, producing results as close to the real world as possible. For instance, the effect of background traffic on the emergency messages can be investigated for situations in which there are no application priorities. More accurate mobility models can be incorporated into the simulations, containing elements for changing lanes, keeping the safety distance, platooning, and driver behaviour. Concerning the wireless communication infrastructure, more realistic PHY conditions can be made part of the simulation if appropriate channel error and propagation loss models are included. Our research plan for the near future is to address some of these issues and, currently, we are working on an adaptive selective broadcast algorithm and the integration of a new propagation loss model based on real-life measurements into our simulations.

Acknowledgment

This work is partly funded by Excellence Center at Linköping-Lund in Information Technology (eLLIIT). K. Bür and M. Kihl are members of Lund Center for Control of Complex Engineering Systems (LCCC), a Linnaeus Center at Lund University, funded by the Swedish Research Council. M. Kihl is partly funded by the VINNMER program at the Swedish Governmental Agency for Innovation Systems (VINNOVA).

References

[1] P. L. Olson and M. Sivak, "Perception-response time to unexpected roadway hazards," *Human Factors*, vol. 28, no. 1, pp. 91–96, 1986.

[2] S. Biswas, R. Tatchikou, and F. Dion, "Vehicle-to-vehicle wireless communication protocols for enhancing highway traffic safety," *IEEE Communications Magazine*, vol. 44, no. 1, pp. 74–82, 2006.

[3] P. Papadimitratos, A. La Fortelle, K. Evenssen, R. Brignolo, and S. Cosenza, "Vehicular communication systems: enabling technologies, applications, and future outlook on intelligent transportation," *IEEE Communications Magazine*, vol. 47, no. 11, pp. 84–95, 2009.

[4] Y. Toor, P. Muhlethaler, and A. Laouiti, "Vehicle ad hoc networks: applications and related technical issues," *IEEE Communications Surveys and Tutorials*, vol. 10, no. 3, pp. 74–88, 2008.

[5] M. Kihl and M. Sichitiu, "Inter-vehicle communication systems: a survey," *IEEE Communications Surveys and Tutorials*, vol. 10, no. 2, pp. 88–105, 2008.

[6] F. Li and Y. Wang, "Routing in vehicular ad hoc networks: a survey," *IEEE Vehicular Technology Magazine*, vol. 2, no. 2, pp. 12–22, 2007.

[7] W. Chen, R. K. Guha, T. J. Kwon, J. Lee, and I. Y. Hsu, "A survey and challenges in routing and data dissemination in vehicular ad-hoc networks," in *Proceedings of IEEE International Conference on Vehicular Electronics and Safety*, pp. 328–333, Columbus, Ohio, USA, 2008.

[8] H. Hartenstein and K. P. Laberteaux, "A tutorial survey on vehicular ad hoc networks," *IEEE Communications Magazine*, vol. 46, no. 6, pp. 164–171, 2008.

[9] M. Kihl, "Vehicular network applications and services," in *Vehicular Networks: Techniques, Standards, and Applications*, CRC Press, 2009.

[10] A. F. Molisch, F. Tufvesson, J. Karedal, and C. F. Mecklenbräuker, "A survey on vehicle-to-vehicle propagation channels," *IEEE Wireless Communications*, vol. 16, no. 6, pp. 12–22, 2009.

[11] D. W. Matolak, "Channel modeling for vehicle-to-vehicle communications," *IEEE Communications Magazine*, vol. 46, no. 5, pp. 76–83, 2008.

[12] C. X. Wang, X. Cheng, and D. Laurenson, "Vehicle-to-vehicle channel modeling and measurements: recent advances and future challenges," *IEEE Communications Magazine*, vol. 47, no. 11, pp. 96–103, 2009.

[13] R. Uzcategui and G. Acosta-Marum, "Wave: a tutorial," *IEEE Communications Magazine*, vol. 47, no. 5, pp. 106–133, 2009.

[14] T. Kosch, I. Kulp, M. Bechler, M. Strassberger, B. Weyl, and R. Lasowski, "Communication architecture for cooperative systems in Europe," *IEEE Communications Magazine*, vol. 47, no. 5, pp. 116–125, 2009.

[15] X. X. Diao, J. J. Li, K. M. Hou, H. Y. Zhou, and A. Jacquot, "Cooperative inter-vehicle communication protocol dedicated to intelligent transport systems," in *Proceedings of the New Technologies, Mobility and Security Conference and Workshops (NTMS '08)*, pp. 1–5, Tangier, Morocco, November 2008.

[16] M. Nekovee, "Epidemic algorithms for reliable and efficient information dissemination in vehicular ad hoc networks," *IET Intelligent Transport Systems*, vol. 3, no. 2, pp. 104–110, 2009.

[17] R. Fracchia and M. Meo, "Analysis and design of warning delivery service in intervehicular networks," *IEEE Transactions on Mobile Computing*, vol. 7, no. 7, pp. 832–845, 2008.

[18] M. Mariyasagayam, T. Osafune, and M. Lenardi, "Enhanced Multi-Hop Vehicular Broadcast (MHVB) for active safety applications," in *Proceedings of International Conference on Intelligent Transport Systems Telecommunications*, pp. 1–6, Sophia Antipolis, France, 2007.

[19] E. Fasolo, A. Zanella, and M. Zorzi, "An effective broadcast scheme for alert message propagation in vehicular ad hoc networks," in *Proceedings of IEEE International Conference on Communications*, vol. 1, pp. 3960–3965, Istanbul, Turkey, 2006.

[20] P. Muhlethaler, A. Laouiti, and Y. Toor, "Comparison of flooding techniques for safety applications in VANETs," in *Proceedings of International Conference on Intelligent Transport Systems Telecommunications*, pp. 1–6, Sophia Antipolis, France, 2007.

[21] T. Nadeem, P. Shankar, and L. Iftode, "A comparative study of data dissemination models for VANETs," in *Proceedings of International Conference on Mobile and Ubiquitous Systems*, pp. 1–10, San Jose, Calif, USA, 2006.

[22] R. Bauza, J. Gozalvez, and M. Sepulcre, "Operation and performance of vehicular ad-hoc routing protocols in realistic environments," in *Proceedings of IEEE Vehicular Technology Conference*, pp. 1–5, Calgary, Canada, September 2008.

[23] L. Briesemeister and G. Hommel, "Role-based multicast in highly mobile but sparsely connected ad hoc networks," in *Proceedings of Mobile and Ad Hoc Networking and Computing*, pp. 45–50, Boston, Mass, USA, 2000.

[24] The ns-3 network simulator, 2010, http://www.nsnam.org/.

[25] The network simulator ns-2, 2010, http://www.isi.edu/nsnam/ns/.

[26] N. Wisitponghpan, F. Bai, P. Mudalige, V. Sadekar, and O. Tonguz, "Routing in sparse vehicular ad hoc wireless networks," *IEEE Journal on Selected Areas in Communications*, vol. 25, no. 8, pp. 1538–1556, 2007.

[27] Y. H. Ho, A. H. Ho, and K. A. Hua, "Routing protocols for inter-vehicular networks: a comparative study in high-mobility and large obstacles environments," *Computer Communications*, vol. 31, no. 12, pp. 2767–2780, 2008.

Hindawi Publishing Corporation
International Journal of Vehicular Technology
Volume 2011, Article ID 486975, 12 pages
doi:10.1155/2011/486975

Research Article

Time in Privacy Preserving LBSs: An Overlooked Dimension

Luciana Marconi,[1] Roberto Di Pietro,[2] Bruno Crispo,[3] and Mauro Conti[4]

[1] *Dipartimento di Informatica, Sapienza Università di Roma 00185, Roma, Italy*
[2] *Dipartimento di Matematica, Università di Roma Tre, Roma, Italy*
[3] *Dipartimento di Ingegneria e Scienza dell'Informazione, Università di Trento 38122, Trento, Italy*
[4] *Department of Computer Science, Vrije Universiteit Amsterdam, 1081 Amsterdam HV, The Netherlands*

Correspondence should be addressed to Luciana Marconi, marconi@di.uniroma1.it

Received 16 October 2010; Revised 23 January 2011; Accepted 27 January 2011

Academic Editor: Cristina Pinotti

A new privacy model for Location-Based Services (LBSs) has been recently proposed based on users' footprints-these being a repre-sentation of the amount of time a user spends in a given area. Unfortunately, while the model is claimed to be independent from the specific knowledge of the adversary about users' footprints, we argue that an adversary, that has a more structured knowledge over time, can pose a threat to the privacy guarantees of the model. The major contribution of this paper is to show that time is a relevant dimension that needs to be taken into consideration when investigating LBSs privacy issues. In particular, we show that applying our considerations, user privacy can be violated. We support our claim with analysis and a concrete example. Furthermore, by analyzing a real data set of vehicular traces, we show that the threat is actually present in a real scenario and that its effect on jeopardizing user privacy is relevant.

1. Introduction

Location-Based Services (LBSs) can be defined as services that add value to a user integrating his mobile device's location with additional information. Hence, the localization feature can be considered the main characteristic of a Location-based service. LBSs can be regarded as a subset of context-aware applications [1], the most basic context being the user's location. Context information is used to deliver a service and to add value to the service by adapting it to the user's personal context.

LBSs are widely spreading, particularly leveraging the use of mobile devices. As an example, we can consider the vehicular services that many national transportation infrastructures are developing: traffic monitoring, hazard warning, congestion-based, and "pay-as-you-go" road pricing [2, 3]. However, this type of services are subject to a privacy threat: the possibility to identify the user that requests a given service and her location at the time of the request. Even when privacy mechanisms are taken into consideration to anonymize the users, a user might be reidentified correlating the access information with other kind of information (e.g., the mobility of the user or some specific location-bound feature). In particular, there are three main issues related to the privacy of users in LBSs (i) how to anonymize a user; (ii) how to specify the level of anonymity; and, (iii) how to guarantee to a given user the same level of desired anonymity for all of her requests. Common anonymization techniques leverage the concept of k-anonymity (i) consisting in cloaking the user within a set of k potential users. The *feeling*-based model, recently introduced [4, 5], also leverages the concept of k-anonymity. However, this model is motivated by the fact that specifying a practical value of k could be a difficult choice for the user. Hence, the feeling-based model allows a user to define her desired level of anonymity (ii) by specifying a given area (e.g., a shopping mall). The entropy of the selected area is used to describe its popularity. In turns, the popularity is expressed in terms of footprints of the visitors in the selected area. The popularity of the user-specified area is considered later on, in the subsequent user's LBSs requests, as the anonymization level that the LBS has to guarantee to the user (iii).

While the feeling-based approach seems to be promising from the point of view of user's awareness of privacy, we

argue that the specific proposed solution is missing an important variable: time. In fact, the threat model considered in the proposals [4, 5] assumes an adversary having the same amount of information on the users as the one leveraged by the anonymizer. While this might seem a strong adversary model, it actually does not take into consideration practical aspects related to the distribution of such a knowledge over time. In particular, we consider both of the following situations to be practical. First, the adversary might have the information of the users footprints structured over time (e.g. how many footprints in the *morning* and how many in the *afternoon*). Second, the adversary might just be able to observe a subset of the footprints (e.g., the adversary is only able to get footprints information during the *morning*). While in the first case the adversary is stronger than the one consider in [4, 5]—having more structure data—the second scenario describes a weaker (but more realistic) adversary—basing its decisions on depleted information. We further underline that both of these adversary models fall into the assumption given in [4, 5] about the adversary.

In this work, we highlight the importance of the time when providing privacy in Location-based Services. We first show how user privacy can be violated leveraging time, with respect to the solutions in [4, 5]. In particular, we investigate on the provided privacy considering a different, more realistic adversary model. We argue that the newly introduced adversary is realistic and that it can also be weaker in terms of the amount of users information available, but still effective. We introduce our claim through a practical example; we then support and verify the claim with simulations and analysis on a real data set of vehicles' traces. The rest of the paper is organized as follows. Section 2 describes the related work in the area. Section 3 defines the notion of time and presents the threat model and the feeling-based privacy model. Section 4 shows how user privacy can be violated applying our considerations; we support our claim with both analysis and a practical example. Section 5 discusses and compares results from the analysis of a real data set. Section 6 argues about a viable approach under assumptions sligthly different from the ones in [4, 5]. Finally, Section 7 reports some concluding remarks.

2. Related Work

One of the main issues that slow down the large-scale adoption of LBSs is privacy [6]. In particular, given the peculiarity of these services (e.g., particularly relevant to mobile user devices), the privacy solutions already designed for other environments—like the ones based on k-anonymity [7–9]—result not portable into this context.

The main aspect related to the anonymization of LBSs regards the users mobility. In fact, mobile users ask for LBSs from different locations that correspond either to their current position or other positions of their interest. The first approach [10] for location anonymity aimed at applying the k-anonymity concept. The proposal was to reduce the accuracy of the definition of the user location (defined by both space and time) when asking for an LBS. The aim of reducing this accuracy was to cloak the requesting user within $k - 1$ other users, present in a broader area and consider a broader time frame. However, increasing the area would lead to a coarser service, while increasing the time frame would lead to a delay of the user's request.

Several works leveraged on the basic concept introduced in [10]. For example, the CliqueCloak algorithm [11] aims at minimizing the size of the cloaking area, while allowing the user to specify the value of k. However, this solution is practicable only for small values of k and requires a high computation overhead. The work in [12] generates a cloaking area in polynomial time and also considers attacks that correlate periodic location updates. The possibility of choosing k is also considered in [13], without considering the minimization of the cloaking area. Further work [14] provides a solution for mobile peer-to-peer environment, where the cloaking area is determined in a distributed way. The spatial cloaking algorithm proposed in [15] distinguishes between location privacy (i.e., a user willing to hide her location) and query privacy (i.e., a user can have her location revealed, but not her query). The aim is to prevent the adversary to link the user location to the submitted query. The motivation stems from the fact that in many applications the locations of mobile users is publicly known.

All these works do not explicitly consider the fact that nodes move, and their location-related request might be correlated. This issue has been first addressed by some works [16, 17] intended to cope with nodes tracing. However, these solutions were not developed having LBSs privacy in mind. In fact, they all report the actual user location. In particular, the work in [16] introduced the concept of mix zone—a zone where nodes avoid reporting their locations and exchange their identification instead. The aim of a mix zone is to make it hard for an adversary to correlate the pseudonym that a node used before entering the mix zone, and its pseudonym once it is out of the mix zone. Selfish behaviour of the nodes in mix zones has also been considered recently [18], as well as how pseudonyms aging affects privacy [19]. An idea similar to the one of mix zone is *path confusion* [17, 20]—pseudonyms are exchanged between nodes that have paths close to each other. The mix zone concept is also applied in [21] to protect the location privacy of drivers in vehicular networks (Vanet). The idea is to combine mix zones with mix networks that leverage on the mobility of vehicles and the dynamics of road intersections to mix identifiers.

The solution proposed in [22] requires that each LBSs request comes together with at most $k - 1$ dummy requests that simulate the movement of nodes. However, the dummy traces do not take into consideration the actual geography of the area where the corresponding dummy user is expected to be—such type of anomalies could let the adversary identify the dummy requests. Trajectory anonymization is also considered in [23], increasing the cloaking area to include exactly $k - 1$ other users. Unfortunately, continuously increasing the cloaking area degrades the precision of the LBSs.

The special case of providing location privacy in Vanet has been addressed in [24]. In this work, authors observed how Vanet poses specific constraints to mobility of nodes (vehicles)—the movement being spatially restricted (to lanes and freeways) and dependent (among vehicles). To tackle these unique characteristics and they proposed a scheme

that leverages pseudonyms with some enhancing features (i) increasing silent period between subsequent broadcast messages to obtain pseudonyms' unlinkability; (ii) grouping vehicles in geographical proximity to avoid overhearing of pseudonyms. As for vehicle-to-infrastructure communication, a privacy preserving mechanism can be found in [25].

A slightly different problem, that is avoiding reporting information about sensitive areas (e.g., a night club), has also been addressed [26]. Here, anonymization is achieved using areas instead of users. In fact, the reported location should include k sensitive areas instead of k users. Similarly, the framework proposed in [27] provides obfuscation of sensitive semantic locations-based on the privacy preference specified by each user. The solution uses a probabilistic model of space—the semantic locations being expressed in terms of spatial features—and does not take time into account. The solution proposed in [28] aims to avoid reporting the user location. The technique applies a Private Information Retrieval protocol to let the user of the service to download directly the LBSs information without requiring a trusted anonymizer. However, as the amount of data to be downloaded by the user depends on the total amount of data stored by the service provider, it may be impractical for a mobile device.

A problem strictly related to the protection of the user location privacy is the quantification of the "privacy level" guaranteed by several solutions. The solution in [20] quantifies location privacy as the duration over which an attacker could track a subject. The expected error in distance between a person's current location and an attacker's uncertain estimate of that location is used in [17]. The number of users k represents the level of privacy in [10] where k-anonymity is introduced for location privacy. Other works derive metrics from information theory [29]. For instance, entropy is the privacy quantifier used in [5, 16]. Whatever location privacy metric is adopted, it is maximized if no one knows a subject's location. Hence, the majority of the proposed solutions can be considered a trade-off between location privacy and quality of service. Some interesting solutions to location privacy in WSNs (Wireless Sensor Networks), sharing some common points with LBSs, have already been proposed. In particular, solutions in [30, 31] achieve privacy when querying a WSN, but sensors are required to partake logical hierarchy. Open problems highlights and related solution guidelines for a general privacy model in WSNs are in [32].

The problem of anonymity of trajectories has also been considered in other contexts. For instance, the work in [33] proposes a privacy-aware data publishing perspective. Differently from the LBS context, where the anonymity is centered on the Location-based service, authors of [33] consider an off-line and data-centric anonymity on a database of moving objects. The anonymization is enforced before the database is made public—the aim being to preserve privacy of people releasing the data to the public.

In our work, we show that leveraging time-frame provides an adversary with a powerful tool to compromise privacy in LBSs. A preliminary investigation, without real data analysis and consequent discussion, appeared in [34]. In particular, we show an application of this concept by compromising the privacy claimed in [4, 5], where the feeling-based model is introduced. Being a reference also for this paper, we recall this model in Section 3.3. Finally, our findings are consistent with the recent proposal in [35] where time is considered one of the aspects to take into account to protect user location.

3. Preliminaries and Notation

In this section, we propose models and definitions used in the paper. Section 3.1 introduces the system model. Section 3.2 formalizes the notion of time applied to time-related concepts analyzed throughout this work. Section 3.3 gives an overview of the solutions proposed in [4, 5], while the threat model description can be found in Section 3.4.

3.1. System Model. We consider the same system architecture used in [4, 5]. We assume mobile nodes (users) communicating with location-based services (LBSs) providers through a central anonymity server, the location depersonalization server (LDS), which is considered trusted. The LDS is managed by some mobile service provider allowing the (mobile) users to access to wireless communications. The provider offers the depersonalization service as an added value service and supplies the LDS with an initial footprints database derived from users phone calls.

3.2. Formalizing Time. Consistently, with the literature [35], we consider a discrete timeline, starting from time t_0—this time corresponding to the deployment of the system. Hence, we formalize the notion of time with the following definitions.

Definition 1 (time unit). The smallest measurable time unit we consider in our discrete time-line.

Definition 2 (time period). A time period is a predetermined number (ℓ) of contiguous time units, $\ell \in \mathbb{N}^+$. We denote periods with p_i, $0 \leq i \leq \rho$, ρ being the number of periods from the system start-up.

Definition 3 (time slice). A time slice of a period p is defined to be a time interval of a predetermined length $s < \ell$. We denote time slice j of time period p with T_j^p.

Thus, a time period is composed of $q = \ell/s$ time slices. We assume, without loss of generality, that $q \in \mathbb{N}$.

Definition 4 (time frame). A time frame is defined to be the set obtained as the union of the ith time slice of each period. We denote a time frame with $\widehat{T}_i$. Hence, $\widehat{T}_j = \{T_j^{p_0}, T_j^{p_1}, \ldots, T_j^{p_\rho}\}$.

For a practical discussion, time parameters to be fixed are thus the length ℓ of the period and the length of the time slice s. As an example, if we fix ℓ to be one week, and s to be one day, the period p is set to be the pth week, T_1^p = Sunday, T_2^p = Monday, $\ldots$, T_7^p = Saturday represent the days of the pth week.

3.3. Feeling-Based Privacy Model. The aim of the work in [5] is to provide location privacy protection for users requesting location-based services enhancing the k-anonymity model. The privacy model proposed introduces the concept of feeling-based privacy, based on the intuition of privacy being mainly a matter of feeling. The user is allowed to express a privacy requirement by specifying a spatial region in which she would feel comfortably cloaked (public region). Their solution then transforms the intuitive notion of user privacy feeling, in a quantitative evaluation of the level of protection provided, using the user-specified region. They define the entropy of a spatial region to measure the popularity of that region. This popularity is then used as the quantity describing the user privacy requirement: the popularity of the location disclosed by the anonymizer on behalf of the user, is required to be at least that of the specified public region. Formally, they provide the following definitions.

Definition 5 (entropy). Let R be a spatial region and $S(R) = \{u_1, u_2, \ldots, u_m\}$ be the set of users having footprints in R. Let $n_i (1 \leq i \leq m)$ be the number of footprints that user u_i has in R, and $N = \sum_{i=1}^{m} n_i$. The entropy of R is defined as $E(R) = -\sum_{i=1}^{m} (n_i/N) \cdot \log(n_i/N)$.

Definition 6 (popularity). The popularity of R is defined as $P(R) = 2^{E(R)}$.

The entropy is used to address the problem of the possible dominant presence of some users in a certain region. This phenomenon makes the number of visitors of a region not sufficient to quantify its popularity. The property that $P(R)$ is higher if m is larger is preserved even using entropy: a region is more popular if it has more visitors. Also, a skewed distribution of footprints significantly reduces the $P(R)$ with respect to a symmetric distribution. The entropy is also intended by the authors as the amount of additional information needed for the adversary to identify the service user from $S(R)$ when R is reported as her location in requesting an LBSs.

3.4. Threat Model. In this section, we present the threat model we consider. In particular, we define two types of adversary: ADV and ADV^T, both satisfying the assumptions provided in [5]. In particular, ADV mimics the adversary considered in [4, 5]. ADV is able to identify users in a cloaking region correlating with restricted spaces. However, it will not be able to reidentify the user who requests the service. We assume the adversary being present from time t_0, that is from the system deployment. Hence, we observe that the adversary may coincide with the LBSs provider. In fact, it could be highly interested in exploiting the location knowledge (historical) of the LDS anonymizer—potentially motivated by commercial or marketing purposes. Thus, ADV and LBSs will be used interchangeably throughout the paper.

Some existing techniques use current location of k neighbours of the service requester to protect from the adversary and to calculate the cloaking area. These techniques protect the anonymity of the service users but not their location privacy. An adversary identifying the users in the cloaking area knows their locations as it is aware of their presence in the cloaking area at the time of the service request.

The idea to use footprints, that is historical data, makes the adversary weaker as it is not able to know neither who requested the service nor who was really there at the time of the service request. From this core idea, introduced in [4] and applied by the same authors to mobile user's trajectory can be extracted in [5], another implicit assumption: the indistinguishability for the ADV between current and historical visitors of the cloaking area. This is equivalent to assume that ADV can not have instantaneous access to current users location data. If this will be the case, the usage of historical locations would not be suitable to compute the cloaking box for depersonalization. As an example, let us suppose the LDS reporting a cloaking area for a user, based on a five footprints (historical) calculation. If the user is the only one actually in that area and the LBSs knows the user location at each time instant, the latter would immediately identify the service requester. Thus, we also assume the users location knowledge held by the adversary to be the footprints information provided by the LDS anonymizer. We denote such a knowledge with LK.

In this work, we also consider a time-aware adversary, ADV^T, that has just additional information on time frames. Hence, we assume ADV^T has the same knowledge of ADV (the footprints information database), with the difference that such a knowledge takes also into account the different time frames $\hat{T}_j$. We denote ADV^T knowledge with LK^T. We can observe that the knowledge of ADV^T might be lower than the knowledge of ADV as it could know footprints information regarding just a portion of the time slices. Figure 1 illustrates the comparison of the knowledge of the two adversaries. For example, Table *daily* stands for the footprints data information of ADV. Table *morning* and Table *afternoon* stand for the footprints data information in Table *daily*, split on two time frames. We assume that ADV^T may know both Table *morning* and Table *afternoon* or, in a weaker version, just one of the two.

Hence, two scenarios may apply to ADV^T: it has the same user footprints information of ADV split on time frames, or ADV^T has less user footprints information than ADV, having footprints information only for some time frames.

Table 1 summarizes the notation used in this work.

4. Time Warp: Facing The Time-Aware Adversary

In this section, we aim to investigate on the privacy guaranteed by the solution in [5] when facing ADV^T. Section 4.1 introduces the adversary model used and an example showing how user privacy can be violated. Section 4.2 provides an evaluation of the adversary effectiveness against the privacy guarantees of the protocol in [5].

4.1. The Time-Aware Adversary Model. Our adversary model is motivated by the fact that the privacy of user's location may be highly influenced by the time frames considered. For instance, we might refer to several real scenarios: a theatre is

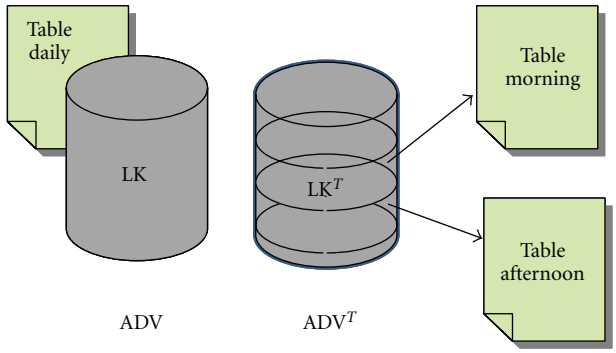

Figure 1: ADV and ADV^T footprints location knowledge.

Table 1: Notation table.

R	A spatial region
$S(R)$	Set of users having footprints in R
$E(R)$	Entropy of region R
$P(R)$	Popularity of region R
p_i	ith time period, $0 \le i \le \rho$
ρ	Number of periods from system start-up
T_i^p	ith time slice of a period p
q	l/s, number of slices composing a period
$\hat{T}_j$	Time frame $\hat{T}_j = \{T_j^{p_0}, T_j^{p_1}, \ldots, T_j^{p_\rho}\}$
$E(R, \hat{T}_j)$	Entropy of region R, during time slice x of time period p
$P(R, \hat{T}_j)$	Popularity of region R, for time frame $\hat{T}_j$
u_i	Generic ith user of a set of users, $1 \le i \le m$, $m \in \mathbb{N}$
$u_{i,\hat{T}_j}$	Generic ith user who have footprints in R in time frame $\hat{T}_j$
n_i	Number of footprints of user u_i in R
$n_{i,\hat{T}_j}$	Number of footprints of user u_i in R in time frame $\hat{T}_j$
N	Total number of footprints in a region R

a physical place where users concentrate only on particular days and in specific time frames, restaurants are most likely to be crowded at lunch and dinner time, and, office buildings are supposed to be almost empty during night. We show that with the knowledge held by ADV^T, the LDS is no more able to guarantee to users the claimed level of privacy. Further, we will also show scenarios where the entropy of the user public region is actually lower than the entropy calculated by the LDS. Therefore, the adversary will need less effort—with respect to what assumed by the LDS—to identify the user. Further, We will show that ADV^T may be more effective than ADV even if provided with less knowledge. This, as we will formally show at the end of this section, is due to the fact that time severely affects the entropy and the popularity of a cloaking region. This may result in a reduced amount of additional information needed for the adversary to identify the service user (see Section 3.3).

Definition 7 (entropy in $\hat{T}_j$). Let R be a spatial region and $S(R, \hat{T}_j)$ the set of users who have footprints in R, if observed during time frame $\hat{T}_j$, that is, $S(R, \hat{T}_j) = \{u_{1,\hat{T}_j}, u_{2,\hat{T}_j}, \ldots, u_{m,\hat{T}_j}\}$, where $n_{i,\hat{T}_j} (1 \le i \le m)$ is the number of footprints that user u_i has in R during the time frame $\hat{T}_j$ and $N_{\hat{T}_j} = \sum_{i=1}^{m} n_{i,\hat{T}_j}$. We define the entropy of R at time $\hat{T}_j$ as $E(R, \hat{T}_j) = -\sum_{i=1}^{m} (n_{i,\hat{T}_j}/N_{\hat{T}_j}) \cdot \log(n_{i,\hat{T}_j}/N_{\hat{T}_j})$.

Definition 8 (popularity in $\hat{T}_j$). We define the popularity of R at time frame $\hat{T}_j$ as $P(R, \hat{T}_j) = 2^{E(R,\hat{T}_j)}$.

We observe that we can rewrite the quantities in Definition 5, using our Definition 7. More formally, we consider: $N = \sum_{x=1}^{q} N_{\hat{T}_j}$ and $n_i = \sum_{x=1}^{q} n_{i,\hat{T}_j}$.

We use the following example to support our discussions and to compare with the privacy model in [4, 5].

Example 1. Let us consider a user, Alice, requesting a LBS from her office building. She feels her privacy is preserved when specifying her office as the public region. In Alice's office, employees are organized on work shifts. Part of the employees are on a *morning* shift and the remaining ones on an *afternoon* shift. Let us consider $m = 4$ users (u_1, u_2, u_3, u_4) for the region corresponding to Alice's office (later on also referred as region R_1), each of them having 16 footprints in the LDS footprints database. This scenario is depicted in Figure 2. The corresponding footprints data for u_1, u_2, u_3, u_4 are provided and highlighted in the first column of Tables 2(a), 2(b), and 2(c), respectively.

Data in Table 2(a) represent the footprints information used by the LDS to calculate the entropy and the popularity of Alice's office. The results of the calculation determine a corresponding spatial region R_j (column labels in Table 2) used to cloak the user location. Hence, Table 2(a) also represents the knowledge of ADV. Tables 2(b) and 2(c) instead represent the structured knowledge of ADV^T, that is the same information of ADV when taking into account two time frames: $\hat{T}_1$ = *morning* and $\hat{T}_2$ = *afternoon*. Each table is provided with additional column data to show that both the entropy and the popularity depend on footprints distribution among visitors. In fact, it is possible to check that in each reported scenario the total number of footprints per user remains unchanged. Let us take the values of entropy and popularity in Table 2(a) as reference point to evaluate entropy and popularity calculations reported for each data column in Tables 2(b) and 2(c). As it is shown in Table 2(a) column 1, the maximum is obtained from footprints uniform distribution (column 1). We can observe that a more structured knowledge, like that of ADV^T in Tables 2(b) and 2(c) may result in the following possible scenarios. (i) ADV^T entropy and popularity values are strictly less than that of ADV. This is the case for the first and the second data columns in Table 2(c) and for the first column in Table 2(b), compared to the corresponding columns in Table 2(a). (ii) ADV^T entropy and popularity values are equal to that of ADV (see Tables 2(b) and 2(c)

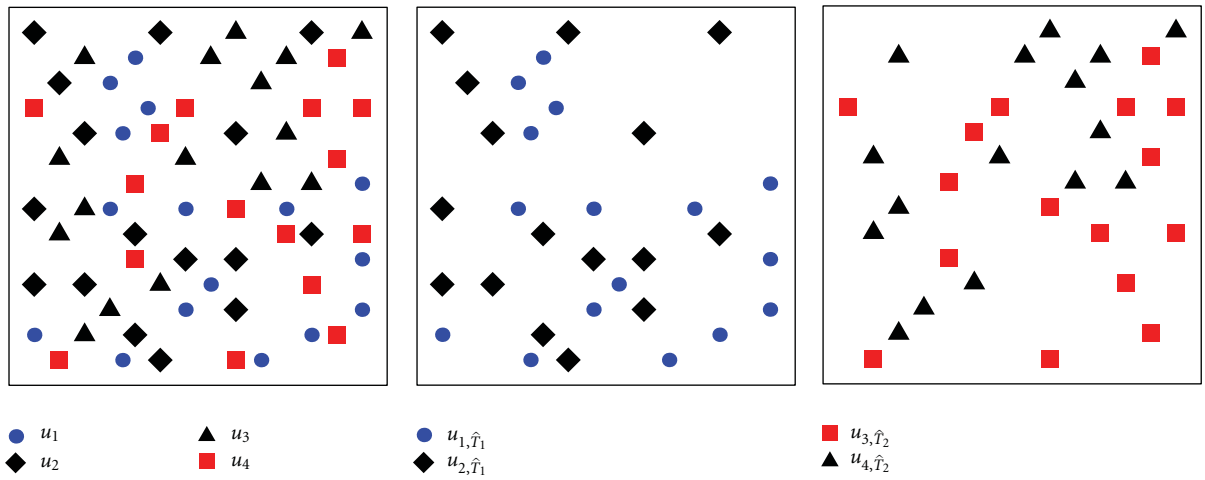

(a) ADV: daily (b) ADVT: *morning* (c) ADVT: *afternoon*

FIGURE 2: ADV and ADV^T knowledge.

TABLE 2: ADV and ADV^T table data.

(a) ADV: *daily*

User	R_1	R_2
u_1	**16**	9
u_2	**16**	16
u_3	**16**	18
u_4	**16**	21
$E(R)$	2	1.94
$P(R)$	4	3.84

(b) ADV^T: *morning*

User	R_1	R_2	R_3
$u_{1,\hat{T}_1}$	**16**	4	8
$u_{2,\hat{T}_1}$	**16**	8	8
$u_{3,\hat{T}_1}$	**0**	9	8
$u_{4,\hat{T}_1}$	**0**	11	8
$E(R,\hat{T}_1)$	1	1.92	2
$P(R,\hat{T}_1)$	2	3.78	4

(c) ADV^T: *afternoon*

User	R_1	R_2	R_3
$u_{1,\hat{T}_2}$	**0**	5	8
$u_{2,\hat{T}_2}$	**0**	8	8
$u_{3,\hat{T}_2}$	**16**	9	8
$u_{4,\hat{T}_2}$	**16**	10	8
$E(R,\hat{T}_2)$	1	1.96	2
$P(R,\hat{T}_2)$	2	3.88	4

column 3). (iii) ADV^T entropy and popularity values are greater than that of ADV. This is the case for the second column in Table 2(b) with entropy 1.51—greater than the corresponding 1.49 in Table 2(a).

In the following, we formally prove that an anonymizer using the aggregated data can guarantee the level of privacy requested by the user only if it is facing the adversary ADV. In fact, we prove that when the anonymizer is facing ADV^T, the following two cases can also happen: (i) the anonymizer is not able to guarantee to the user the requested level of privacy. (ii) the anonymizer is degrading the accuracy of the location information for the LBSs, exceeding the level of privacy requested by the user.

Theorem 1. *Given a spatial region R and footprints data $\hat{T}_i$ related to the ith time slice, footprints distributions exist such that $E(R,\hat{T}_i) \neq E(R)$.*

Proof. The proof is a direct consequence of the two following cases.

Case 1. If $n_{i,\hat{T}_j}$ satisfies $n_{i,\hat{T}_j} \leq n_i \cdot N_{\hat{T}_j}/N$, then $E(R,\hat{T}_j) \leq E(R)$. In fact, the condition can be rewritten as: $(n_{i,\hat{T}_j}/N_{\hat{T}_j}) \leq (n_i/N)$. Since the log function is monotonically increasing, $\log n_{i,\hat{T}_j}/N_{\hat{T}_j} \leq \log n_i/N$. As a consequence, $E(R,\hat{T}_j) \leq E(R)$.

Case 2. If $n_{i,\hat{T}_j}$ satisfies $n_{i,\hat{T}_j} > n_i \cdot (N_{\hat{T}_j}/N)$, then $E(R,\hat{T}_j) > E(R)$. The proof is similar to the proof of Case 1. □

Case 1 shows that with a time-aware adversary, ADV^T, and the LDS is not always able to guarantee the level of privacy requested by the user. This happens when $E(R,\hat{T}_i) < E(R)$. In fact, if this is the case, the region R does not achieve an entropy at least equivalent to the public region specified by the user in order to meet her privacy requirement. Case 2 shows that with a time-aware adversary, ADV^T, the LDS is not always able to guarantee the maximum level of accuracy for the LBSs service requested by the user. This happens when $E(R,\hat{T}_i) > E(R)$. If this is the case, the LDS introduces a loss

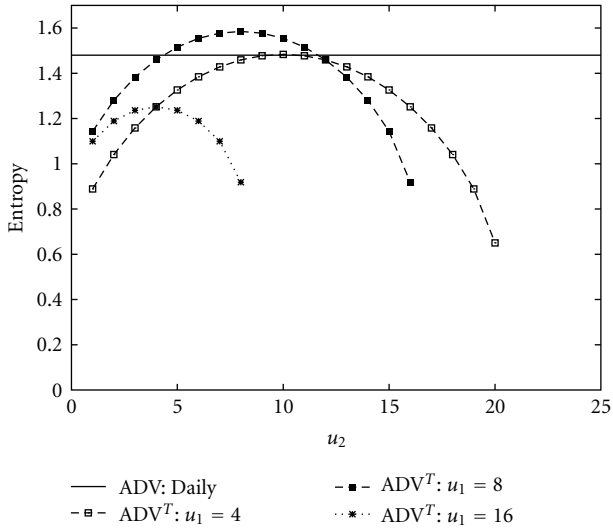

FIGURE 3: Comparing entropy between ADV and ADV^T: $\hat{T}_2$ (*afternoon*) footprints distribution, $u_{1,\hat{T}_2} = 4,\ 8,\ 16$.

in service accuracy—since a region larger than necessary is used to guarantee the user requested level of privacy.

4.2. Evaluating the Adversary Effectiveness. In this section, we highlight the importance of the time when providing LBSs privacy.

To show the influence of the time frames, we evaluated the adversary effectiveness against the privacy guarantees of the protocol in [5]. To do so, we plot the analytical results of some example data. The aim of the graph is to show how footprints distribution impacts the entropy values used to measure the required adversary effort. We remind that the entropy is a measure for the adversary effort needed to compromise the user privacy. Let us assume the user selected a desired level of privacy (entropy). On the one hand, if the anonymizer behaves in such a way that the effort required to ADV^T to compromise privacy is less than the expected one, the anonymizer is failing in guaranteeing the claimed level of privacy. On the other hand, each time the actual level of entropy for ADV^T is greater than the one sufficient for guaranteeing the user's chosen level of privacy, the anonymizer is decreasing the quality of the LBSs.

In our example, we assume the user sets the entropy value (that is the privacy level) to 1.48, represented by the straight line parallel to the x-axis in Figure 3. We also assume—as for the example in Section 4—three users being visiting the region for a total of 48 footprints, while the ADV^T knowledge is split in two time frames: $\hat{T}_1$ = *morning* and $\hat{T}_2$ = *afternoon*. We use the fixed entropy value (as the one that would be considered by the solution in [5]) to compare with different ADV^T footprints distributions, sampled as possible ADV^T knowledge at time frame $\hat{T}_2$ = *afternoon*. The different scenarios for footprints in $\hat{T}_2$ are obtained as follows: (i) we fix the subset of total ADV footprints for the time frame $\hat{T}_2$, 24 out of 48 in our example, (ii) we fix the number of footprints for user $u_{1,\hat{T}_2}$, and (iii) we let $u_{2,\hat{T}_2}$ vary (x-axis), $u_{3,\hat{T}_2}$ being determined once u_1 and u_2 are known. We report the entropy values computed for $u_{1,\hat{T}_2}$, $u_{2,\hat{T}_2}$, and $u_{3,\hat{T}_2}$ on the y-axis. The analytical results computed on these example scenarios are reported in Figure 3. The results confirm the claim of Theorem 1—the actual level of entropy for ADV^T can be smaller or greater than the one expected for ADV.

In Figure 3, three curves are plotted for ADV^T, setting, respectively $u_{1,\hat{T}_2} = 4$, $u_{1,\hat{T}_2} = 8$, and $u_{1,\hat{T}_2} = 16$. Consistently with Theorem 1, varying footprints distributions may result in ADV^T entropy values (thus adversary effort) much lower than the one calculated for ADV. This is the case for the two curves in Figure 3 obtained with $u_{1,\hat{T}_2} = 4$ and $u_{1,\hat{T}_2} = 16$. ADV^T entropy values greater than 1.48 (see Figure 3, ADV^T curve $u_{1,\hat{T}_2} = 8$) raise another issue. Indeed, on the one hand, a greater entropy for ADV^T (compared to the one for ADV) might imply a privacy level higher than the one requested; on the other hand, this implies a loss in the service accuracy—cloaking the user in an area bigger than necessary. While we plotted only the results for the entropy, the curves we computed for the popularity reflect a shape similar to the ones for entropy—popularity curves have the maximum value of 3 for the uniform distribution obtained setting $u_{1,\hat{T}_2} = 8$, $u_{1,\hat{T}_2} = 8$, and $u_{1,\hat{T}_2} = 8$.

Theorem 1 proves that the problem related to considering time in designing privacy solutions is relevant. However, one might ask how much likely is that the distributions of footprints falls in the case of Theorem 1. In fact, if the chances to fall into such a scenario were very small, this could be considered not a big concern. In the sequel, we show that this is not the case, that is, the chances to match the conditions for which Theorem 1 holds are not negligible.

To investigate this aspect, we considered the following example. In a scenario with two users, we set the number of footprints for the two users, respectively to $u_1 = 5$ and $u_1 = 8$. We vary all the possible distributions of the user footprints split into two time frames $\hat{T}_1$ = *morning* and $\hat{T}_2$ = *afternoon*. For each possible distribution we calculate the corresponding entropy. Assuming each distribution to be equally probable, we thus calculate the ratio between the number of occurrences of each entropy value obtained and the total number of possible distributions, 54 in our example. The resulting probability density function is shown in Figure 4. In particular, Figure 4 reports on the probability density of the observed entropy. The entropy calculated for the total number of user footprints is 0.96. It is represented as a vertical line to highlight the points closest to this value. Small squares represent the relation between entropy values (x-axis) and their corresponding probability density (y-axis). We can also observe that the highest probability (0.26) is reached for the entropy value zero obtained for all the distributions, in which at least one of the two users has zero footprints—14 cases in our example.

Figure 5 reports the entropy values obtained for each footprints distribution considered at time frame $\hat{T}_1$ = *morning*. On the x-axis we, vary the footprints value for user $u_{1,\hat{T}_1}$, on the y-axis the ones for user $u_{2,\hat{T}_1}$, and on the z-axis we show the resulting entropy. We notice that the values for $u_{2,\hat{T}_2}$ and $u_{2,\hat{T}_2}$ can be derived, once determined the value

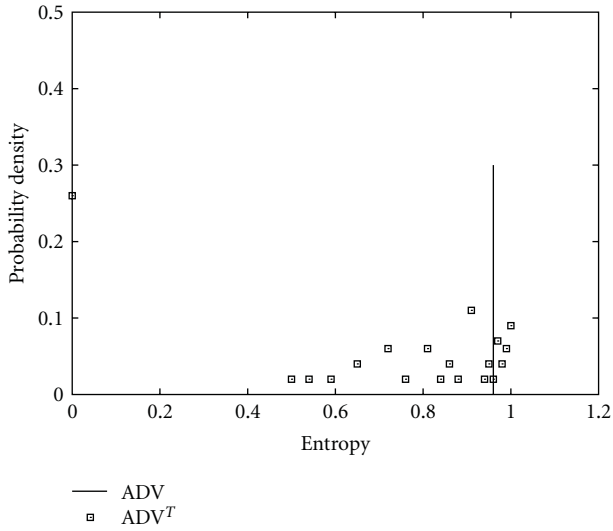

FIGURE 4: ADV^T entropy: probability density function ($u_1 = 5, u_2 = 8$).

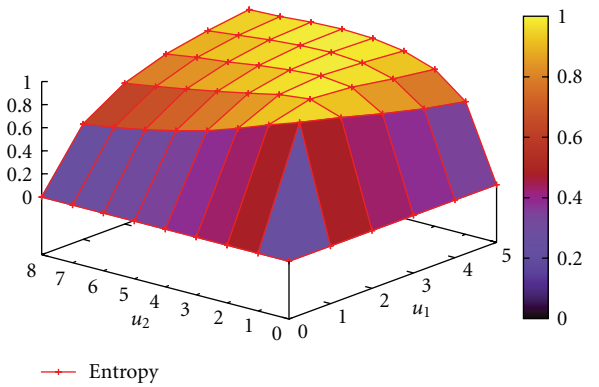

FIGURE 5: ADV^T entropy: $\hat{T}_1$ (*morning*) footprints distributions ($u_1 = 5, u_2 = 8$).

for $u_{1,\hat{T}_1}$ and $u_{2,\hat{T}_1}$, leveraging the above assumptions on the total number of footprints per user. From Figure 5, we can observe that the maximum entropy is obtained, as expected, when the numbers of footprints for user u_1 and user u_2 are the same. We can observe this in the diagonal that goes from point $\langle u_1 = 0,\ u_2 = 0\rangle$ to the point $\langle u_1 = 5, u_2 = 5\rangle$. From this diagonal, when the values for u_2 remains in the high range (e.g., $u_2 = 8$), the entropy remains high. However, when one of the two values decreases, the entropy decreases accordingly. In particular, as already noticed, when one of the two values is equal to zero, the entropy also goes to zero.

5. Comparisons and Discussions

The aim of this section is to discuss the results from the analysis of an existing data set of footprints information. The series of experiments using real data confirms the observation that the feeling-based model, and in particular the solution proposed in [4, 5], while promising in terms of

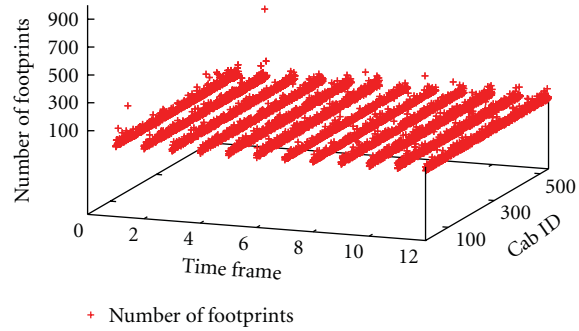

FIGURE 6: R_g global dataset view: cabs footprints per time frames.

user capability to specify the anonymity level, has a problem in dealing with a realistic adversary such as ADV^T.

5.1. Experimenting with Real Data. The *San Francisco Cabs data set* is provided by the Crawdad project [36] and contains traces of 536 cabs vehicles, collected over approximately 30 days in the San Francisco Bay Area (USA). Cab mobility traces are provided by the cabspotting project [37]. Each record in the data set takes the form (*id*, *p*, *t*, *fare*), where $p = (x, y)$ is the location of the vehicle identified by *id* at time *t* and fare formalizes whether the cab itself is busy or not at time *t*. We transform the latitude and longitude coordinates (x, y) provided by the data set in the UTM (Universal Transverse of Mercator) system obtaining a grid-based representation for locations.

We consider for the simulations the region that delimits the Golden Gate Park in San Francisco (referred as R_g). Figure 6 reports an overall view of the footprints in the data set for this region. In particular, on the *x*-axis we vary the time frames starting from $\hat{T}_1$—indicating the 00AM : 02AM time interval—to $\hat{T}_{12}$—indicating the 10P M : 12 PM one. On the y-axis we represents the cab *id*, and, on the *z*-axis we show the corresponding number of footprints for each cab in each time frame.

Among the 536 cabs, we select for the simulation the four cabs (54, 293, 404, 475) with the highest variance as for the number of footprints, with respect to time frames. The footprints trend for these cabs is depicted in Figure 7. We can observe that the footprints of the cab 404 show the highest variation in the time frame $\hat{T}_3$ (04 AM : 06 AM), with 632 footprints; at the same time, they show the same value, 0, in three time frames ($\hat{T}_7$, $\hat{T}_9$, $\hat{T}_{10}$). This means that data for cab 404 vary in a large range but do not vary so much between time frames. On the contrary, the other three cabs vary in a smaller range: from 0 to approximately 250. Thus, they present a higher variation with respect to time frames (see cab 475). Table 3 reports footprints data for the four selected cabs in the region R_g. More specifically, Table 3(a) contains the total number of footprints in the data set while Table 3(b) shows the same data split into 12 time frames.

Similarly to Figure 3, we plotted the results for the entropy corresponding to the footprints distribution in Table 3(b). In Figure 8, the points represent the entropy values calculated for each time frame; the straight line

Table 3: ADV and ADV^T cabs data.

(a) ADV.

R_g	daily
$id = 54$	989
$id = 293$	808
$id = 404$	858
$id = 475$	565
$E(R_g)$	5.62
$P(R_g)$	49.20

(b) ADV^T : $\widehat{T}_j$, $1 \le j \le 12$ (2 hours)

R_g	$\widehat{T}_1$	$\widehat{T}_2$	$\widehat{T}_3$	$\widehat{T}_4$	$\widehat{T}_5$	$\widehat{T}_6$	$\widehat{T}_7$	$\widehat{T}_8$	$\widehat{T}_9$	$\widehat{T}_{10}$	$\widehat{T}_{11}$	$\widehat{T}_{12}$
$id = 54$	244	118	52	52	13	85	207	35	72	45	29	37
$id = 293$	14	48	9	10	14	50	26	67	229	80	160	101
$id = 404$	12	33	632	111	14	17	0	6	0	0	27	6
$id = 475$	27	19	23	81	81	159	47	4	13	34	39	38
$E(R_g, \widehat{T}_j)$	1.94	2.43	1.33	2.50	2.65	2.67	1.92	1.77	2.29	2.67	2.63	2.61
$P(R_g, \widehat{T}_j)$	3.85	5.39	2.51	5.65	6.30	6.36	3.79	3.43	4.90	6.35	6.22	6.09

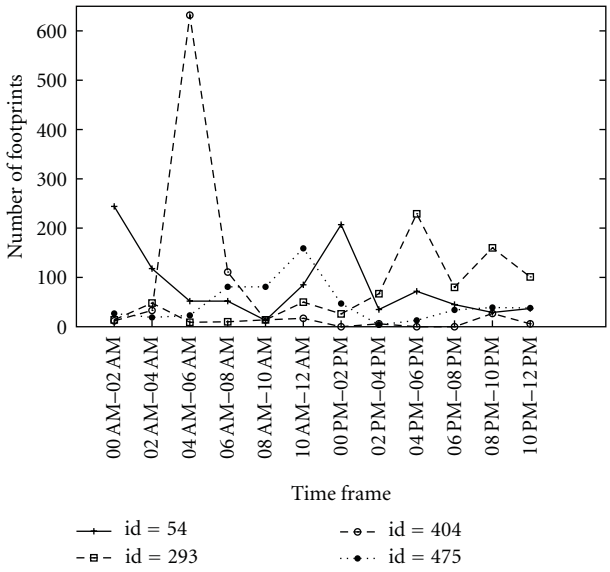

Figure 7: Footprints distribution of four sample cabs, $\widehat{T}_j$, $1 \le j \le 12$ (2 hours).

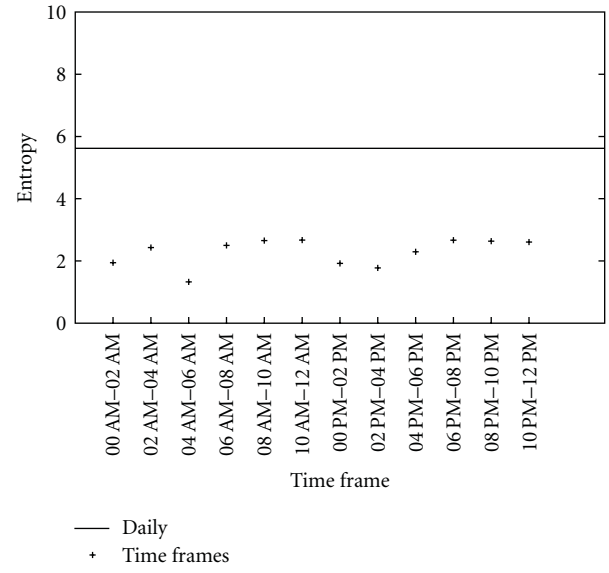

Figure 8: Comparing entropy between ADV and ADV^T for cabs: daily and time frames.

represents the entropy value obtained from the data set considered as a whole. Consistently, with the example in Section 4.1 and with Theorem 1, Figure 8 shows that considering time frames may result in ADV^T entropy values (e.g., 2.65 for time frame $\widehat{T}_5$) much lower than the one calculated for ADV (i.e., 5.62).

We also notice that all the entropy values depicted in Figure 8 are lower with respect to the ADV value of 5.62; also the maximum gap between ADV and ADV^T is quite significant (i.e., 4.30 for time frame $\widehat{T}_3$ (04 AM : 06 AM)). This is due to the choice of cabs with a number of footprints with high variance between time frames. In fact, this choice implies obtaining the minimum entropy values and thus the worst case in the lack of privacy guarantees.

As this is exactly what we expected, we have further confirmed our preliminary findings through real data analysis. Figure 9 shows how much the service quality can be influenced by considering time frames. In particular, we considered three regions: $R_1 = R_g$, R_2, R_3 of 5.83, 10.22, and 13.98 km^2 area, respectively. The region $R_1 = R_g$ matches the area of the Golden Gate Park, while R_2 and R_3 expand the park area. Figure 9(a) reports R_1, R_2, and R_3 on the map of San Francisco. While one might expect that significantly increasing the area of the region (from 5.83 to 13.98, in our

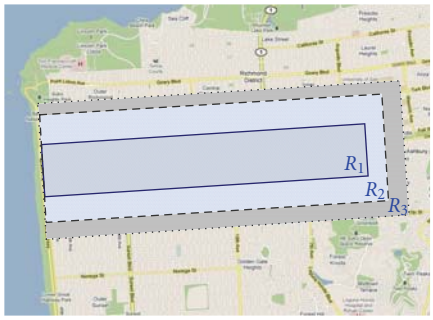

(a) R_1, R_2, R_3 on the map of San Francisco

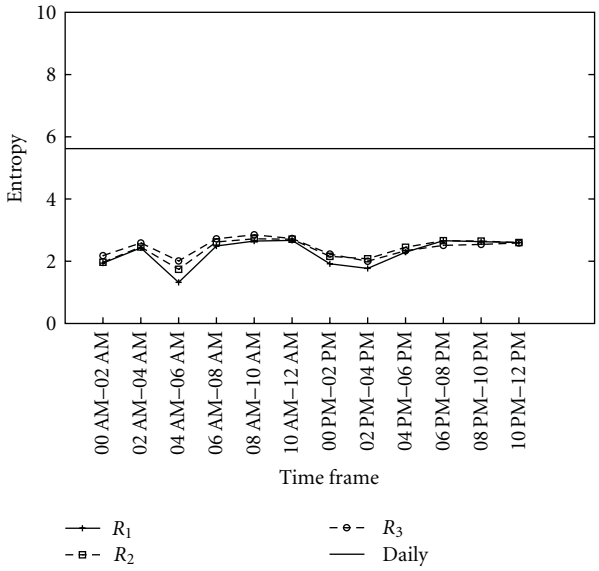

(b) Comparing entropy of R_1, R_2, R_3

Figure 9: San Francisco cabs: comparing service quality (region area) and privacy for ADV^T

case) will significantly increase the entropy (e.g., being closer to the ADV entropy value of 5.62), there are cases where this does not happen. In fact, as we can notice from Figure 9(b), even significantly increasing the size of the considered region, the gain in the entropy values is negligible. In particular, varying time frames (x-axis) and the area of the regions (R_1, R_2, R_3), the resulting entropy values (y-axis) are very similar. This highlights how, considering a time-aware adversary, affects both the privacy and the quality of the service.

6. Revisiting Assumptions and Approaches

We observed how the feeling-based model [4, 5], while promising in terms of user capability to specify the anonymity level, has a problem in dealing with a realistic adversary such as ADV^T.

Conducting our experiments on a data set of real vehicles traces strengthens the validity of assertions, with respect to experiments performed on synthetically generated datasets only. Our results also show how the threats to user privacy in LBSs are realistic and motivates further investigations. In fact, the results suggest that the problem of protecting location privacy requires to tackle the assumption that the adversarial knowledge is unknown to the anonimyzer. We believe this scenario to be the most challenging and realistic to consider. In fact, depending on the knowledge that the anonymizer has about the adversary, the following scenarios are possible.

(i) The anonymizer knows that the adversary has traces information structured in time slices of equal size. In particular, the anonymizer also knows the size of such time interval.

(ii) The anonymizer knows that the adversary has traces information structured in time slices of different size. In particular, the anonymizer also knows the size of the smaller time slice.

(iii) The anonymizer does not have any information about the adversary knowledge over the traces.

Let us consider (i) and (ii), that is the hypothesis in which the anonymizer has some knowledge of the adversary. Under these hypothesis, a possible direction could be extending the protocol in [4, 5] in order to handle time in a finer manner, so as to thwart ADV^T. For example, it could be argued that for each time frame (e.g., $\widehat{T}_2$), the LBSs requests in that time frame should be anonymized-based on the footprints of that time frame. We assume the anonymizer being able to restructure the possessed traces over any possible time frame. The point is that the anonymization should be computed considering time frame with time slices that are so small as the ones considered by the adversary, that is, the LDS anonymizes against the worst case scenario. This could be an acceptable solution (that assure the level of privacy promised to the user), even if at a cost of a worse service than the one that might be required (i.e., LBS referred to a broader region). In particular, in case of scenario (i), the anonymizer needs to anonymize the request-based on the traces in the same time frame. For scenario (ii), the anonymizer can do anonymization considering always the smallest time slice used by the adversary. As an example, if the adversary has information structured on time slices of three, two and one hours, the anonymizer should always use time frame of one hour to compute the anonimization region. Furthermore, we assume that time slices can only start at multiples of the smaller time slice. For instance, in the cited example the time slice can only start at the beginning of an hour—8.00 AM, 9.00 AM, and so on. Anonymizing the user in a consistent way (i.e., assuring her always the promised level of privacy) using the footprint model and making no assumption about the knowledge of the adversary, that is, scenario (iii) still an open issue that calls for further investigations.

7. Conclusion

We showed that an adversary that has a time-related knowledge different from the one used by the anonymizer poses a serious threat to the privacy of users of Location-based Services. We specifically considered a recently proposed

footprints privacy model. We showed that, once the time is taken into consideration, the claimed privacy assurance does not hold anymore, even when the adversary knowledge about footprints is partial compared to the one of the anonymizer. We supported our claim with both analysis and a concrete example. In particular, we considered real mobility traces of cabs of San Francisco. The analysis of this data set not only confirmed our claim on a real vehicular network scenario. It also showed that the size of the highlighted problem is all but negligible. In practical scenarios, the distance between the expected (claimed) privacy level is far away from the one actually granted by the system. We concluded the paper highlighting further research directions.

Acknowledgments

The work of this paper is partly supported by the project S-MOBILE, contract no. VIT.7627 funded by STW Sentinels (The Netherlands), and by the grant no. HPC-2010 from CASPUR (Italy).

References

[1] M. Conti, V. T. N. Nguyen, and B. Crispo, "CRePE: context-related policy enforcement for android," in *Proceedings of the 13th Information Security Conference (ISC '10)*, 2010.

[2] "Electronic toll collection california (USA)," http://www.bayareafastrak.org/.

[3] "London congestion charge," http://www.tfl.gov.uk/road-users/congestioncharging/.

[4] T. Xu and Y. Cai, "Exploring historical location data for anonimity preservation in location-based services," in *Proceedings of the 27th IEEE Communications Society Conference on Computer Communications (INFOCOM '08)*, pp. 547–555, Phoenix, Ariz, USA, April 2008.

[5] T. Xu and Y. Cai, "Feeling-based location privacy protection for location-based services," in *Proceedings of the 16th ACM Conference on Computer and Communications Security (CCS '09)*, pp. 348–357, November 2009.

[6] J. Krumm, "A survey of computational location privacy," *Personal and Ubiquitous Computing*, vol. 13, no. 6, pp. 391–399, 2009.

[7] K. LeFevre, D. J. DeWitt, and R. Ramakrishnan, "Incognito: efficient full-domain K-anonymity," in *ACM SIGMOD International Conference on Management of Data (SIGMOD '05)*, pp. 49–60, June 2005.

[8] A. Solanas and R. Di Pietro, "A linear-time multivariate micro-aggregation for privacy protection in uniform very large data sets," in *Proceedings of the 5th International Conference on Modeling Decisions for Artificial Intelligence (MDAI '08)*, vol. 5285 of *Lecture Notes in Computer Science*, pp. 203–214, 2008.

[9] L. Sweeney, "k-anonymity: a model for protecting privacy," *International Journal of Uncertainty, Fuzziness and Knowlege-Based Systems*, vol. 10, no. 5, pp. 557–570, 2002.

[10] M. Gruteser and D. Grunwald, "Anonymous usage of location-based services through spatial and temporal cloaking," in *Proceedings of the 1st International Conference on Mobile Systems, Applications and Services (MobiSys '03)*, pp. 31–42, 2003.

[11] B. Gedik and L. Liu, "A customizable k-anonymity model for protecting location privacy," in *Proceedings of IEEE International Conference on Distributed Computing Systems (ICDCS '05)*, pp. 620–629, 2005.

[12] T. Xu and Y. Cai, "Location anonymity in continuous location-based services," in *Proceedings of the 15th Annual ACM International Symposium on Advances in Geographic Information Systems (GIS '07)*, pp. 1–8, 2007.

[13] M. F. Mokbel, C. Chow, and W. G. Aref, "The new casper: query processing for location services without compromising privacy," in *Proceedings of the 32nd International Conference on Very Large Data (VLDB '06)*, pp. 763–774, 2006.

[14] C. Y. Chow, M. F. Mokbel, and X. Liu, "A peer-to-peer spatial cloaking algorithm for anonymous location-based service," in *Proceedings of the 14th Annual ACM International Symposium on Advances in Geographic Information Systems (GIS '06)*, pp. 171–178, November 2006.

[15] C.-Y. Chow and M. F. Mokbel, "Enabling private continuous queries for revealed user locations," in *Proceedings of the 10th International Symposium on Advances in Spatial and Temporal Databases (SSTD '07)*, vol. 4605 of *Lecture Notes in Computer Science*, pp. 258–275, 2007.

[16] A. R. Beresford and F. Stajano, "Location privacy in pervasive computing," *IEEE Pervasive Computing*, vol. 2, no. 1, pp. 46–55, 2003.

[17] B. Hoh and M. Gruteser, "Protecting location privacy through path confusion," in *Proceedings of the 1st International Conference on Security and Privacy for Emerging Areas in Communications Networks (SecureComm '05)*, pp. 194–205, September 2005.

[18] J. Freudiger, M. H. Manshaei, J. P. Hubaux, and D. C. Parkes, "On non-cooperative location privacy: a game-theoretic analysis," in *Proceedings of the 16th ACM Conference on Computer and Communications Security (CCS '09)*, pp. 324–337, November 2009.

[19] J. Freudiger, M. H. Manshaei, J. Le Boudec, and J. Hubaux, "On the age of pseudonyms in mobile ad hoc networks," in *Proceedings of the 29th Conference on Information Communications (INFOCOM '10)*, pp. 1577–1585, San Diego, Calif, USA, March 2010.

[20] B. Hoh, M. Gruteser, H. Xiong, and A. Alrabady, "Preserving privacy in GPS traces via uncertainty-aware path cloaking," in *Proceedings of the 14th ACM Conference on Computer and Communications Security (CCS '07)*, pp. 161–171, November 2007.

[21] J. Freudiger, M. Raya, M. Felegyhazi, P. Papadimitratos, and J. Hubaux, "Mix-zones for location privacy in vehicular networks," in *Proceedings of the 1st International Workshop on Wireless Networking for Intelligent Transportation Systems (WiN-ITS '07)*, 2007.

[22] H. Kido, Y. Yanagisawa, and T. Satoh, "An anonymous communication technique using dummies for location-based services," in *Proceedings of the 2nd International Conference on Pervasive Services (ICPS '05)*, pp. 88–97, July 2005.

[23] C. Bettini, X. S. Wang, and S. Jajodia, "Protecting privacy against location-based personal identification," in *Proceedings of the 2nd VLDB Workshop on Secure Data Management*, pp. 185–199, 2005.

[24] K. Sampigethaya, L. Huang, M. Li, R. Poovendran, K. Matsuura, and K. Sezaki, "Caravan: providing location privacy for vanet," in *Proceedings of Embedded Security in Cars (ESCAR '05)*, 2005.

[25] P. Cencioni and R. Di Pietro, "A mechanism to enforce privacy in vehicle-to-infrastructure communication," *Computer Communications*, vol. 31, no. 12, pp. 2790–2802, 2008.

[26] M. Gruteser and X. Liu, "Protecting privacy in continuous location-tracking applications," *IEEE Security and Privacy*, vol. 2, no. 2, pp. 28–34, 2004.

[27] M. L. Damiani, E. Bertino, and C. Silvestri, "The PROBE framework for the personalized cloaking of private locations," *Transactions on Data Privacy*, vol. 3, no. 2, pp. 123–148, 2010.

[28] G. Ghinita, P. Kalnis, A. Khoshgozaran, C. Shahabi, and K. L. Tan, "Private queries in location based services: anonymizers are not necessary," in *ACM SIGMOD International Conference on Management of Data (SIGMOD '08)*, pp. 121–132, June 2008.

[29] A. Serjantov and G. Danezis, "Towards an information theoretic metric for anonymity," in *Proceedings of the International Symposium on Privacy Enhancing Technologies (PETS '02)*, pp. 41–53, 2002.

[30] R. Di Pietro and A. Viejo, "Location privacy and resilience in wireless sensor networks querying," *Computer Communications*, vol. 34, no. 3, pp. 515–523, 2011.

[31] R. Di Pietro, P. Michiardi, and R. Molva, "Confidentiality and integrity for data aggregation in WSN using peer monitoring," *Security and Communication Networks*, vol. 2, no. 2, pp. 181–194, 2009.

[32] S. Ortolani, M. Conti, B. Crispo, and R. Di Pietro, "Event handoff unobservability in WSN," in *Proceedings of the IFIP Open Research Problems in Network Security Conference (iNetSec '10)*, 2010.

[33] O. Abul, F. Bonchi, and M. Nanni, "Never walk alone: uncertainty for anonymity in moving objects databases," in *Proceedings of the 24th IEEE International Conference on Data Engineering*, pp. 376–385, IEEE Computer Society, Washington, DC, USA, 2008.

[34] L. Marconi, R. Di Pietro, B. Crispo, and M. Conti, "Time warp: how time affects privacy in LBSs," in *Proceedings of the 12th International Conference on Information and Communications Security (ICICS '10)*, pp. 325–339, 2010.

[35] R. Shokri, J. Freudiger, and J. Hubaux, "Unified framework for location privacy," in *Proceedings of the 9th International Symposium on Privacy Enhancing Technologies (PETS '10)*, pp. 203–214, 2010.

[36] M. Piorkowski, N. Sarafijanovic-Djukic, and M. Grossglauser, "CRAWDAD data set epfl/mobility (v. 2009-02-24)," February 2009, http://crawdad.cs.dartmouth.edu/epfl/mobility.

[37] "San francisco exploratorium—cabspotting project," http://cabspotting.org/.